1.25 Deep Earth Structure: *Q* of the Earth from Crust to Core

BA Romanowicz, University of California, Berkeley, CA, USA
BJ Mitchell, Saint Louis University, St. Louis, MO, USA

1.25.1	**Introduction**	789
1.25.2	**Early Studies**	790
1.25.3	**Frequency Dependence of *Q***	791
1.25.4	**1D Global Mantle *Q* Models**	793
1.25.4.1	Normal Mode and Surface-Wave-Based 1D *Q* Mantle Models	793
1.25.4.2	Body-Wave-Based 1D Mantle *Q* Models	794
1.25.5	***Q* in the Core**	796
1.25.5.1	The Outer Core	796
1.25.5.2	Attenuation in the Inner Core	796
1.25.5.2.1	Hemispheric variations	797
1.25.5.2.2	Anisotropic attenuation	798
1.25.6	**Global 3D Attenuation Structure in the Upper Mantle**	799
1.25.6.1	Normal Modes and Long-Period Surface Waves	799
1.25.6.1.1	Early studies	799
1.25.6.1.2	Anelasticity and focusing	799
1.25.6.1.3	Current status	800
1.25.6.2	Global Body-Wave Studies	803
1.25.6.3	Body-Wave Studies of Regional Extent	804
1.25.6.3.1	Multiple ScS studies	804
1.25.6.3.2	Body-wave attenuation studies in North America	805
1.25.6.3.3	Body-wave studies of upper mantle *Q* around subduction zones	805
1.25.6.3.4	Regional studies of upper mantle *Q* in mid-oceanic settings	807
1.25.7	**Regional *Q* Variations in the Crust and Uppermost Mantle**	807
1.25.7.1	Introduction	807
1.25.7.2	*Q* or Attenuation Determinations for Seismic Waves in the Crust	808
1.25.7.2.1	Spectral decay methods in which source effects cancel: regional phases	808
1.25.7.2.2	Spectral decay methods in which source effects cancel: fundamental-mode surface waves	809
1.25.7.2.3	Spectral decay methods in which source effects cancel: Lg coda	810
1.25.7.2.4	Spectral decay methods for which assumptions are made, or information can be learned, about the source spectrum: regional phases	811
1.25.7.2.5	Spectral decay methods for which assumptions are made about the source spectrum: fundamental-mode surface waves	812
1.25.7.3	Tomographic Mapping of Crustal *Q*	812
1.25.7.3.1	Q_{Lg}^{C}, Q_{Lg}, and Q_{μ} tomography in regions of Eurasia	814
1.25.7.3.2	Q_{Lg}^{C} tomography in Africa	815
1.25.7.3.3	Q_{Lg}^{C} and Q_{Lg} tomography in South America	815
1.25.7.3.4	Q_{Lg}^{C} tomography in Australia	815
1.25.7.3.5	Q_{Lg}^{C}, Q_{Lg}, and P/S tomography in North America	816
1.25.7.3.6	Q_{P} variation near ocean ridges	820
1.25.7.3.7	Variation of crustal *Q* with time	820
1.25.8	**Conclusions**	820
Acknowledgment		821
References		821

1.25.1 Introduction

Seismic waves have long been known to attenuate at a rate greater than that predicted by geometric spreading of their wave fronts. Knopoff (1964) pointed out more than four decades ago that much of that attenuation must occur because of the intrinsic anelastic properties of the Earth. Were it not for that fortunate circumstance, waves generated by all past earthquakes, as noted by Knopoff, would still be reverberating in the Earth today. Since it redistributes rather than absorbs wave energy, scattering would not have the same effect.

A commonly used measure of the efficiency of wave propagation is the quality factor Q or its inverse, the internal friction Q^{-1}. The latter quantity is most often defined by the expression

$$Q^{-1} = \Delta E / 2\pi E_{\max} \quad [1]$$

where ΔE is the elastic energy lost per cycle and $E_{\max}$ is the maximum elastic energy contained in a cycle. O'Connell and Budiansky (1978) proposed replacing maximum energy by average stored energy in eqn [1], a change that requires the integer 4 replace 2 in that equation. That form of the definition permits writing Q as the ratio of the real to imaginary part of the complex elastic modulus. However, most seismologists use eqn [1].

Because of its strong dependence on temperature, partial melting, and water content, mapping anelastic attenuation in the Earth has the potential to provide valuable information on Earth's three-dimensional (3D) structure and dynamics, in complement to what can be learned from mapping elastic velocities. A significant challenge is to separate the effects of anelastic (or intrinsic) attenuation from those of elastic scattering and focusing due to propagation in elastic 3D structure.

Practical aspects of seismic-wave attenuation include the need to account for it when determining earthquake magnitudes and when computing realistic synthetic seismograms. In addition, seismologists must know the attenuation structure in the Earth if they wish to determine dispersion that is produced by anelasticity (Jeffreys, 1967; Liu et al., 1976), which is needed, in particular, to interpret seismic models in the light of other observables such as the geoid (e.g., Romanowicz, 1990). The principle of causality requires that such velocity dispersion accompany intrinsic attenuation (Futterman, 1962; Lomnitz, 1957; Strick, 1967).

The following sections present a review of our current knowledge about seismic-wave attenuation from earliest studies to the present. It is a rapidly growing field for which measurements have only recently become sufficiently numerous and reliable to allow mapping at relatively small scales. It has consistently been observed that measurement errors are large, and it has recently become clear that systematic, rather than random, errors are the greatest cause of concern in Q determinations.

A major consideration is the frequency dependence of Q. After a brief review of earliest studies, we thus begin by describing the state of understanding of this issue. Next, we discuss 1D models of Q: Even now, only the average variation of Q with depth is reasonably constrained in the deep Earth, and frequency-dependent differences between the upper and lower mantle are emerging from the analysis of high-quality global data accumulated over the last 20 years. Following that, we discuss regional variations of Q in the upper mantle and in the crust, for which robust constraints are beginning to emerge. Earlier reviews on this topic can be found in Mitchell (1995) for the crust, Romanowicz (1998) for the mantle, and, most recently, Romanowicz and Durek (2000) for the whole Earth. This review is an updated version of Romanowicz and Mitchell (2007).

1.25.2 Early Studies

Although seismic-wave attenuation did not become a popular area of research until the 1970s, the first contributions appeared not long after global deployments of seismographs in the early 1900s. Here, we describe several important studies completed before 1970, which, in addition to providing the first estimates of Q for several phases, provided the first inklings of the difficulties associated with amplitude measurements.

Angenheister, working in Göttingen, Germany, in 1906, reported the first known measurements of the attenuation rate of a seismic wave. Instruments at that time were still primitive and surface waves consequently dominated most seismograms recorded by Göttingen's Wiechert seismometers. Angenheister (1906) used records from those instruments to measure the amplitude decay of 20 s surface waves for three different segments of the same great-circle path and found the decay rate to be about 0.00025 km^{-1}. For group velocities near 3 km s^{-1}, that rate corresponds to a Q value of about 200, a value implying that the measured attenuation coefficient lies within the range of commonly measured 20 s values today. He later published what was probably the first report of regional variations of surface-wave attenuation (Angenheister, 1921) in which he found that the decay of surface-wave amplitudes along oceanic paths was greater than that along continental paths. This result holds only for those cases where attenuation over relatively low-Q oceanic paths is compared to attenuation over high-Q continental paths (Mitchell, 1995).

Gutenberg also made some early determinations of Q using surface waves. He determined a Q value of 70 for Love waves at 100 s period (Gutenberg, 1924) and a value of 200 for Rayleigh waves at 20 s period (Gutenberg, 1945b). The latter value corresponds well with Angenheister's earlier measurement of Rayleigh-wave attenuation at that period. Gutenberg also determined Q for body phases, first finding a Q of 1300 for 4 s P and PKP waves (Gutenberg, 1945a). He then measured Q for three body-wave phases at different periods (Gutenberg, 1958), finding Qs of 2500 for P and PP at 2 s and 400 for P and PP at 12 s. In the same study, he also measured Q for S waves, finding values of 700 at 12 s and 400 at 24 s. Press (1956) also determined Q for S waves, finding it to be 500 or less.

Evernden (1955) studied the arrival directions of SV-, Rayleigh-, and Love-wave phases using a tripartite array in California and found that all of those phases deviated from great-circle paths between the events and the array. Although Evernden did not address Q, he brought attention to the fact that seismic waves may deviate from a great-circle path during propagation, a problem that continues, to this day, to plague determinations of Q from amplitude measurements.

The 1960s produced the first definitive evidence for lateral variations of body-wave Q even over relatively small distances. Asada and Takano (1963), in a study of the predominant periods of teleseismic phases recorded in Japan, found that those periods differed at two closely spaced stations and attributed that to differences in crustal Q. Ichikawa and Basham (1965) and Utsu (1967) studied spectral amplitudes at 0.5–3.0 Hz frequencies and concluded that P-wave absorption beneath a seismic station at Resolute, Canada, was greater than that beneath other stations in northern Canada.

Tryggvason (1965) devised a least-squares method for simultaneously obtaining Rayleigh-wave attenuation coefficients and source amplitudes using several stations located at varying distances from an explosive source. Since he assumed the source radiation pattern in this method to be circular, he had no need to determine that pattern or know the crustal velocity structure. In the same year, Anderson et al. (1965)

developed equations that allowed measured surface-wave attenuation to be inverted for models of Q_μ variation with depth and applied it to long-period surface waves that were sensitive to anelasticity at upper mantle depths.

Sutton et al. (1967) studied radiation patterns for Pg and Lg phases recorded at several stations in the United States and found that focusing and regional attenuation differences affected both waves. They concluded that the nature of the tectonic provinces traversed by the waves was more important than initial conditions at the source in determining the observed radiation patterns.

1.25.3 Frequency Dependence of *Q*

Determinations available in the 1960s from seismic observations and laboratory measurements suggested that Q was only weakly dependent on frequency (Knopoff, 1964). That conclusion, however, conflicted with the frequency dependence known for single relaxation mechanisms that exhibit rather narrowly peaked spectra for Q^{-1} centered at a characteristic frequency. Liu et al. (1976) reconciled those two observations by considering that, over the seismic frequency band in the Earth, Q^{-1} consists of a superposition of many thermally activated relaxation mechanisms for which maxima occurred at different frequencies. That superposition produces a continuous absorption band with a nearly frequency-independent Q^{-1} distribution in the seismic frequency band (**Figure 1**). The high- and low-frequency limits of the absorption band are described by relaxation times τ_1 and τ_2 and result in the following expression for the absorption band model (Kanamori and Anderson, 1977):

$$Q^{-1}(\omega) = (2/\pi)Q_m^{-1}\tan^{-1}\left[\omega(\tau_1 - \tau_2)/\left(1 + \omega^2\tau_1\tau_2\right)\right] \qquad [2]$$

where Q_m represents the maximum within the absorption band. A more realistic distribution of relaxation times yields a mild frequency dependence $Q \approx \omega^\alpha$ within the absorption band (Minster and Anderson, 1981; Mueller, 1986), with $Q^{-1} \sim \omega^{+1}$ at the higher end of the absorption band and $Q^{-1} \sim \omega^{-1}$ at the low end (Minster and Anderson, 1981). Measurements of attenuation of multiple ScS phases (Sipkin and Jordan, 1979) and other body waves (e.g., Der et al., 1982; Lundquist and Cormier, 1980; Sacks, 1980; Ulug and Berckhemer, 1984) have provided evidence that the high-frequency corner is located in the band 0.1–1 Hz. A later model (Anderson and Given, 1982) constructed to explain variations of Q for various depths in the Earth from the comparison of surface wave, free oscillation, and body-wave data obtained a single absorption band with $Q_\mu = 80$, $\alpha = 0.15$, and a width of five decades centered at different frequencies for different depths in the mantle, with a shift of the absorption band to longer periods at greater depth. Such a model could satisfy many of the known values of Q in the early 1980s. In particular, $\alpha = 0.15$ is compatible with a study of the damping of the Chandler wobble (Smith and Dahlen, 1981).

Many years of body-wave studies have since constrained the frequency dependence $Q \propto \omega^\alpha$ in the body-wave band to have $\alpha \sim 0.1$–1. Ulug and Berckhemer (1984) used spectral ratios of S/P waves in the frequency range 0.04–1.5 Hz and found

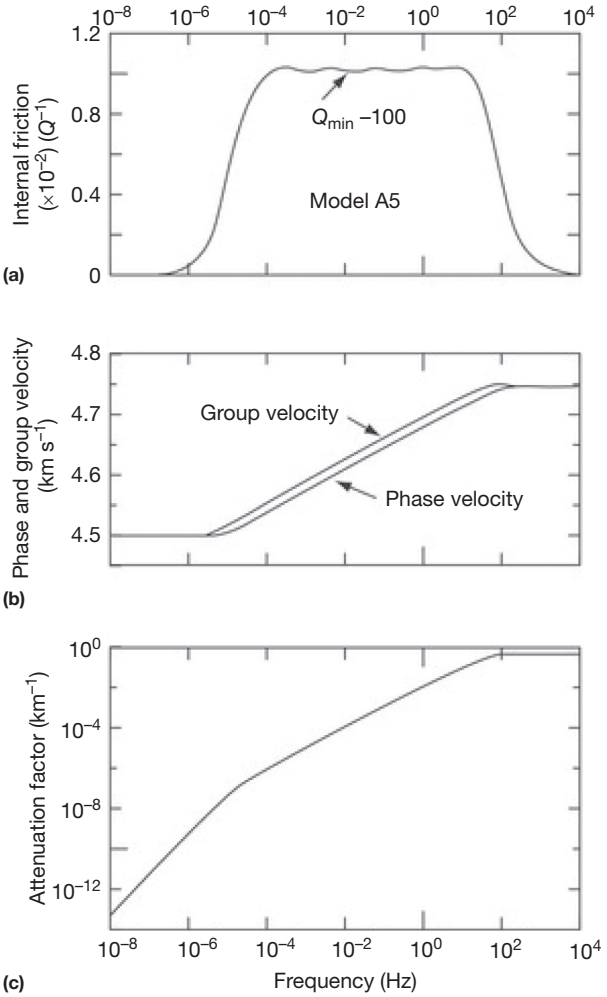

Figure 1 (a) Internal friction (Q^{-1}), (b) phase and group velocity dispersion, and (c) attenuation coefficient as functions of frequency. Reproduced from Liu HP, Anderson DL, and Kanamori H (1976) Velocity dispersion due to anelasticity: Implication for seismology and mantle composition. *Geophysical Journal of the Royal Astronomical Society* 47: 41–58, with permission from Blackwell Publishing.

$\alpha \sim 0.25$–0.6. This frequency range was extended to 6 Hz by Cheng and Kennett (2002), who found $\alpha \sim 0.2$–1 in Australia. Flanagan and Wiens (1998) found a factor of 2 difference in Q measured from sS/S and pP/P phase pairs in the Lau back-arc region, implying a strong frequency dependence in the 1–10 s period range, and inferred $\alpha \sim 0.1$–0.3.

More recently, Shito et al. (2004) used regional waveform data in western Pacific subduction zones to estimate α from P–P spectral ratios in the frequency range 0.08–8 Hz and found a range of $\alpha \sim 0.1$–0.4, which is in agreement with laboratory studies for solid olivine (e.g., Gueguen et al., 1989; Jackson, 2000) and seems to indicate that solid-state processes are the primary mechanism for the observed attenuation. Indeed, according to laboratory results, partial melting results in weak frequency dependence in a broad frequency range (e.g., Jackson et al., 2004), which is inconsistent with these observations.

In order to reconcile teleseismic S–P differential travel times measured by handpicking, on the one hand, and by

comparison of observed and synthetic seismograms, on the other, Oki et al. (2000) found that a frequency dependence with $\alpha \sim 0.04$ needs to be introduced in the reference preliminary reference Earth model (PREM) Q model (Dziewonski and Anderson, 1981), a value much smaller than in other studies.

More recently, Lekic et al. (2009) applied a Backus–Gilbert approach to globally averaged normal mode and surface-wave measurements in order to isolate the frequency dependence from that due to the frequency dependence reflecting the depth sensitivity of Q_μ. They found that α varies with frequency within the period range considered (80–3000 s), with $\alpha \sim 0.3$ at periods shorter than 200 s (compatible with most body-wave results), decreasing to ~0.1 between 300 and 800 s and possibly becoming negative at even longer periods (**Figure 2**). From most recent comparisons of global 1D Q models obtained from surface waves and free oscillations, on the one hand, and teleseismic P and S body waves, on the other, it appears that this frequency dependence is manifested primarily in the lower mantle (see **Section 1.25.4**).

At crustal depths, the frequency dependence of Q is usually described by the equation $Q = Q_0 f^{\zeta}$ where Q_0 is a reference frequency and ζ is the frequency dependence parameter. For shear-wave Q (Q_μ), it appears to be between about 0.0 and 1.0 and varies regionally, with depth in the crust and with frequency, as will be described in more detail in a later section.

An important consequence of the frequency dependence of Q in the Earth is the presence of velocity dispersion due to attenuation. Velocity dispersion was first recognized to be important when comparing global mantle elastic velocity models based on free oscillation and body-wave travel time data centered at 1 s. A dispersion correction of 0.5–1.5% helped reconcile these models (Kanamori and Anderson, 1977; Liu et al., 1976) and has been applied systematically in global seismology (e.g., Dziewonski and Anderson, 1981), although Montagner and Kennett (1996) showed that attenuation alone is insufficient to reconcile both types of data and suggested the need to perturb the density structure and introduce radial anisotropy in different parts of the mantle. In the presence of large lateral variations in Q in the upper mantle, which could be in excess of 100%, it is also necessary to account for velocity dispersion when interpreting global tomographic models in the light of other geophysical data, such as the geoid, as illustrated by Romanowicz (1990) in the case of very long wavelength structure. Karato (1993) estimated the contribution of anelasticity to the calculation of partial derivatives of elastic velocities with temperature and concluded that it should be important in the deep mantle, as anelastic effects might dominate anharmonic effects at high pressures, a conclusion confirmed by Karato and Karki (2001), who used an improved model for the calculation of anelastic effects, including the nonlinear dependence of attenuation on temperature.

In order to interpret seismologically derived 1D and 3D Q models in the Earth, it is necessary to confront them with laboratory experiments, which should provide constraints on (1) the physical mechanisms responsible for attenuation (i.e., grain boundary or dislocation processes (e.g., Jackson, 1993; Karato, 1998)) and the related frequency dependence and (2) the dependence of Q on temperature and pressure. Unfortunately, this has proven to be a major challenge, particularly for the deep mantle, due to the difficulties of reproducing in the laboratory both the high P and high T conditions, the low frequency range of seismic observations, and the location of the absorption band far from the frequency range of ultrasonic experiments, preventing ready extrapolation of seismic frequencies.

The variation of Q_μ with temperature can be expressed as (e.g., Jackson, 1993; Karato, 1993)

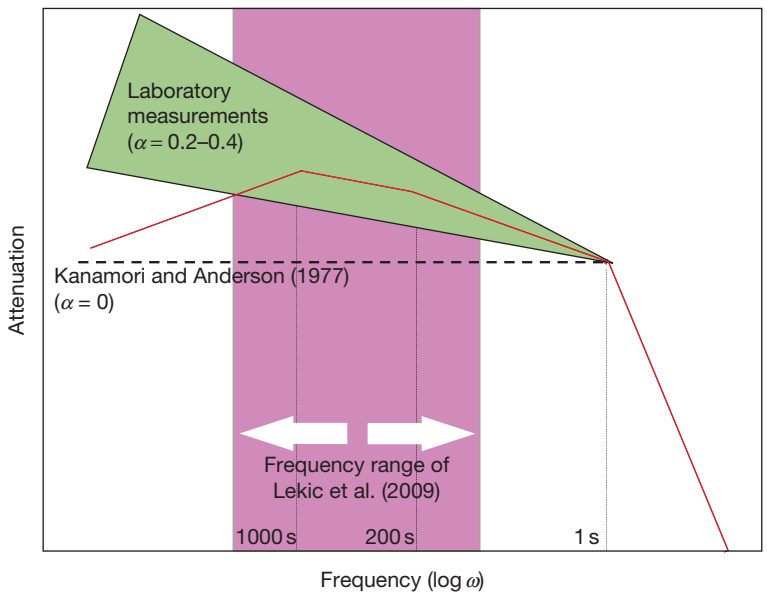

Figure 2 Frequency dependence of attenuation within the absorption band obtained from low-frequency data. A corner frequency is assumed at 1 Hz, beyond which $\alpha = 1$ (Sipkin and Jordan, 1979). Seismically inferred values (pink) are compared to those obtained from laboratory measurements (green) and the estimates assuming no frequency dependence (broken line). After Lekic V, Matas J, Panning M, and Romanowicz B (2009) Measurement and implications of frequency dependence of attenuation. *Earth and Planetary Science Letters* 282: 285–293.

$$Q^{-1} = A\omega^{-\alpha}\exp(-\alpha H/RT) \quad [3]$$

where $H = E^* + PV^*$ is the activation enthalpy, which depends on pressure through the activation volume V^*, a quantity that is not precisely known. One way to circumvent this is to parametrize this expression in terms of homologous temperature T_m/T (e.g., Cammarano et al., 2003; Karato, 1993; Sato et al., 1989):

$$Q^{-1} = A\omega^{-\alpha}\exp(-\alpha g T_m/T) \quad [4]$$

where g is a dimensionless factor, which depends on H, the melting temperature T_m, and the gas constant R. Such a parametrization removes the need for accurate knowledge of the activation volume and also allows the use of a simple scaling law to relate grain size to frequency (Sato et al., 1989). The pressure dependence is folded into T_m, which is easier to measure in the laboratory.

Much progress in the measurement of attenuation at seismically relevant frequencies has been achieved in the last 15 years (e.g., Faul et al., 2004; Getting et al., 1997; Jackson, 1993; Jackson and Faul, 2010; Karato and Spetzler, 1990). Recently, reliable results for olivine have become available at pressures and temperatures down to asthenospheric depths. There is some evidence that attenuation scales with diffusion creep viscosity (e.g., McCarthy and Takei, 2011), that hydration of mantle minerals causes significant increases in attenuation (Aizawa et al., 2008), and that water (Shito et al., 2006) and melt (Faul et al., 2004; McCarthy et al., 2011) can significantly increase attenuation. Research continues into the mechanism of attenuation, including grain boundary sliding (Morris and Jackson, 2009), diffusion creep (Sundberg and Cooper, 2010), and the effect of dislocations (Farla et al., 2012). These recent advances are described in more detail in **Chapter 2.21**.

While most physical mechanisms invoked consider volumetric contributions to attenuation in the Earth (e.g., Jackson, 2007), several authors have pointed out recently that solid–solid phase transitions may play a role in bulk dissipation of seismic energy, through the finite character of their kinetics. However, this process is clearly strongly frequency-dependent, and there is no agreement yet on the relevance of the attenuation band to seismically relevant frequencies (e.g., Durand et al., 2012; Li, 2010; Ricard et al., 2009). Nevertheless, global 1D mantle Q profiles are generally readily interpreted in terms of thermally activated, viscoelastic relaxation mechanisms (e.g., Faul and Jackson, 2005; see also **Chapter 2.21**).

1.25.4 1D Global Mantle *Q* Models

Our knowledge of the 1D Q structure of the Earth comes from two types of data spanning different ranges of frequencies: normal modes/surface waves, on the one hand, and body waves, on the other. Because of the suggestive evidence for frequency dependence of Q, with an upper frequency limit for the corresponding absorption band falling in the range of body-wave studies, it is important to consider these two types of models separately before comparing them. Another issue is that of lateral variations in Q and how representative the sampling might be in different types of studies: for example, normal mode data, by the nature of their global sampling, will likely provide models that are more representative of the true global average than multiple ScS data, which sample primarily subduction zone regions and their vicinities. A third issue is that some bulk attenuation appears to be needed to explain normal mode data, but different authors locate it in different parts of the mantle.

1.25.4.1 Normal Mode and Surface-Wave-Based 1D *Q* Mantle Models

As noted in a previous review of this topic (Romanowicz and Durek, 2000), early studies based on normal mode and surface-wave data developed measurement and inversion methodologies and established the main features of the variation of Q_μ with depth (e.g., Anderson and Archambeau, 1966; Buland and Gilbert, 1978; Deschamps, 1977; Geller and Stein, 1978; Gilbert and Dziewonski, 1975; Jobert and Roult, 1976; Kanamori, 1970; Roult, 1975; Sailor and Dziewonski, 1978). These studies found that

1. shear-wave attenuation is low in the lithosphere;
2. there is a high-attenuation zone roughly corresponding to the low-velocity zone generally associated with the asthenosphere;
3. below 200 km depth, Q_μ increases with depth with a sharp gradient across the transition zone; and
4. Q_μ is higher on average in the lower mantle than in the upper mantle.

In the last decades, an intriguing discrepancy has emerged between the measurements of fundamental mode Q_R obtained for spheroidal modes using a propagating wave approach (e.g., Durek and Ekström, 1996; Durek et al., 1993; Dziewonski and Steim, 1982; Romanowicz, 1990, 1994a) and those using a standing-wave approach (Roult and Clévédé, 2000; Smith and Masters, 1989; Widmer et al., 1991). In the period band 150–300 s, where measurements by the two methods overlap, Q_R estimates derived from standing-wave observations are systematically higher than those derived from surface waves by about 15–20%, which translates into higher Q_μ in the transition zone for models based on free oscillation data (**Figure 3**). The cause of this discrepancy was first investigated by Durek and Ekström (1997) who explored the influence of realistic background noise on normal mode-based measurements, which require the use of long time series. This issue is particularly relevant in the light of the discovery of continuously excited background free oscillations (e.g., Suda et al., 1998). While the background noise does contribute to a bias toward higher Q values, if measurements are done with care, the bias does not exceed about 5–10%, failing to explain the larger observed discrepancy. On the other hand, Masters and Laske (1997) questioned the accuracy of surface-wave Q measurements at very long periods, pointing out the difficulty in finding an appropriate time window isolating the fundamental mode in the presence of overlapping wave trains and overtones. A more recent study by Roult and Clévédé (2000) confirms the higher Q values obtained from mode-based measurements (**Figure 3**). These authors concluded that mode Q measurements are more reliable than measurements

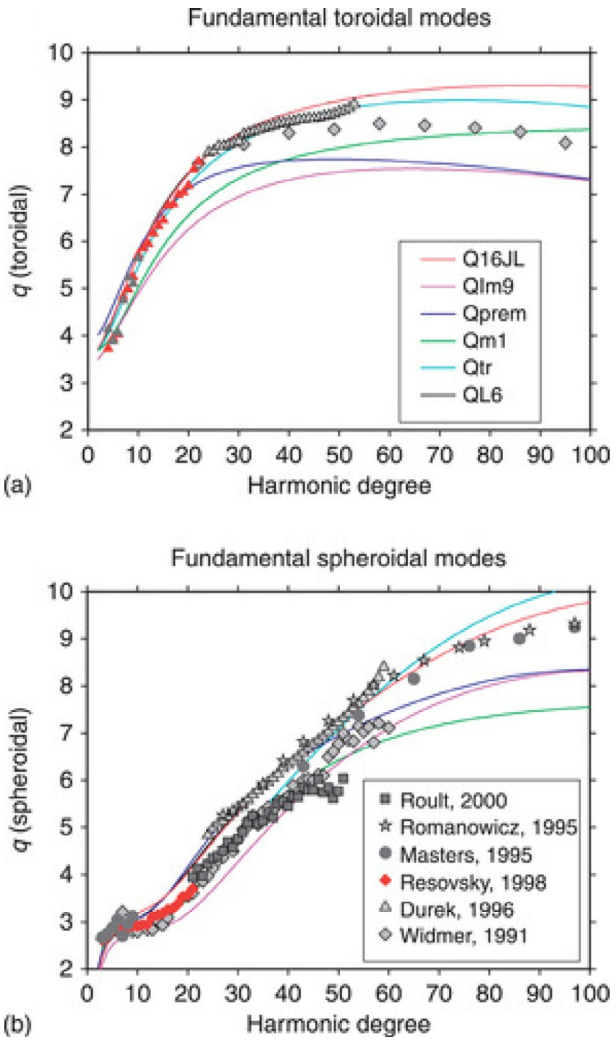

Figure 3 Fundamental-mode Q measurements obtained using either a standing mode approach (Masters and Laske, 1997; Roult and Clévédé, 2000; Widmer et al., 1991) or a propagating surface-wave approach (Durek and Ekström, 1996; Romanowicz, 1995). Note the discrepancy between the two approaches in the frequency band where both methods can be applied. Also shown are fits to the data for several models of Q_μ shown in Figure 3. (a) Toroidal modes and (b) spheroidal modes. Data are from the REM website.

based on great-circle surface-wave amplitude ratios, which they attribute to contamination by higher modes and to the relative deficiency in low frequencies of the first arriving R1 train. We note however that the QL6 model of Durek and Ekström (1996) was derived from traveling surface-wave data using a different method than tested by Roult and Clévédé (2000). QL6 (**Figures 3** and **4**) not only fits surface-wave data better than mode-based models such as QM1 (Widmer et al., 1991) but also fits toroidal mode Q data better than both QM1 and PREM (Dziewonski and Anderson, 1981). Therefore, it seems that the question of the mode/surface-wave discrepancy has not been resolved yet. A more recent study by Resovsky et al. (2005) revisited the construction of a 1D Q model of the Earth using a forward modeling approach based on the neighborhood algorithm and produced a family of acceptable models with robust error estimates. Their mode data set was augmented through recent measurements of the attenuation of low-angular-order modes (e.g., He and Tromp, 1996; Resovsky and Ritzwoller, 1998). They circumvented the mode/surface-wave discrepancy problem by including both fundamental-mode surface-wave and spheroidal mode measurements in the period range 150–300 s and attributing a low weight to these incompatible data. Their final family of models appears to be in good agreement, on average, with the surface-wave-based model QL6, in particular in the transition zone (**Figure 4**). While PREM and QL6 have constant Q_μ in the lower mantle, the Resovsky et al. (2005) study tentatively includes three layers in the lower mantle and confirms the presence of a mild Q_μ maximum in the mid-lower mantle (Qtr, **Figure 3**), as was found in earlier models (SL8, Anderson and Hart (1978); PAR2C, Okal and Jo (2002); QM1, Widmer et al. (1991); and Q7U15L, Durek and Ekström (1996); see the review by Romanowicz and Durek (2000)). What is perhaps not yet well constrained is the precise location of this maximum.

1.25.4.2 Body-Wave-Based 1D Mantle *Q* Models

Body-wave studies typically derive Q structure from the measurement of t^* ('t-star'), which is defined as follows:

$$t^* = \int \frac{ds}{Qv} \qquad [5]$$

where the integral is taken along the body-wave path and v is the wave velocity. See **Section 1.25.6.2** for more details on how t^* is measured.

Nearly vertically traveling multiple ScS waves provided early constraints on the average Q_μ in the whole mantle (e.g., Kovach and Anderson, 1964; Yoshida and Tsujiura, 1975) and confirmed the increase in Q_μ in the mid-mantle. Studies of amplitude ratios of body-wave phases interacting with the core–mantle boundary (CMB) provided early evidence for a possible lower Q_μ zone at the base of the mantle (e.g., Kuster, 1972; Mitchell and Helmberger, 1973).

More recently, Lawrence and Wysession (2006a) developed a Q_μ model based on a large global data set of differential ScS/S amplitude measurements, using a niching genetic algorithm to fit the variations of these amplitudes with distance. Because of the nature of their data, their model (QLM9, **Figure 4**) is best constrained in the lower mantle, so they chose to fix the top 400 km of the mantle to the PREM value. The resulting model also provides evidence for the existence of a Q_μ maximum in the lower mantle, in this case right above the D″ region. However, the high Q values that they obtain in the transition zone are incompatible with the fundamental-mode spheroidal and toroidal data (**Figure 3(a)**). Replacing their upper mantle with that of QL6 solves this problem (**Figure 3(b)**), and little adjustment is needed in the lower mantle to fit the ScS/S amplitude data (Lawrence, personal communication).

Most recently, Durand et al. (2013) applied a method based on instantaneous frequency measurements (Ford et al., 2012; Gao et al., 2011) to obtain differential t^*_{S-ScS} estimates in the northeast Pacific and under Central America with a strict data quality selection. These authors infer a 1D Q_μ profile of the mantle that is generally in good agreement with QLM9

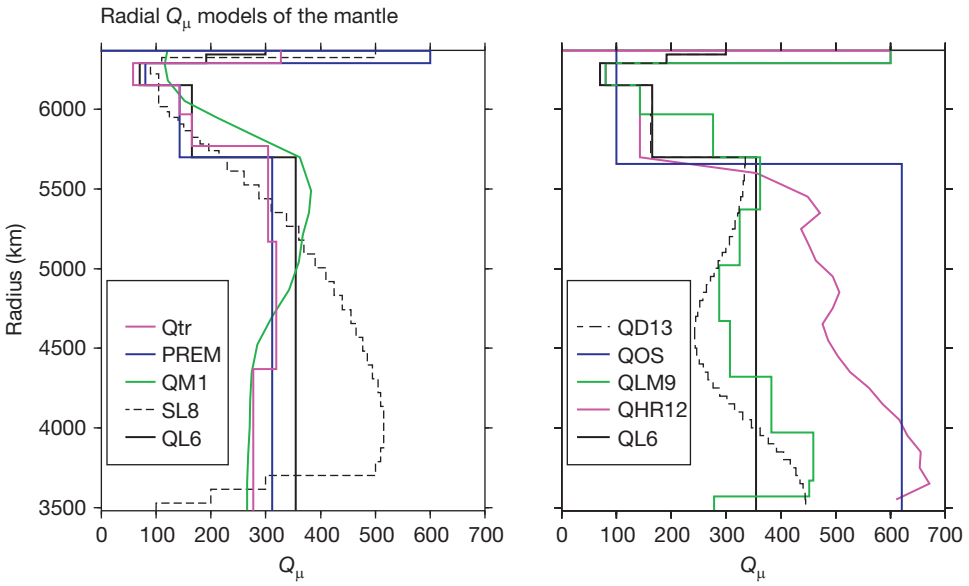

Figure 4 Radial models of Q_μ in the mantle. (Left panel) Free oscillation and surface-wave-based models. Models QM1 (Widmer et al., 1991); SL8 (Anderson and Hart, 1978); PREM (Dziewonski and Anderson, 1981); QL6 (Durek and Ekström, 1996); and Qtr (Resovsky et al., 2005). PREM and QL6 fit fundamental-mode Rayleigh-wave data, but only QL6 also fits fundamental-mode toroidal mode data. (Right panel) Body-wave-based models: QLM9 (Lawrence and Wysession, 2006a) from ScS/S amplitude data; QI6JL: a model that fits both ScS/S amplitude data and fundamental-mode surface-wave data (Lawrence, personal communication); QOS08 (Oki and Shearer, 2008); QHR12 (Hwang and Ritsema, 2011). The latter two models are based on teleseismic P and S waves.

(Figure 4). They suggest that differences can be attributed to a slight frequency dependence with $\alpha \sim 0.1$.

The typical frequency range of studies based on ScS and multiple ScS is about 0.02–0.2 Hz. Higher frequency studies have been based on a combination of P and S waves or P and PP waves. Warren and Shearer (2000) derived a series of 1D global Q_α models from stacked spectra of P and PP waves in the frequency band 0.16–0.86 Hz. While frequency dependence cannot be ignored in this frequency band, as discussed further in the following text, when assuming no frequency dependence, these authors find that the upper mantle is five times more attenuating than the lower mantle.

Recently, Oki and Shearer (2008) constructed a two-layered 1D Q_μ model for short-period body waves (3–10 s), using a large data set of measurements from teleseismic P and S waves from broadband seismograms and extracting differential t^*_{S-P} measurements. They obtained similar average Q_μ in the upper mantle as derived from long-period surface-wave/mode measurements but higher Q_μ (by a factor of 2) in the lower mantle, which they inferred to indicate stronger frequency dependence of Q_μ in the lower mantle. Hwang and Ritsema (2011) reexamined this question with an order of magnitude larger data set and confirmed the larger Q_μ in the lower mantle. Their proposed model (model HR11, Figure 4), which has a fixed upper mantle Q_μ profile equal to that of PREM (Dziewonski and Anderson, 1981), features increasing Q_μ from 360 at the top of the lower mantle to 670 in the lowermost mantle. The authors point out that this difference with depth is as large as lateral differences in Q_μ between tectonic and stable areas of the continents. The details of the lower mantle structure may change if the upper mantle model QL6 (Durek and Ekström, 1996) is used rather than PREM, as would be appropriate to fit long-period surface waves. However, the general trend of Q_μ increasing with depth in the lower mantle, which is the most robust feature of model HR11, would not change.

Clearly, the large differences between the Q values obtained from body waves, especially those including P waves in the analysis, and low-frequency surface waves and free oscillations suggest a frequency-dependent effect. Moreover, this effect may be different in the upper and lower mantle. To accommodate both normal mode and body-wave observations, Anderson and Hart (1976, 1978) proposed a model with a Q_μ maximum in the lower mantle, a feature that has successively appeared and disappeared in subsequent whole mantle models based on normal mode and surface-wave data (Giardini and Woodhouse, 1988; Li, 1990; Masters and Gilbert, 1983; Okal and Jo, 2002; Smith and Masters, 1989; Widmer et al., 1991). Anderson and Given (1982) proposed that the absorption band is shifted to lower frequencies in the lower mantle, compared to the upper mantle, resulting in a more prominent frequency dependence in the lower mantle. This is in agreement with the results of Oki and Shearer (2008). On average, the large differences between lower mantle Q values derived from low-frequency and high-frequency data can be accommodated with a frequency dependence with $\alpha \sim 0.1$, as also noted by Lekic et al. (2009) (Figure 2).

In these body-wave studies, it is generally assumed that bulk attenuation (Q_κ^{-1}) can be neglected. Using the relationship between Q_α, Q_β, and Q_κ (Anderson and Hart, 1978)

$$Q_\alpha^{-1} = \frac{4}{3}(V_S/V_P)^2 Q_\beta^{-1} + \left[1 - \frac{4}{3}(V_S/V_P)^2\right] Q_\kappa^{-1} \qquad [6]$$

this leads to the commonly used conversion between Q_α and Q_β, assuming a Poisson solid ($V_S = \sqrt{3}V_P$):

$$Q_\alpha = \frac{9}{4} Q_\beta$$

However, some regional studies in subduction zones suggest that bulk attenuation could be as large as 1/3 of attenuation in shear (e.g., Roth et al., 1999).

Bulk attenuation is necessary to simultaneously fit high-Q radial mode data and surface-wave data, and some models such as SL8 (Anderson and Hart, 1978) and the widely used PREM (Dziewonski and Anderson, 1981) locate it in the inner core, while others prefer to place it in the upper mantle (e.g., Sailor and Dziewonski, 1978), in the outer core (Anderson and Given, 1982; Widmer et al., 1991), and, more recently, in the asthenosphere (Durek and Ekström, 1995). Resovsky et al. (2005) also revisited this question and found bulk attenuation to be negligible in the inner core and preferentially located in the outer core and lower mantle. The issue of the location of bulk attenuation in the Earth is not resolved.

New constraints on average shear and bulk attenuation in the Earth and the core and their frequency dependence, from a combination of body-wave and normal mode analysis, may be forthcoming, owing to the high-quality digital data set assembled in the last 20 years on the global broadband seismic network and owing to the occurrence of several very large earthquakes, especially great earthquakes such as that in Sumatra on 26 December 2004 and Tohoku (Japan) on 12 March 2010. In particular, these data are providing an opportunity to revisit the Qs of the gravest modes of the Earth, in particular the radial mode ${}_0S_0$, and, for the first time, measure the Q of individual singlets of modes such as ${}_0S_2$ or ${}_2S_1$ (e.g., Rosat et al., 2005; Roult et al., 2006).

1.25.5 *Q* in the Core

1.25.5.1 The Outer Core

In the liquid outer core, Q is very high, and generally well approximated by $Q_\kappa \sim \infty$, to fit both free oscillation and body-wave data. Finite Q_κ is, however, required to explain some free oscillation data in the outer core, but the depth range where it is located is still the subject of debate (Anderson and Given, 1982; Durek and Ekström, 1996; Resovsky et al., 2005; Widmer et al., 1991) and, in general, the upper mantle and the inner core are preferred locations for finite Q_κ. Likewise, while some evidence for finite Q_κ from short-period core phases has been suggested, it is not clear that it is resolvable (Cormier and Richards, 1976). There is some indication for the existence of a thin layer of relatively low Q just above the inner core boundary (ICB) (Zou et al., 2008), which could be due to the presence of suspended solid particles in the F-layer (Jeffreys, 1939; Loper and Roberts, 1981).

1.25.5.2 Attenuation in the Inner Core

Attenuation in the inner core is investigated using inner core-sensitive modes, as well as spectral amplitude ratios of different core phases. Topics that have been the subject of recent work include

- the compatibility of normal mode and body-wave measurements and implications for the frequency dependence of Q in the inner core,
- variations with depth,
- anisotropy in Q_α, and
- hemispheric variations at the top of the inner core.

From early on, measurements of amplitude ratios of PKP(DF) (sampling the inner core) and PKP(BC) (sampling the outer core) constrained Q_α in the top 500 km of the inner core to be in the range 200–600 (e.g., Bhattacharyya et al., 1993; Bolt, 1977; Choy and Cormier, 1983; Cormier, 1981; Doornbos, 1974, 1983; Ivan et al., 2005; Niazi and Johnson, 1992; Sacks, 1969; Song and Helmberger, 1993; Tseng et al., 2001). Most studies have suggested an increase of Q_α with depth, although some find that Q_α is constant with depth (e.g., Bhattacharyya et al., 1993; Niazi and Johnson, 1992). In these studies, the sampling depth range was limited by the narrow distance range in which the phase PKP(BC) is observed. Extending the depth range sampled by previous studies to 600 km by including diffracted PKP(BC) phases, Souriau and Roudil (1995) proposed a two-layered model with $Q_\alpha \sim 200$ in the topmost 100 km of the inner core and $Q_\alpha \sim 440$ below. Cormier et al. (1998) designed a new approach that allowed them to investigate the variation of Q_α deeper in the inner core, by comparing observed and synthetic PKIKP waveforms in the distance range 150–180°. The synthetic waveforms are built using the source time history of each earthquake, determined from the analysis of P waveforms, and include the effects of mantle attenuation. In a recent improved implementation of this method, which takes into account surface reflections and reverberations near the source, Li and Cormier (2002) obtained a mean for the inner core of Q_α 307 ± 90 and much stronger attenuation in the top 300 km of the inner core. Testing the hypothesis of an innermost inner core, Cormier and Stroujkova (2005) found a rapid change in the magnitude and variance of seismic attenuation of PKIKP in the middle of the inner core, in the interval 400–600 km in Earth radius (**Figure 4**), which supports the existence of a distinct innermost inner core (e.g., Ishii and Dziewonski, 2002). Recently, Waszek and Deuss (2013) have suggested the presence of a high-Q_α layer in the top 30 km of the inner core.

While the analysis of core-sensitive PKP phases provides constraints on Q_α, normal modes primarily provide constraints on Q_μ. If there were no significant attenuation in bulk, and no frequency dependence, the inferred Q_μ from body-wave studies would be on the order of ~40. Confronting this value with measurements based on inner core-sensitive normal mode data has resulted in some puzzles. Early normal mode studies found very large values of Q_μ (1500–3500) based on the measurement of attenuation of spheroidal core modes (Buland and Gilbert, 1978; Masters and Gilbert, 1981), whereas most more recent models have much lower Q_μ, such as PREM ($Q_\mu = 85$; Dziewonski and Anderson, 1981) or QM1 ($Q_\mu = 110$; Widmer et al., 1991), which is also compatible with measurements of Giardini and Woodhouse (1988). On the other hand, applying the Sompi method, Kumazawa et al. (1990) and Suda and Fukao (1990) measured Q_μ of modes sensitive to shear in the top part of the inner core and found very large values and an increase with depth, with $Q_\mu = 1500$ in the top 200 km and $Q_\mu = 3800$ at greater depth. However, their identification of modes has been questioned, and, recently, Andrews et al. (2006) have shown that measurements of

inner core Q_μ could be biased by neglecting mode coupling. Through the comparison of observations and synthetic predictions including mode coupling effects, these authors found that models with very high Q_μ are incompatible with the observations, which favor moderate values of $Q_\mu \sim 80–100$. While such moderate values are now established in the top part of the inner core, where normal modes concentrate their sensitivity, a recent observation of PKJKP, which samples deep into the inner core (Cao et al., 2005), has provided the opportunity to estimate the average Q_μ in the inner core, which was found to be >150, possibly as large as 300 (Cao and Romanowicz, 2009), and which would imply an increase with depth, like that for Q_α. This result, however, needs to be confirmed by additional observations of PKJKP.

Even the lowest proposed values for Q_μ currently favored are incompatible with the Q_α results, unless one invokes either (1) significant bulk attenuation in the inner core, or (2) significant frequency dependence of Q, or (3) a significant scattering component. The rather low value for Q_α found is compatible with the existence of a mushy zone in the top part of the inner core, whose presence is related to the process of solidification of iron alloy (Fearn et al., 1981; Loper and Fearn, 1983; Loper and Roberts, 1981) involving a solid matrix and fluid inclusions. This would result primarily in compressional attenuation and could explain some of the observations of seismic anisotropy in the inner core (e.g., Singh et al., 2000). Bowers (2000) cautioned that the large scatter observed in Q_α measurements from PKP amplitude ratios could be due to the effects of lateral variations in structure near the CMB and in particular the presence of ultralow-velocity zones. On the other hand, Krasnoshchekov et al. (2005) suggested that variability in the amplitudes of ICB reflected PKiKP phases could be due to a mosaic of partially molten patches of scale length 10–100 km.

In a series of papers, Cormier and collaborators recently explored two different interpretations for the attenuation in the inner core, invoking a viscoelastic mechanism and a scattering mechanism, respectively (Cormier and Li, 2002; Cormier et al., 1998; Li and Cormier, 2002). In the viscoelastic interpretation, they considered the absorption band model of Cormier and Richards (1988) and, through a parameter search approach, sought to constrain the low-frequency corner τ_1, as well as the peak attenuation Q_m^{-1} and the attenuation at 1 Hz (Li and Cormier, 2002). While constraining τ_1 turned out to be problematic, they found that the data are consistent with frequency-dependent attenuation in the inner core and weak velocity dispersion in the seismic body-wave band. The existence of scattering, at least at the top of the inner core, was clearly documented by Vidale and Earle (2000) through the modeling of PKiKP coda and more recently by Leyton and Koper (2007). In the scattering interpretation, Cormier and Li (2002) investigated a model of inner core attenuation due to forward scattering by 3D fabric caused by solidification texturing, which could also be responsible for the observed depth-dependent inner core anisotropy. They found a mean scale length of heterogeneity of 9.8 ± 2.4 km and a mean velocity perturbation of $8.4 \pm 1.8\%$. They confirmed the depth dependence found in the viscoelastic interpretation but with a sharper transition between the highly attenuating upper part of the inner core and the lower attenuating center (e.g., Figure 13 in Souriau and Calvet, 2015). They suggested that scattering plays a dominant role in attenuating inner core traversing phases in the frequency band 0.02–2 Hz, as it can also explain elastic and anelastic anisotropy and their depth dependence and helps reconcile the body-wave and normal mode Q measurements. A synthesis of waveform and travel time observations led Cormier (2007) to propose a model of texture of the uppermost inner core that may reflect the solidification process of the inner core.

1.25.5.2.1 Hemispheric variations

Another observation in favor of the presence of a mushy transition zone at the top of the inner core is that of hemispheric differences, first observed in elastic velocity using differential travel time measurements of the pair of phases PKP(BC), PKP(DF) (Creager, 1999; Tanaka and Hamaguchi, 1997). A pair of useful phases for the study of hemispheric variations in attenuation is (PKiKP, PKIKP) in the distance range 120–144°. In this distance range, PKiKP is postcritically reflected at the ICB and PKIKP samples the top ~100 km of the inner core (Garcia, 2002; Niu and Wen, 2001). These phases have almost the same ray paths in the mantle and in the outer core, so the differences in travel times and amplitudes can be attributed to the vicinity of the ICB. Indeed, in a study covering the epicentral distance range 131–141°, the faster eastern hemisphere (40–180 °E) was also found to have lower Q_α than the slower western hemisphere (Wen and Niu, 2002). In order to better constrain the depth dependence of the hemispheric variations in Q_α, Cao and Romanowicz (2004) extended the epicentral distance range to 144° and found large differences in Q_α, with $Q_\alpha \sim 335$ in the western hemisphere and ~160 in the eastern hemisphere, which they interpreted as resulting from small lateral temperature variations at the top of the inner core. Such temperature variations could be imposed on the inner core by heterogeneities at the CMB (e.g., Sumita and Olson, 1999) and would influence the connectivity of fluid inclusions in the mushy zone. Below about 85 km depth, the hemispheric differences appeared to wane. However, several studies found evidence for persisting differences at greater depth. Oreshin and Vinnik (2004) measured spectral ratios of PKP(DF) and either PKP(AB) or PKP(BC) in the distance range 150–170° and found differences in Q_α between the hemispheres down to 600 km depth. Yu and Wen (2006a) combined observations of PKiKP/PKIKP in the distance range 120–141° and PKP(BC)/PKIKP in the distance range 146–160°, along equatorial paths, and proposed that they could resolve hemispheric differences in Q down to at least 200 km (**Figure 5**). However, in the distance range 149–155°, PKP(BC) interferes with PKiKP, causing large scatter in the data. On the other hand, Li and Cormier (2002) did not find evidence for such hemispheric variations in the deeper inner core using PKIKP data at larger distances.

Recently, depth-dependent attenuation structure was constrained in the inner core below the north East Pacific (western hemisphere), using PKP data from the dense short-period HiNet array in Japan (Iritani et al., 2010; Kazama et al., 2008). These authors found evidence for a peak in attenuation around 200–250 km depth, which may provide constraints on the mode of growth of the inner core. Most recently, lopsided growth of the inner core has been proposed to explain seismic

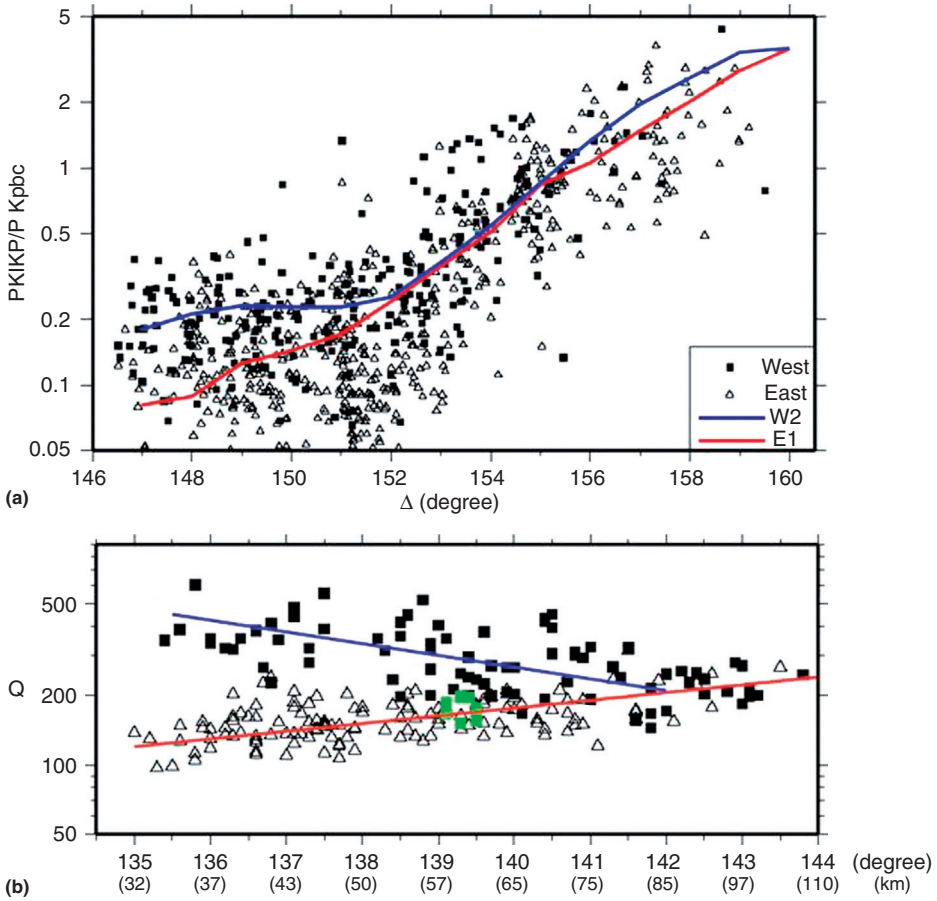

Figure 5 Hemispheric variations of *Q* in the inner core. (a) Variations of amplitude ratios of PKIKP/PKP(BC) as a function of distance and predictions of *Q* models for the western (W2) and eastern (E1) hemispheres. Adapted from Yu W and Wen L (2006a) Seismic velocity and attenuation structures in the top 400 km of the Earth's inner core along equatorial paths. *Journal of Geophysical Research* 111: http://dx.doi.org/10.1029/2005JB003995. (b) *Q* measurements as a function of distance from amplitude ratios of PKIKP/PKiKP showing differences between the western (triangles) and eastern (squares) hemispheres. Reproduced from Cao A and Romanowicz B (2004) Hemispherical transition of seismic attenuation at the top of the Earth's inner core. *Earth and Planetary Science Letters* 228: 243–253.

hemispheric variations in the inner core (Alboussière et al., 2010; Monnereau et al., 2010).

1.25.5.2.2 Anisotropic attenuation

The presence of velocity anisotropy is well documented for the inner core (e.g., Creager, 1992; Morelli et al., 1986; Shearer, 1994; Su and Dziewonski, 1990; Vinnik et al., 1994; Woodhouse and Wong, 1986). Theoretical studies indicate that anisotropy in attenuation should accompany anisotropy in velocity, and several authors have noted the stronger attenuation of PKP(DF) phases traveling along polar paths (Creager, 1992; Song and Helmberger, 1993). Anisotropy in attenuation was first proposed by Souriau and Romanowicz (1996), who examined a carefully selected data set of PKP(DF)/PKP(BC) amplitude ratios for paths whose turning points were located under western Africa and for which good azimuthal coverage was available. They found a significant correlation between high attenuation and high velocity and inferred that the origin of anisotropy in the top half of the inner core must be due to the orientation of iron crystals, which would produce this type of correlation (Carcione and Cavallini, 1995), rather than fluid inclusions, which would result in correlation of high velocity with low attenuation (Peacock and Hudson, 1990). These results were subsequently extended to a global data set (Souriau and Romanowicz, 1997) and to antipodal paths (Cormier et al., 1998). Using an effective medium theory, Singh et al. (2000) proposed that both velocity and attenuation anisotropy could be explained by a model of oblate fluid inclusions aligned in the equatorial plane. Li and Cormier (2002) suggested that anisotropy in attenuation also varies with depth and preferred a scattering interpretation. Oreshin and Vinnik (2004) confirmed the correlation of anisotropy in attenuation with that in velocity, which, however, may not be present at high latitudes (Helffrich et al., 2002). Yu and Wen (2006b) confirmed these global trends from measurements of amplitude ratios of PKIKP/PKiKP and PKIKP/PKPbc, finding an average Q_α for polar paths of 200–250, in contrast to 600 for equatorial paths in the top 200 km of the inner core. More recently, the need for attenuation anisotropy in the inner core was challenged by Waszek and Deuss (2013), who analyzed an extended data set of PKIKP/PKiKP amplitude ratios, confirming the hemispheric variations in Q_α. These

authors noted that most previous studies did not take into account hemispheric variations in velocity when interpreting amplitude ratios of core-sensitive phases and suggested that these velocity variations alone could account for apparent attenuation anisotropy.

For more details on inner core attenuation, see **Chapter 1.23**.

1.25.6 Global 3D Attenuation Structure in the Upper Mantle

1.25.6.1 Normal Modes and Long-Period Surface Waves

1.25.6.1.1 Early studies

In the 1970s, after the occurrence of the 1960 Great Chilean Earthquake (Mw 9.6), and with the accumulation of data from the World-Wide Standardized Seismographic Network, measurements of long-period surface-wave attenuation, then based on relatively few records, showed large disagreements (e.g., Ben-Menahem, 1965; Jobert and Roult, 1976; Mills and Hales, 1978; Smith, 1972). At that time, it was realized that (1) elastic effects were important in limiting the accuracy of Q measurements; (2) anelastic attenuation caused frequency dependence of elastic velocities, which needed to be taken into account (Akopyan et al., 1976; Kanamori and Anderson, 1977; Liu et al., 1976; Luh, 1974; Randall, 1976); and (3) large systematic lateral variations existed, correlated with those of phase velocities and suggesting significant differences in attenuation under different tectonic regions, with low attenuation under shields and high attenuation under oceans and tectonically active provinces (e.g., Dziewonski and Steim, 1982; Lee and Solomon, 1979; Nakanishi, 1978, 1979b, 1981; Roult, 1982).

Most global upper mantle 3D Q models up to now, as we will discuss in the succeeding text, have been on surface waveform or amplitude data. However, several authors attempted to measure lateral variations in Q from normal mode data, which in principle should provide sensitivity at greater depths in the mantle. Because the mode amplitude data set is very contaminated by elastic effects (e.g., Smith and Masters, 1989), it was possible to recover only the longest wavelengths in the even-degree structure (Romanowicz et al., 1987; Roult et al., 1984; Suda et al., 1991). The most important result of these early studies is the presence of a long wavelength, degree 2, structure in Q_μ in the transition zone, shifted toward the west with respect to the degree 2 in the shallower mantle, with lowest Q centered in the central Pacific Ocean and under Africa.

1.25.6.1.2 Anelasticity and focusing

One of the main issues limiting resolution in global mantle attenuation tomography is the contamination of amplitudes by elastic focusing effects. Numerous cases of such contamination in Earth circling mantle waves have been reported. For example, for moderate size earthquakes, for which the effect of source directivity can be ruled out, one expects successive Rayleigh-wave trains to gradually decrease in amplitude, due to the effects of attenuation and geometric spreading. However, it is sometimes observed that an R_{n+1} train has larger amplitude than R_n, where n is the orbit number of the Rayleigh wave (e.g., Lay and Kanamori, 1985; Romanowicz, 1987, 2002), and such observations can be qualitatively reproduced by including focusing effects in synthetic seismograms obtained by normal mode summation (e.g., Romanowicz, 1987). Also in the frequency domain, long-period surface-wave amplitude spectra are often irregular, with many 'holes' that cannot be attributed to intrinsic attenuation or source effects (e.g., Romanowicz, 1994a).

To first order, in the framework of single scattering and in the high-frequency approximation, analytic expressions have been obtained for the focusing effect, both in a propagating wave formalism (Woodhouse and Wong, 1986) and in a normal mode asymptotic formalism (Park, 1987; Romanowicz, 1987). Using asymptotic approximations in the framework of normal mode theory, it was shown that focusing effects depend on the transverse gradients of elastic structure, as expressed in terms of phase velocity perturbations, in the case of propagating waves, and of local frequency perturbations, in the case of normal modes. The expressions obtained in both approaches are equivalent (Romanowicz, 1987). In the propagating surface-wave case and in the frequency domain,

$$\ln \delta A_F(\omega) = \frac{1}{2}\operatorname{cosec}\Delta \int_0^\Delta \left[\sin(\Delta-\phi)\sin\phi\,\partial_\theta^2 - \cos(\Delta-2\phi)\partial_\phi\right]\frac{\delta c}{c_0}(\omega)\,\mathrm{d}\phi \qquad [7]$$

where Δ is epicentral distance, ϕ is the angular distance along the source-station great-circle path, $\delta c/c_0$ is the relative perturbation in phase velocity along the path, and $\delta A_F(\omega)$ is the contribution to the amplitude at frequency ω due to focusing.

In the standing-wave case and time domain, for an isotropic source,

$$\delta F_k(\Delta) = \frac{a\Delta}{U}\left(\frac{\hat{D}_k - \widetilde{D}_k}{2k} + \frac{\cot\Delta}{8k}\left(\delta\hat{\omega}_k - \delta\widetilde{\omega}_k\right)\right) \qquad [8]$$

where $F_k = (1+\delta F_k(\Delta))$ is the perturbation to the time domain amplitude of the seismogram for multiplet k and $\delta\hat{\omega}_k$ and $\delta\widetilde{\omega}_k$ are the perturbations to the great-circle average and minor are average local frequencies for that multiplet respectively, $k = l + 1/2$, where l is the angular order of the mode, and we have defined

$$\widetilde{D} = \frac{1}{\Delta}\int_0^\Delta \partial_\Gamma(\delta\omega_k(s))\,\mathrm{d}s$$
$$\hat{D} = \frac{1}{2\pi}\int_0^{2\pi} \partial_\Gamma(\delta\omega_k(s))\,\mathrm{d}s \qquad [9]$$

where ∂_Γ denotes the second transverse derivative along the great-circle path, which reduces to the integrand in eqn [7]. Accounting for the radiation pattern in eqn [8] is equivalent to using eqn [7] together with ray tracing.

Because the focusing effects are so strongly dependent on the transverse gradients of the elastic structure, and because those are not generally well constrained, compounded by the fact that these expressions are approximate and valid only to first order, it has been a difficult challenge, for the last decade, to properly account for focusing effects in surface-wave attenuation tomography. Indeed, if the corrections made on the basis of an existing elastic model are inaccurate, they can potentially introduce more biases than they can correct.

Noting that focusing effects and attenuation behave very differently as Rayleigh waves circle around the Earth, with the

sign of attenuation always the same, while focusing/defocusing depends on the direction of propagation along the great circle, Romanowicz (1990) and Durek et al. (1993) showed that, by using four consecutive Rayleigh-wave trains, one can eliminate, at least to first order, the effect of focusing, as well as uncertainties in the source amplitude. This resulted in the first, low-degree, even-degree global tomographic models of attenuation in the upper mantle, which confirmed the existence of a strong degree 2 in attenuation, as first suggested in studies based on normal modes. These models showed that attenuation in the uppermost mantle was correlated with seismic velocities, at least at the longest wavelengths (~4000 km). There are two drawbacks to this approach: First, only even-degree structure can be retrieved in this fashion, as only great-circle average attenuation can be measured, and second, elastic effects become increasingly more pronounced as distance increases, and the first-order approximation is not suitable for higher orbit trains, leading to a decrease in the ability to retrieve the intrinsic attenuation signal. Moreover, higher orbit trains are more dispersed, limiting the frequency range in which consecutive Rayleigh-wave trains do not interfere with each other and/or with overtones.

In order to be able to retrieve odd-degree structure while not explicitly correcting for unknown focusing effects, and avoiding the drawbacks of using multiple orbit wave trains, a different approach was proposed by Romanowicz (1995), using three consecutive Rayleigh-wave trains (R1, R2, and R3). She noted that the R1 and R2 trains are the least contaminated by focusing effects. However, their amplitudes also depend on uncertainties in the source amplitude. The source amplitude shift varies slowly with frequency and can be estimated by comparing the overall level of the amplitude spectrum computed in two different fashions: (1) directly from R1 (or R2) and (2) using a linear combination of R1, R2, and R3 (Romanowicz, 1994a). This approach, combined with a rigorous data selection in which all R1 and R2 amplitude spectra that were not smoothly varying with frequency were rejected, led to the first low-degree (equivalent to about degree 5) tomographic model of upper mantle shear attenuation, QR19 (Romanowicz, 1995). Even though this first model had very low resolution, it confirmed the correlation of lateral variations of Q with V_S in the top 250 km of the upper mantle and a shift to a different pattern in the transition zone, dominated by low Q in the central Pacific and Africa and correlated with hotspots. Romanowicz (1994b) showed that, in the transition zone, at least at the longest wavelengths, anelastic attenuation correlated with the hotspot distribution, whereas the velocity structure correlates better with the slab distribution, consistent with expectations that Q is more sensitive to high temperature regions. The desensitizing approach used, however, limited the lateral resolution of the model obtained, since a relatively small number of paths qualified for inclusion in the inversion.

The applicability of the linear asymptotic approximation to the computation of focusing (eqns [7]–[9]) has been tested by Selby and Woodhouse (2000) on a large data set of Rayleigh-wave amplitudes on minor and major arcs, in the period range 73–171 s. These authors derived maps of lateral variations of $q_R(\omega) = Q_R^{-1}(\omega)$ at different frequencies, assuming that the amplitude of a fundamental-mode Rayleigh wave observed at distance Δ and angular frequency ω can be written as

$$A(\omega, \Delta) = A_0(\omega)(1 + F(\omega))\exp[-\omega a \Delta \widetilde{q}_R(\omega)]/2U_0(\omega) \quad [10]$$

where U_0 is group velocity, a is the radius of the earth, $A_0(\omega)$ is source term, and $\widetilde{q}_R(\omega)$ is the average Rayleigh-wave attenuation along the source-station path:

$$\widetilde{q}_R(\omega) = \frac{1}{\Delta}\int_0^{\Delta} q_R(\omega, s)\mathrm{d}s \quad [11]$$

$F(\omega)$ represents the effect of focusing, which can be calculated from a reference elastic 3D model using expression [6]. Selby and Woodhouse (2000) compared the maps obtained by (1) inverting the observed amplitude data set for lateral variations in Q_R without correcting for focusing, (2) inverting synthetic maps of apparent attenuation obtained by assuming the amplitudes are only affected by focusing and using the elastic phase velocity model of Trampert and Woodhouse (1995), and (3) inverting the observed amplitude data set for Q_R after correcting for focusing. In these experiments, a degree-20 model of 3D apparent attenuation was obtained. They concluded that at the longer periods (e.g., 146 s), the amplitude signal is not severely affected by focusing, whereas at the shorter periods (e.g., 73 s), the contaminating effect is stronger. Also, Selby and Woodhouse (2000) found that low-degree attenuation structure (up to degree 8 in a spherical harmonics expansion) is not significantly affected by focusing in the entire period range considered. In a subsequent study, they inverted the maps of $Q_R(\omega)$ with and without corrections for focusing to obtain a series of models of lateral variations in attenuation in the upper mantle up to degree 8 (Selby and Woodhouse, 2002). In the latter study, they also considered the effect of uncertainties in the source term and found that a frequency-dependent correction factor is necessary to combine the $Q_R(\omega)$ maps into a successful depth-dependent model of attenuation. They concluded that the details of focusing and source corrections did not affect the robustness of their models up to degree 8, but would be more important at shorter wavelengths.

1.25.6.1.3 Current status

An important result of the Selby and Woodhouse studies was the confirmation that surface-wave amplitudes contained information not only on anelastic structure but also on elastic structure that could be exploited, as already suggested by Woodhouse and Wong (1986) and Wong (1989). At about the same time, Billien and Lévêque (2000) made the first attempt at inverting simultaneously Rayleigh-wave amplitude and phase data, for maps of phase velocity and Q_R between 40 and 150 s. The effects of focusing were included using eqn [7], which allowed them to consider shorter periods and shorter wavelengths. The maps obtained at short periods indicate significant correlation between phase velocity and attenuation, and therefore, tectonics and the even-degree part (degrees 2, 4, and 6) of their longer-period maps are compatible with those of other studies. However, their odd-degree part is dominated by degree 5, a feature not found in other studies.

In a recent study, Dalton and Ekström (2006a,b) considered a large global data set of Rayleigh-wave amplitudes in the period range 50–250 s. They inverted this data set, simultaneously, for maps of lateral variations in phase velocity up to spherical harmonics degree 20, attenuation up to degree 12, as well as source and receiver correction factors. As in previous

studies, the focusing effect is also included using expression [7]. A notable result of their study is the high-quality phase velocity maps that they were able to obtain by using only the amplitude constraints in their inversion (Dalton and Ekström, 2006b). Inclusion of the source and receiver correction factors was also found to improve the attenuation mapping. They constructed maps of Rayleigh-wave attenuation at different periods and also found a good correlation of the Q^{-1} distribution with tectonics for periods sensitive to the first 250 km of the upper mantle (Dalton and Ekström, 2006a).

The studies described so far considered only fundamental-mode surface waves, which, in practice, limits the resolution in depth to the top 300–400 km of the upper mantle, even though some attempts at interpreting deeper structure were shown. These studies also used a two-step approach, and often only the results of the first step, inverting for maps of lateral variations of $Q_R(\omega)$ at different periods, were presented (e.g., Billien and Lévêque, 2000; Dalton and Ekström, 2006a; Romanowicz, 1990). The more recent 3D attenuation models include both even and odd terms of lateral heterogeneity in Q_μ (Dalton et al., 2008; Romanowicz, 1995; Selby and Woodhouse, 2002) or in Q_R (Dalton and Ekström, 2006a). **Figure 6** compares maps of Q^{-1} at a depth of ~150 km obtained in different recent studies and shows that while details are still variable from model to model, the large-scale features, with high Q in shield areas low Q under ridges and back arcs, are quite consistent.

In order to improve the depth resolution in the transition zone, it is desirable to develop a methodology that includes information from surface-wave overtones, as well as Love waves. Because overtones are not easily separable due to their similar group velocities, a waveform methodology is desirable. Such a methodology uses a comparison of observed and synthetic seismograms in the time domain. The synthetics can be computed using normal mode theory, taking into account 3D effects at various degrees of approximation. However, to obtain accurate amplitude information from surface-wave data, it is necessary to employ an approach based on the measurement of envelopes or to first align the phase of waveforms before comparing observed and synthetic waveforms. Following these considerations, Gung and Romanowicz (2004) recently developed an iterative waveform inversion approach, in which a large global data set of three-component fundamental and overtone waveforms, filtered in the frequency range 80–250 s, is first inverted for elastic 3D structure, using the nonlinear asymptotic coupling theory approach developed by Li and Romanowicz (1995), up to spherical harmonics degree 24. Different elastic models are computed for Love and Rayleigh waves, to account for the strong radially anisotropic signal in the uppermost mantle (e.g., Ekström and Dziewonski, 1997; Gung et al., 2003; Montagner and Tanimoto, 1991). In a second step, the waveforms, corrected for the 3D elastic structure obtained in the previous step, are inverted for lateral variations of $Q_\mu(r)$ in the upper mantle, up to degree 8. In this process, the waveforms are directly inverted for depth dependence in elastic and anelastic structure.

Although Gung and Romanowicz (2004) did not include focusing effects in deriving their model QRLW8, subsequent tests indicated that the model was robust with respect to these effects, in agreement with the predictions of Selby and Woodhouse (2000). In particular, Gung and Romanowicz (2004) compared the degree-8 $Q_\mu(r)$ model obtained with and without focusing terms, the latter computed using expression [8] in the 3D elastic model obtained in the first step, and found no significant changes. Including focusing in the second step of the inversion justifies inverting for a higher-degree Q_μ model. **Figure 7** shows a comparison of the models obtained

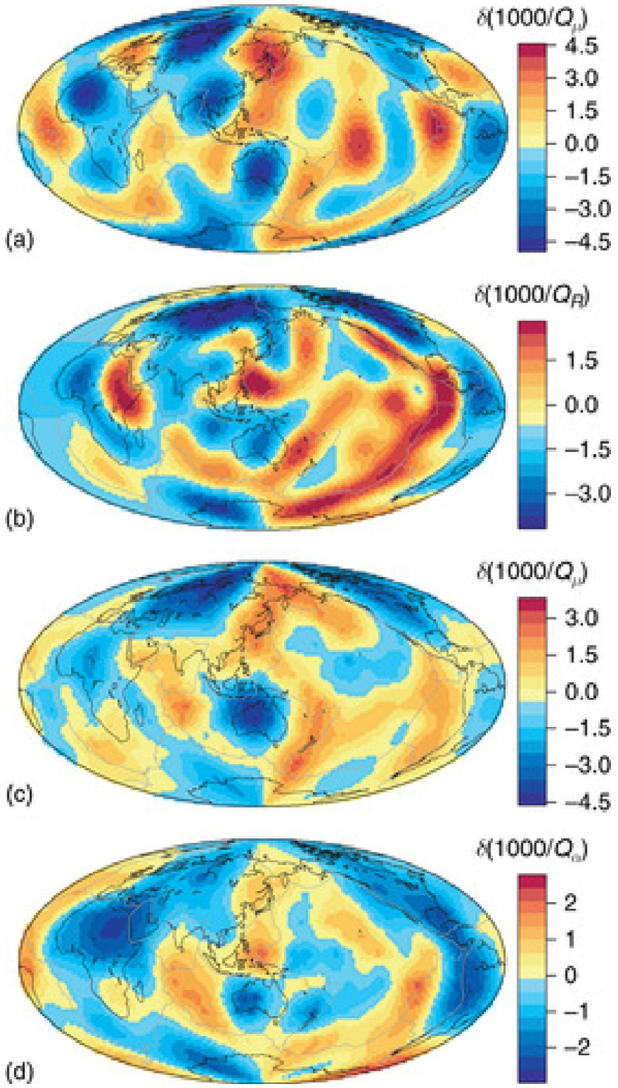

Figure 6 Comparison of global Q models in the uppermost mantle. (a) QRLW8 model (Gung and Romanowicz, 2004), from inversion of three-component surface-wave and overtone waveform data, presented is Q_μ at a depth of 160 km. (b) Map at 150 km of the Rayleigh-wave-based Q model QRFS12 of Dalton et al. (2008). (c) Average Q_μ in the depth range 0–250 km from Selby and Woodhouse (2002) and also from Rayleigh waves. (d) Average variations in Q_α in the first 250 km of the mantle from amplitude ratios of P and PP (Warren and Shearer, 2002). Some of the differences observed may be due to the different depth ranges sampled: in models (a), (c), and (d), the global ridge and back-arc systems all stand out as low Q_μ features, whereas the Atlantic ridge is not as prominent in model (b), while the Red Sea region lights up more strongly. This may be due to the fact that (b) has not been inverted with depth and therefore may include some effects of structure deeper than 250 km.

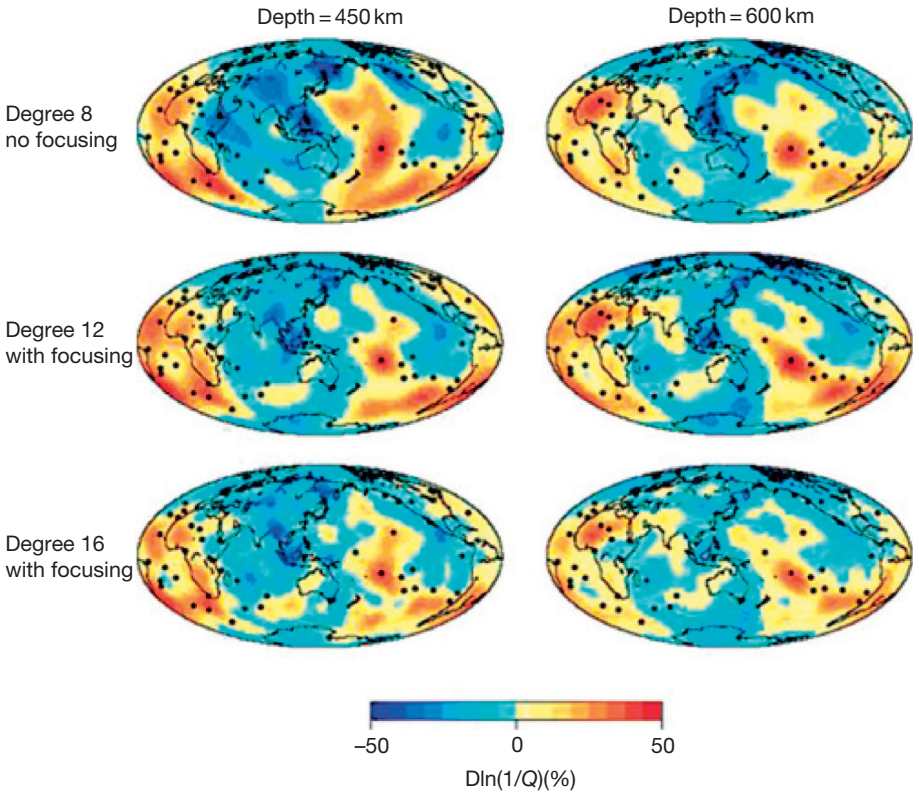

Figure 7 Lateral variations of Q_β in the upper mantle transition zone. (Top) Degree-8 model QRLW8 (Gung and Romanowicz, 2004). In this relatively low-degree model, no corrections for elastic focusing have been included. (Middle/bottom) Inversion of the same three-component long-period seismograms for a degree-12 model (middle) and a degree-16 model (bottom). In both cases, the waveforms have been corrected for focusing effects before inversion, using an asymptotic higher-order formalism (Romanowicz, 1987). The main features of these models, namely, strong low-*Q* anomalies in the South Pacific and under Africa, correlated with the hotspot distribution of Davies (1990) (black dots) and high-*Q* anomalies under the western Pacific, remain stable, but the low-*Q* features sharpen up in the higher-resolution models.

up to degrees 12 and 16, in the transition zone, when focusing terms are included. Clearly, the large-scale features remain stable among the models, with some variability in the details. They indicate that, in contrast to the upper 200–300 km of the mantle, the main features in Q_μ in the transition zone are two large low-Q regions in the south-central Pacific and under Africa, which correlate with the distribution of elastic velocities at the base of the mantle (Romanowicz and Gung, 2002), as well as the distribution of hotspots, confirming earlier results (Romanowicz, 1994b).

The most recent global 3D upper mantle model of Q_μ was developed by Dalton et al. (2008) based on fundamental-mode Rayleigh-wave data using the methodology of Dalton and Ekström (2006b). The resulting model (QRFSI12), expressed to degree 12 in spherical harmonics, takes into account source and station terms as well as focusing effects. It confirms the correlation of Q_μ^{-1} with surface tectonics in the first 200–250 km of the upper mantle (e.g., **Figure 6**) and a shift at greater depth to a structure dominated by high attenuation beneath the central Pacific and Africa and low attenuation in subduction zone regions. Dalton et al. (2009) found strong correlations between attenuation distribution (in model QRFSI12) and shear velocity in different tectonic regions and inferred that lateral variations in temperature of 150–200 °C can explain most of the observed variability in velocity and attenuation in the top 250 km of the upper mantle, except in cratonic regions where compositional differences may be required, in agreement with earlier studies. In particular, inversion of long-period seismic waveforms assuming only lateral variations in temperature results in temperatures in the cratonic upper mantle that are more than 100 °C colder than estimated from heat flow measurements and the analysis of xenoliths (e.g., Cammarano and Romanowicz, 2007). Dalton and Faul (2010) compared the seismological trends to experimental trends in dry olivine samples and concluded that in regions of the upper mantle where the relationship between attenuation and velocity cannot be explained by temperature variations alone, the discrepancies can be explained by a combination of the presence of partial melt (oceans at depths ~100 km) or compositional differences (cratons at depths <250 km), although the composition that would give rise to the observed mismatch in cratons remains elusive.

Some variability in the correlation between velocity and attenuation maps may be due to the effects of anelastic dispersion due to attenuation, as also investigated by Zhou (2009). Assuming a 3D Q model derived from an existing 3D shear velocity model under the assumption that all lateral variations of structure in the upper mantle are due to temperature

variations, Zhou (2009) calculated finite frequency kernels and found that dispersion corrections in the phase due to attenuation are important enough in the period range 50–200 s (up to 25% of the elastic effect) so that they cannot be neglected in global surface-wave tomography.

With the advent of accurate global 3D numerical computations of the seismic wavefield, it has become possible to evaluate more precisely the effects of 3D elastic structure on the amplitudes of long-period surface waveforms and, vice-versa, the effect of 3D Q variations on velocity modeling, through anelastic dispersion. Savage et al. (2010) incorporated attenuation into their spectral element code (Specfem, e.g., Komatitsch et al., 2002) and investigated competing effects on amplitudes due to elastic and anelastic 3D structure at the regional scale. Ruan and Zhou (2010) used the same spectral element method to quantify the effects of 3D Q structure on surface-wave phase delays and found that about 15–20% of the phase delays may be due to 3D Q structure through the mechanism of anelastic dispersion, especially in the period range 60–150 s, less so at longer periods. Using a similar approach, Ruan and Zhou (2012) confirmed, in turn, that the effects of elastic focusing and scattering on surface-wave amplitudes are as important as those of 3D Q and cannot be ignored, even at long periods. Such numerical techniques hold promise for advances in the resolution of Q structure at global and regional scales.

1.25.6.2 Global Body-Wave Studies

In the same way as differential travel times of teleseismic body-wave phases are used to obtain information on the distribution of upper mantle velocities, global-scale lateral variations in attenuation can be inferred from differential amplitude measurements (i.e., amplitude ratios). These measurements are difficult, however, as they are sensitive to the window chosen for each phase, as well as to contamination by complex structure near the source, receiver, and bounce points. Komatitsch et al. (2002) have called attention to the importance of considering the effects of focusing and scattering in the crust. **Chapter 1.06** provides details about the theoretical computation of the effects of attenuation on body waves.

Only three published studies to date have developed models of upper mantle Q based on differential body-wave measurements, two for Q_μ using S phases (Bhattacharyya et al., 1996; Reid et al., 2001) and one for Q_α (Warren and Shearer, 2002). Each of them used slightly different methods, but the basic principle remains the same.

The amplitude spectra of recorded body waves can be expressed as

$$A(\omega) = cS(\omega)R(\omega)I(\omega)A_c(\omega)F(\omega)\exp(-\omega t^*/2) \qquad [12]$$

where c is a constant expressing the radiation pattern and the geometric spreading, $S(\omega)$ is the source spectrum, $R(\omega)$ is the crustal response, $I(\omega)$ is the instrument response, A_c is the crustal layering/reflectivity at the bounce point for reflected waves, F is a hypothetical factor that includes possible effects of focusing, and t^* is defined in eqn [5]. In body-wave studies, the frequency dependence of Q needs to be taken into account, because the measurements are performed at higher frequency (typically 0.15–1 Hz for P waves and 0.05–0.1 Hz for S waves), closer to the high-frequency cutoff in the Earth's absorption band. The frequency dependence of Q is often expressed in terms of an absorption band model (eqn [2]). However, Warren and Shearer (2002) estimated the effect of frequency dependence on the attenuation of P waves around a period of 1 s and concluded that neglecting it did not significantly bias their measurements of lateral variations in Q_α. On the other hand, Reid et al. (2001) suggested that the frequency dependence might be absorbed in the source terms.

Pairs of phases (1,2) are selected so as to eliminate as many factors as possible from their spectral amplitude ratio. The differential δt^* can then be obtained by measuring the slope of the remaining spectral ratio as a function of frequency:

$$\ln(A_2/A_1) = -\omega/2(\delta t^*) + \varepsilon \qquad [13]$$

where $\delta t^* = t_2^* - t_1^*$ and ε is a constant containing the effects of differential radiation pattern, geometric spreading, and focusing for the two phases. The assumption of frequency independence needs to be verified even if dispersion corrections have been applied, and this is usually done by checking the linearity of the slope, as well as the constancy of the phase of the complex spectral ratio.

Because the lateral variations of Q in the lower mantle are thought to be much smaller than in the upper mantle, the differential t^* thus obtained is attributed to lateral variations of structure in the upper mantle under the bounce point of the reflected phase. Given the steep approach of the reflected rays at the bounce point and the relatively sparse global sampling, these measurements provide information about the average upper mantle lateral variations in Q but have little depth resolution.

This general principle of slope measurement was used by Bhattacharyya et al. (1996) and Warren and Shearer (2002). However, these authors used different approaches to correct for potential receiver and source biases. Bhattacharyya et al. (1996) considered the spectra of S and SS from the same records, in the distance range 40–120° and the period range 15–25 s, and then estimated the differential t^* by applying a multiple-record stacking technique, grouping the records by bounce point location, and assuming that effects of source, receiver, and path, outside of the common upper mantle path of the SS waves with common bounce location, would average out in the stacks. The bounce point location area over which the stacking was performed was caps of 5° radius, larger than the estimated Fresnel zones of the corresponding reflected waves. These authors used a frequency domain multitaper technique to minimize the effects of finite source duration and near-source or near-receiver structure complexity. They found a correspondence between the cap-averaged t^* and tectonic provinces, with, as expected, lowest attenuation under platforms and shields and highest attenuation under young oceans. In a second step, they inverted for a depth-dependent model of Q_μ in the upper mantle, expanded laterally up to degree 8 in spherical harmonics, and assuming three layers in depth (20–220, 220–400, and 400–670 km). Resolution experiments indicated that the best resolved layer was the deepest one, and the two shallower ones could not be distinguished uniquely.

Warren and Shearer (2002), on the other hand, considered independent data sets of P waveforms, in the distance range 40–80°, and PP waveforms in the distance range 80–160°.

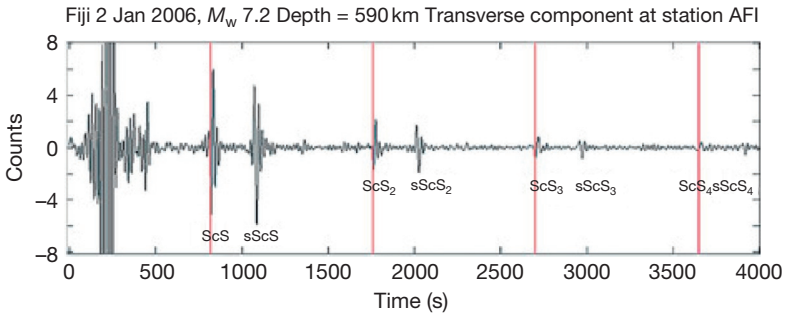

Figure 8 Example of multiple ScS record for a deep earthquake in the Fiji Islands, showing clear multiples out to ScS_4, as well as their depth phases. Courtesy of Ved Lekic.

Working in the frequency domain, they first determined source and receiver terms for the P data set, using an iterative stacking procedure over common sources and common receivers. Then they assumed that the same source and receiver terms could be applied to the PP phases, since the two phases have similar takeoff angles, path lengths, and turning depths, given the distance ranges considered. They thus corrected the PP amplitude spectra using the source and receiver terms determined from the P spectra and estimated the residual t^* attributed to the upper mantle beneath the bounce point. Finally, to reduce the scatter in the data, they estimated cap averages over non-overlapping bounce point areas of 5° radius. They too found the highest Q_α (smallest t^*) under shields and platforms and the lowest Q_α (largest t^*) under young oceans (e.g., **Figure 6**). Unlike Bhattacharyya et al. (1996), these authors considered, however, that their measurements reflected the average structure over the top 220 km of the mantle and derived the corresponding Q_α averaged over that depth range.

Reid et al. (2001) developed a somewhat different method, based on waveform fitting, which they applied to a large data set of SS and S waveforms from seismograms collected in the distance range 50–105° and also to SSS and SS, in the distance range 90–179°. In the process, they included the effects of elastic structure on differential travel times of these phases. These authors considered that their data had sensitivity down to 400 km and inverted their t^* data set for a model of Q_μ expanded laterally to degree 8 and in depth, using a spline parametrization with six knots. However, their resolution tests indicated that the depth resolution was poor and that they could not attribute the lateral variations found to a particular depth.

The most recent attempt at using body-wave phases to constrain 3D Q_μ variations at the global scale is a study that includes differential attenuation measurements between S and a combination of upper and lower mantle-sensitive multiple phases (ScS, SS, and corresponding depth phases; Lawrence and Wysession, 2006b). These authors validate their model in the upper mantle against model QRLW8 (Gung and Romanowicz, 2004), arguing that the qualitative similarities imply robustness of their lower mantle model. The most striking feature of their lower mantle model is a large low-*Q* region in the depth range 700–1400 km beneath the subduction zones in eastern Asia, which they attribute to the presence of water. However, the authors do not evaluate or make any corrections for elastic contaminating effects in this highly heterogeneous region, which makes their model tentative until confirmed by future independent studies.

1.25.6.3 Body-Wave Studies of Regional Extent

1.25.6.3.1 Multiple ScS studies

Although they do not provide a complete global coverage, the most widely used shear-wave phases for large-scale regional mantle attenuation studies have been multiple ScS phases. Measurements of the attenuation of these near-vertical multiply reflected waves are relatively uncontaminated by source, instrument, and geometric spreading effects. They and their depth phases appear very clearly on transverse seismograms in the 'reverberative interval,' after the first arriving surface-wave train (**Figure 8**). In the absence of noise, the spectral domain transfer function relating ScS_n to ScS_{n+1} is

$$H(\omega) = \exp[-\omega T_0/2Q(\omega)]\cdot\exp[i\theta(\omega, T_0)] \qquad [14]$$

where T_0 is the differential travel time between the two phases, θ is a phase function, and $Q(\omega)$ is the quality factor, which is an estimate of the vertically averaged attenuation through the mantle. As in the case of other differential measurements, the estimate of Q_{ScS} is obtained by measuring the slope of the amplitude of the transfer function as a function of frequency. The stability of the phase spectrum is used as an additional indication of the quality of the measurement.

Early studies used spectral ratios measured on hand-digitized and hand-rotated transverse component seismograms and provided evidence for large amplitude lateral variations of Q_{ScS} in the mantle (e.g., Kovach and Anderson, 1964; Press, 1956; Sato and Espinosa, 1967; Yoshida and Tsujiura, 1975). Because of the analog records used, and the measurement methods employed, which did not take into consideration the biasing effects of noise, these early estimates are considered to be less accurate than more recent ones. They are also generally biased toward very high values of Q_{ScS}, compared to normal mode results, which has been attributed not only to the effects of noise but also, potentially, to the effect of frequency dependence of *Q*, as the instruments that produced the records had limited bandwidth. With the advent of digital long-period instrumentation, and the development of more sophisticated methods that were better suited for minimizing the effects of noise (e.g., Jordan and Sipkin, 1977; Nakanishi, 1979a), measurements became more accurate. For example, Jordan and Sipkin (1977) introduced a method of phase equalization, by computing cross correlation between successive ScS multiples, as well as stacking to reduce measurement scatter. Nakanishi (1979a) used a maximum likelihood method to reduce the

effects of noise. Most measurements are performed in the frequency band between 10 and 40–60 MHz, where frequency dependence of Q_{ScS} has been found to be negligible (e.g., Sipkin and Jordan, 1979). These studies have confirmed the existence of large lateral variations in Q_{ScS} (e.g., Chan and Der, 1988; Gomer and Okal, 2003; Lay and Wallace, 1983, 1988; Revenaugh and Jordan, 1989, 1991; Sipkin and Jordan, 1980; Sipkin and Revenaugh, 1994; Suetsugu, 2001). The derived average mantle values for $Q_\mu \sim 220$–240 are, in general, compatible with those obtained from normal modes.

Measurements under oceans and in the vicinity of subduction zones are more numerous, because of the availability of deep earthquakes and the relatively simple effects of the thin crust at the surface reflection points. Measurements under continents are more difficult, because the effect of crustal multiples at the surface reflection point needs to be taken into account (e.g., Isse and Nakanishi, 1997; Sipkin and Revenaugh, 1994). In order to expand the coverage under continents, it is also necessary to consider shallow earthquakes, for which the reverberation interval is more noisy because of the presence of strong multipathing surface waves.

These studies determined that, on average, Q_{ScS} is higher under continents than under ocean basins. Regional variability on relatively short scales has been found in subduction zone regions. In particular, low Q was estimated under the Sea of Japan (e.g., $Q_{ScS} \sim 160$; Nakanishi, 1979a) and under northern South America ($Q_{ScS} \sim 93$; Lay and Wallace, 1983), in regions sampling the upper mantle wedge and/or back-arc region behind subduction zones, which, if primarily attributed to the upper mantle, translates into very low Q. On the other hand, high Q values comparable to continental estimates were obtained on path sampling through slabs (e.g., $Q_{ScS} \sim 232$, in South America, Lay and Wallace (1983); $Q_{ScS} \sim 226$, under Japan/Kuriles, Nakanishi (1979a); and $Q_{ScS} \sim 266 \pm 57$ in Argentina, Sipkin and Jordan (1980)). These older measurements are generally in agreement with a more recent study by Chan and Der (1988), except in the southwest Pacific, where these authors found $Q_{ScS} \sim 214 \pm 42$ compared to the estimate of $Q_{ScS} \sim 157 \pm 17$ (Sipkin and Jordan, 1980). This may however be due to the way the latter averaged their measurements over an extended region where strong lateral variations in Q_{ScS} have since been confirmed (Gomer and Okal, 2003; Suetsugu, 2001). Using short epicentral distance data ($<20°$) filtered between 10 and 50 MHz, Suetsugu (2001) found very low Q under the South Pacific superswell ($Q_{ScS} \sim 70$–80), whereas Gomer and Okal (2003) found very high Q under the Ontong Java Plateau, also using short distances (10–20°) and a bandpass between 10 and 62.5 MHz.

The lateral variations found in Q_{ScS} are attributed primarily to the upper mantle, because of the much higher Q in the lower mantle, which reduces the effects on multiple ScS of any, even significant, lateral variations (e.g., Warren and Shearer, 2002) and the significant correlation of Q_{ScS} with tectonics. Furthermore, the correlation with travel time anomalies from the same multiple ScS phases suggests that they could be primarily related to lateral variations in temperature.

Caution must be exercised, of course, in attributing all of the Q_{ScS} signals to the upper mantle, in particular if there is a low-Q zone at the base of the mantle (e.g., Revenaugh and Jordan, 1991) and significant lateral variations of Q in D″. While attenuation in D″ and its variations have yet to be explored at the global scale, the presence of large variations in velocity implies that at least some lateral variations exist in Q as well. Recently, Fisher and Wysession (2003) showed evidence for the existence of an ~600 km wide high-attenuation, low-velocity region in D″ beneath Central America, using spectral ratios of S and ScS phases.

1.25.6.3.2 Body-wave attenuation studies in North America

A few recent studies have taken advantage of the large quantity of broadband data available over North America to estimate lateral variations in attenuation across the continent, using surface waves (Lawrence et al., 2006) or body waves (Hwang et al., 2009, 2011). In agreement with global studies and early studies (e.g., Der et al., 1982; Solomon and Toksöz, 1970), these studies generally find large-scale lateral variations correlated with tectonics. More such studies are forthcoming, with the growing database from the EarthScope USArray program.

1.25.6.3.3 Body-wave studies of upper mantle Q around subduction zones

High attenuation has been reported in the back of island arcs using other types of body waves (e.g., Wiens et al., 2008). Early estimates were very qualitative (e.g., Barazangi and Isaaks, 1971; Barazangi et al., 1975; Bowman, 1988). This was confirmed by several regional studies (e.g., Flanagan and Wiens, 1990, 1994; Roth et al., 1999, 2000) that utilized shear depth phases from deep earthquakes observed teleseismically or at regional arrays to obtain constraints on the attenuation in the upper mantle wedge above different subduction zones. Flanagan and Wiens (1990) measured differential attenuation between sS–S and sScS–ScS phase pairs beneath the Lau back-arc spreading center in the Fiji–Tonga region. Studying the variation of the estimated Q as a function of depth of the source, they found high attenuation in the first 200–300 km and decreasing attenuation at greater depth. They found very high attenuation ($Q \sim 20$–35) in the uppermost mantle beneath the spreading center and somewhat lower attenuation ($Q \sim 50$) beneath older parts of the Lau Basin. Flanagan and Wiens (1994) extended this approach to the study of several inactive back-arc basins in the western Pacific and confirmed the presence of high attenuation ($Q \sim 40$–50) in the uppermost mantle (depths <160 km), with even lower Qs (<40) in the vicinity of the volcanic centers. They also confirmed a systematic increase of Q with depth ($Q \sim 115$ between 160 and 430 km and $Q \sim 173$ in the transition zone). The frequency band of these two studies was 10–80 MHz.

Following the method of Teng (1968), Roth et al. (1999) assembled a data set of differential S–P and P–P attenuation measurements from a temporary local array of broadband land and ocean bottom stations in the Tonga–Fiji region. The data set they assembled allowed them higher resolution compared to teleseismic data because of the geometry of the source-station distribution, the short paths, and the small Fresnel zones compared to teleseismic phases. These authors measured δt from spectral ratios and obtained an estimate of the best fitting Q_α/Q_β ratio as part of the inversion for Q_α and Q_β, assuming that Q is not frequency-dependent in the

band-pass of their study (0.1–3.5 Hz), which seems to be verified by the data. They confirmed the high-attenuation values in the uppermost mantle found previously beneath the spreading center. In their model, the slab appears as a high-Q zone ($Q_\alpha > 900$) down to at least 400 km, below which it is indistinguishable from the surrounding mantle. An abrupt transition from the high-Q slab to the low-Q back-arc basin occurs approximately at the Tonga volcanic front. The lowest Q_α values (~ 90) are found directly under the Lau back-arc spreading center. There is also evidence for a north–south trend, with attenuation on average higher by 10% in the northern part of the region. This Q tomographic model correlates well with velocity models in the region. The best fitting Q_α/Q_β ratio is ~ 1.75, which is in agreement with a loss in bulk about 1/3 that of the loss in shear, assuming a Poisson solid (Figure 9).

A similar study under the northern Philippine Sea, this time using only S–P spectral ratios (Shito and Shibutan, 2003b), also found high Q in the Philippine and Izu–Bonin slabs and low Q under the spreading center in the Shikoku Basin. However, the lowest values of Q were found at larger depths (250 km) than in the Lau Basin. The authors attributed that to the older age of the Shikoku spreading center. Several other studies in the last decade have investigated different subduction zones and confirmed the presence of strong lateral variations in Q, with lowest values under volcanic centers (as low as $Q_\mu = 40$ at 1 Hz in some areas) and an order of magnitude higher in the slab. These studies have used local earthquake data in Japan (Nakajima and Hasegawa, 2003; Takanami et al., 2000; Tsumura et al., 2000), in New Zealand (Eberhart-Phillips and Chadwick, 2002), in the Andes (Haberland and Rietbrock, 2001; Myers et al., 1998; Schurr et al., 2003), in Alaska (Stachnik et al., 2004), and more recently in Central America (Rychert et al., 2008), and in the Marianas (Pozgay et al., 2009). The recent studies have investigated frequency dependence in Q and, in some cases, have attempted to constrain attenuation in bulk, from Q_P/Q_s ratios. Frequency dependence appears to be in agreement with laboratory measurements ($\alpha \sim 0.1$–0.3), while the amount of attenuation in bulk is not yet very well constrained, reaching 30% of the value of attenuation in shear in some cases (e.g., Roth et al., 2000), but not required at all in some other studies (e.g., Pozgay et al.,

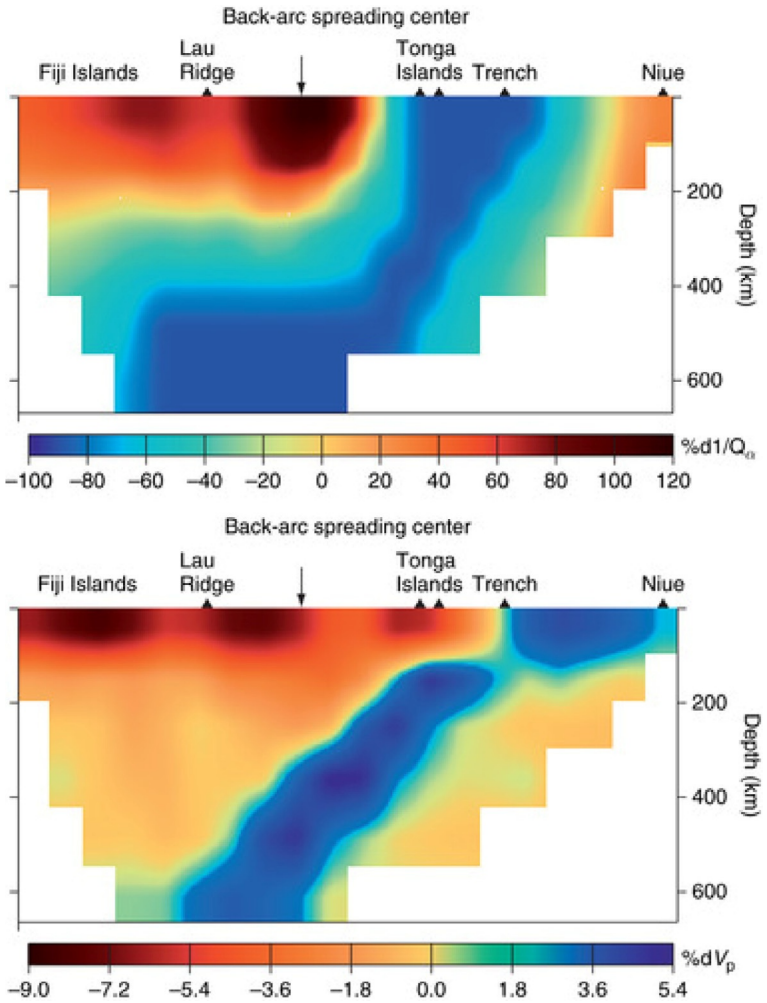

Figure 9 Cross section illustrating lateral variations of structure in the Lau back-arc basin. (Top) Attenuation. (Bottom) Velocity (V_p). Reproduced from Roth E, Wiens DA, and Zhao D (2000) An empirical relationship between seismic attenuation and velocity anomalies in the upper mantle. *Geophysical Research Letters* 27: 601–604.

2009). There may be a suggestion of the need for bulk attenuation only in the slab and not in the wedge (Stachnik et al., 2004). Further high-resolution studies are needed to more clearly separate the effect of frequency dependence from that of bulk attenuation.

1.25.6.3.4 Regional studies of upper mantle Q in mid-oceanic settings

Just as the upper mantle is found to be highly attenuating under back-arc spreading centers, other studies have investigated mid-ocean ridge systems and found very low Q (Ding and Grand, 1993; Molnar and Oliver, 1969; Sheehan and Solomon, 1992; Solomon, 1973). Sheehan and Solomon (1992) used the pair of teleseismic phases S and SS along the North Atlantic ridge and found that SS–S differential attenuation decreases with increasing age of the oceanic plate and that, in order for their measurements to be compatible with surface-wave studies, the high-attenuation region must extend into the asthenosphere. Ding and Grand (1993) performed waveform modeling of multiple S phases (up to S_4) at distances between 30° and 80° along the East Pacific Rise. Because their data have sensitivity to the deep mantle, they found that, in order for their measurements to be compatible with multiple ScS results, a significantly lower average Q in the lower mantle is needed than obtained from normal mode measurements, indicating that lateral variations in Q may also exist in the lower mantle. Note that Sipkin and Jordan attributed a lower Q in the Fiji–KIP corridor from multiple ScS measurements to frequency dependence. In the light of the Ding and Grand (1993) study, it seems more likely that the observations of Sipkin and Jordan (1979) could just be due to lower Qs in the lower mantle, especially as both studies sampled regions of the Pacific superplume. Strong lateral variations in the lower or lowermost mantle would need to be invoked to reconcile these results with the recent 1D mantle Q models constructed using body-wave data of similar frequencies, which exhibit high Qs in the lower mantle (e.g., **Figure 4**).

In the last decade, there have been increasing efforts to interpret tomographic models of the upper mantle at various scales in terms of temperature, degrees of partial melt, water content, and rock composition, using constraints from elastic and anelastic tomography, heat flow, gravity, and experimental data. Thus, Sobolev et al. (1996) found that the Massif Central in France is underlain by a hot mantle body with a potential temperature 100–200 °C higher than the upper mantle average. In an interpretation of velocity and Q tomography under the Philippine Sea, Shito and Shibutan (2003a) found that the deeper upper mantle (300–400 km depth) may contain 10–50 times more water than average. Boyd and Sheehan (2005) measured differential t^* of S-phase waveforms from the Rocky Mountain Front broadband network and found a north–south zone of very low Q_μ in the upper mantle beneath the Rocky Mountains. Combining attenuation and velocity data, they inferred that the Colorado Rocky Mountains are supported by low-density mantle and a thick crust. On the other hand, comparing their laboratory measurements of Q_μ with global seismological Q models, Faul and Jackson (2005) inferred that the upper mantle low-velocity zone could be explained by solid-state processes, without invoking partial melting. Lawrence et al. (2006) applied a waveform cross-correlation method and cluster analysis to the study of upper mantle P- and S-wave attenuation across the North American continent and found that the distribution of attenuation is in general correlated with that of velocity, implying higher temperatures beneath the western tectonic regions than under the more stable east, in agreement with both global and crustal continental-scale studies.

In general, t^* measurements and surface-wave attenuation measurements are interpreted in terms of anelastic attenuation; however, contributions from scattering can be important and need to be considered. For example, in a study of S-wave amplitude variations under Iceland, Allen et al. (1999) found that the low-velocity cylindrical-shaped plume acts as a lens, causing frequency-dependent focusing that dominates over anelastic effects on the amplitudes.

A somewhat puzzling result is that of Yang et al. (2007), who, for the first time, measured attenuation of surface waves in the vicinity of the East Pacific Rise, from a regional ocean bottom network. From a joint inversion for velocity and attenuation, taking into account elastic effects on the amplitudes to some degree, these authors found surprisingly lower attenuation than expected under the youngest ocean (Q_μ not less than 90, which is higher than the global average estimates), while elastic velocities are very low. These results are not compatible with a purely thermal model of attenuation (e.g., Faul and Jackson, 2005) nor with results from back-arc spreading centers in Mariana and Tonga/Lau (e.g., Pozgay et al., 2009). The authors suggest that the presence of water might be partially responsible for the drop in velocity, through the anelastic attenuation effect, and that some partial melting may be present beneath the youngest seafloor. However, this would require the absorption peak to be outside of the seismic frequency band. Reconciling these results with those in back arcs and global averages will necessitate further studies that more accurately take into account the elastic effects on amplitudes.

1.25.7 Regional *Q* Variations in the Crust and Uppermost Mantle

1.25.7.1 Introduction

One of the most interesting aspects of Q in the crystalline crust and upper mantle of the Earth is the large magnitude of its variation from region to region. Whereas broad-scale seismic velocities vary laterally at those depths by at most 10–15%, Q can vary by an order of magnitude or more. **Figure 10** illustrates the large effect that regional Q variations can have on phases that travel through both the upper mantle (P and S waves) and the crust (Lg) by comparing records for paths across the eastern and western United States. Since variations in Q can be so large, seismic-wave attenuation is often able to relate Q variations to variations in geologic and geophysical properties that are not easily detected by measurements of seismic velocities. Factors known to contribute to Q variations in the crust and upper mantle include temperature and interstitial fluids.

In this section, we will emphasize studies of Q variation conducted over regions sufficiently broad to contribute to our knowledge of crust and upper mantle structure and evolution. In so doing, we neglect many studies that have provided useful information on crustal Q over small regions.

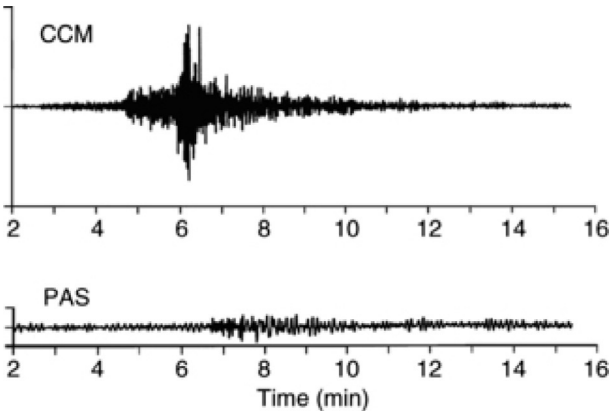

Figure 10 Seismograms recorded at stations CCM (Cathedral Cave, MO) and PAS (Pasadena, CA) for the m_b 4.5 event in southeastern New Mexico that occurred on 2 January 1992 at 11:45:35.6 UT. The epicentral distance to CCM (along a relatively high-*Q* path) is 1256 km and to PAS (along a relatively low-*Q* path) is 1417 km. Reproduced from Mitchell BJ (1995) Anelastic structure and evolution of the continental crust and upper mantle from seismic surface wave attenuation. *Reviews of Geophysics* 33: 441–462.

1.25.7.2 *Q* or Attenuation Determinations for Seismic Waves in the Crust

Investigators have employed different methods, phases, and frequency ranges to study the anelastic properties of the crust and upper mantle. At higher frequencies and shorter distances often employed for crustal studies, some researchers have emphasized determinations of intrinsic Q (Q_i), some have emphasized the scattering contribution (Q_s), and some have sought to determine the relative contributions of Q_i and Q_s. The importance of scattering became apparent from the groundbreaking work of Aki (1969) who first showed that the codae of various regional phases are composed of scattered waves. His work spawned a large literature on both theoretical and observational aspects of scattering that is discussed in Chapter 1.24.

The contributions of the intrinsic and scattering components to total attenuation, $1/Q_t$, can be described by

$$\frac{1}{Q_t} = \frac{1}{Q_i} + \frac{1}{Q_s} \qquad [15]$$

where Q_i and Q_s refer, respectively, to intrinsic Q and scattering Q (Dainty, 1981). Richards and Menke (1983) verified that the contributions of intrinsic and scattering attenuation are approximately additive as described by eqn [15]. Seismologists often wish to focus on Earth's intrinsic anelastic structure. To do so, they must select a phase or work in a frequency range such that the effect of scattering can either be determined or is small relative to the effect of intrinsic Q.

This chapter almost entirely addresses intrinsic Q, but we will discuss one type of scattered wave (Lg coda) quite extensively. Although Lg coda is thought to contain a large amount of scattered energy, some theoretical and computational studies (discussed later) of scattered S-wave energy suggest that measured Q values for that wave may largely reflect intrinsic properties of the crust.

All of the measurements that we discuss in this section can be placed in one of two major categories: (1) those in which seismic source effects cancel and (2) those in which assumptions are made about the seismic source spectrum. For category (1), the cancellation is most often achieved by using ratios of amplitudes recorded by two or more instruments. But it has also been achieved using ratios of amplitudes from different portions of a single time series. The primary application of the latter type of cancellation has been for the determination of Lg coda Q (Q_{Lg}^{C}). We divide this category into three parts that address regional phases, fundamental-mode surface waves, and Lg coda. Category (2) permits studies of Q using a single station but requires knowledge of the source depth, source mechanism, and velocity model for the source region. We divide this category into two parts, one addressing regional phases and the other fundamental-mode surface waves.

Seismologists have measured the dispersion of body waves due to anelasticity and have successfully used that dispersion to infer values for body-wave Q. We will not cover that topic because it has been the subject of relatively few studies and has been applied mainly to small regions.

The following subsections discuss methodology and present some representative results using the cited methods as applied to the crust. Because the number of studies for continents is overwhelmingly greater than for oceans, most of the discussion will pertain to continental regions. A few studies will, however, be described for oceanic regions.

1.25.7.2.1 Spectral decay methods in which source effects cancel: regional phases

Regional phases include P, S, and Lg phases recorded at distances less than about 1000 km. The early portion of this section mostly covers Q determinations for P and S phases, but in cases where researchers measured Q_{Lg}, as well as Q_P and Q_S, all results will be presented. The latter part of this subsection will discuss Lg exclusively since this phase has been widely used in recent years to study variations of Q over broad regions.

In order to cancel source effects, several methods utilize stations that lie on a common great-circle path with the seismic source, but other methods are able to dispense with the need for great-circle path propagation. All studies, however, need to first remove the effect of wave-front spreading before measuring amplitude changes due to attenuation. In this subsection, we will restrict our discussion to studies at frequencies that pertain totally or predominantly to the crust with occasional reference to the upper mantle for studies that include results for both the crust and upper mantle.

Regional and near-distance studies of P- and S-wave attenuation (or their respective quality factors Q_P and Q_S) often cancel the source by utilizing several stations at varying distances (e.g., Carpenter and Sanford, 1985; Nuttli, 1978, 1980; Thouvenot, 1983).

More recently, amplitude measurements in which both the source and sensor reside in boreholes beneath any sediments or weathered layers have provided much-improved estimates of Q_P and Q_S. Abercrombie (1997) used borehole recordings to determine spectral ratios of direct P to S waves and found that they are well modeled with a frequency-independent Q_P distribution in the borehole increasing from $Q_P \sim 26$–133 at depths between the upper 300 m and 1.5–3 km. Q_S increased

from 15 to 47 in the same depth range. Abercrombie (2000), in another borehole study near the San Andreas Fault, found that the rate of attenuation on the northeastern side of the fault is about twice that on the southwestern side.

Lg is very useful for *Q* studies because it both travels predominantly in the crustal waveguide, providing *Q* information for a known depth interval, and is a large and easily recognizable phase. Even relatively small earthquakes can generate useable records; thus, data in many regions are plentiful. Lg can be represented by a superposition of many higher-mode surface waves or by a composite of rays multiply reflected in the crust. It is usually assumed that Q_{Lg} follows a power-law frequency dependence, $Q = Q_0 f^{\eta}$, where Q_0 is the value of Q_{Lg} at a reference frequency and η is the frequency dependence parameter at that frequency. Lg travels through continental crust at velocities between about 3.2 and 3.6 km s^{-1} and is usually followed by a coda of variable duration. That coda is discussed in a later subsection. Since the Lg wave consists of many higher modes, it is often assumed that, even though the radiation patterns for individual modes differ from one another, the totality of modes combines to form a source radiation pattern that is approximately circular. If that assumption is correct, the source and stations need not necessarily line up along the same great-circle path to estimate *Q*.

Early determinations of Q_{Lg}, after correcting for wavefront spreading, compared observed attenuation with distance with theoretically predicted attenuation for the Lg phase and chose the theoretical curve (predicted by selected values of Q_0 and η), which agreed best with observations (e.g., Bollinger, 1979; Campillo et al., 1985; Chavez and Priestley, 1986; Chun et al., 1987; Hasegawa, 1985; Nuttli, 1973; Street, 1976).

Benz et al. (1997) studied four regions (southern California, the Basin and Range Province, the central United States, and the northeastern United States and southeastern Canada) of North America in the frequency range 0.5–14.0 Hz. They found that, at 1 Hz, Q_{Lg} varies from about 187 in southern California to 1052 in the northeastern United States and southeastern Canada and about 1291 in the central United States. They also found that the frequency dependence of *Q* also varies regionally, being relatively high ($\alpha \sim 0.55$–0.56) in southern California and the Basin and Range Province and smaller ($\alpha \sim 0$–0.22) in the other three regions.

Xie and Mitchell (1990a) applied a stacking method to many two-station measurements of Q_{Lg} at 1 Hz frequency in the Basin and Range Province. This method, first developed for single-station determinations of Lg coda *Q* (Q_{Lg}^{C}), will be discussed in the subsection on Lg coda. They found that $Q_{Lg} = (275 \pm 50) f^{(0.5 \pm 0.2)}$ and $Q_{Lg}^{C} = (268 \pm 50) f^{(0.5 \pm 0.2)}$.

Xie et al. (2004) extended the method to multiple pairs of stations in instrument arrays across the Tibetan Plateau. For an array in central Tibet (INDEPTH III), they found very low values for Q_0 (~ 90) that they attributed to very high temperatures and partial melt to the crust. An array in southern Tibet yielded even lower values, ~ 60, for Q_0 in the northern portion of the array but higher values (~ 100) in a central portion and much higher values (>300) in the southernmost portion. Xie et al. (2006) used a two-station method to obtain more than 5000 spectral ratios for 594 interstation paths and obtained Q_0 and η for those paths. They obtained tomographic maps of those values that are described in the subsection on tomographic mapping. With the purpose of obtaining attenuation information in the upper mantle, Xie (2007) studied Pn attenuation beneath the Tibetan Plateau. He obtained Q_0 and η and studied its regional variation across several regions. He found Q_0 to be highest (374, with η being 0.3) in easternmost Tibet and lowest (188 with η being 0.3) in northern Tibet. The high values for Q_0 are comparable to those reported earlier for central Asia. He found regional Pn attenuation varies inversely with Pn velocity.

1.25.7.2.2 Spectral decay methods in which source effects cancel: fundamental-mode surface waves

When using fundamental-mode surface waves to study lateral variations of crustal Q_{μ}, we need to measure the attenuation of relatively short-period (5–100 s) amplitudes. In continents, these waves may be biased by systematic errors associated with laterally varying elastic properties along the path of travel, as discussed earlier. Two-station studies of fundamental-mode surface waves are especially susceptible to these types of error because researchers might incorrectly assume great-circle propagation along a path through the source and the two stations. Non-great-circle propagation would mean that surface-wave energy arriving at two stations along different great-circle paths could originate at different portions of the source radiation pattern. If that pattern is not circular, the two-station method can produce attenuation coefficient values that are either too high or too low, depending on the points of the radiation pattern at which the waves originate.

To determine surface-wave attenuation, measurements for the situation in which a source and two stations lie approximately on the same great-circle path have often been used to determine surface-wave attenuation. The method was described by Tsai and Aki (1969) and determines the average surface-wave *Q* between the two stations after correcting for the different wavefront spreading factors at the two stations. They applied the method to many two-station paths from the Parkfield, California, earthquake on 28 June 1966 and, using the formulation of Anderson et al. (1965), obtained a frequency-independent model of intrinsic shear-wave *Q* (Q_{μ}) with a low-*Q* zone that coincided with the Gutenberg low-velocity zone in the upper mantle. Love-wave *Q* was greater than 800, and Rayleigh-wave *Q* was greater than 1000 in the period range 20–25 s.

Other studies using that method to obtain Q_{μ} models at crustal and uppermost mantle depths include Hwang and Mitchell (1987) for several stable and tectonically active regions of the world, Al-Khatib and Mitchell (1991) for the western United States, and Cong and Mitchell (1998) for the Middle East.

Models have also been obtained in which Q_{μ} varies with frequency. That frequency dependence is described by the relation $Q_{\mu} = Q_0 f^{\zeta}$ where ζ may vary with frequency (Mitchell, 1975) and/or with depth (Mitchell and Xie, 1994). The inversion process for Q_{μ} in those cases requires appropriate extensions of the Anderson et al. (1965) equations. The process requires both fundamental-mode surface-wave attenuation data and *Q* or attenuation information for either an individual higher mode or the combination of higher modes that form the Lg phase. The process proceeds by assuming a simple one- or two-layer distribution of ζ and inverting the

fundamental-mode data for a Q_μ model. ζ is adjusted until a Q_μ model is obtained that explains both the fundamental-mode and higher-mode attenuation data. Mitchell and Xie (1994) applied the method to the Basin and Range Province of the western United States. Example Q_μ models for which ζ varies with depth (Mitchell and Xie, 1994) appear in **Figure 11**.

Other surface-wave studies for which the source is canceled are those that use many stations at various distances and azimuths and simultaneously solve for surface-wave attenuation coefficient values and seismic moments for particular periods by linear least squares. Tryggvason (1965) first did this, as described in our section on early studies, using explosions and assuming circular radiation patterns. Tsai and Aki (1969) extended this method to use earthquake sources and applied it to surface waves generated by the 28 June 1966 Parkfield, California, earthquake. This process was later applied to the central United States (Herrmann and Mitchell, 1975; Mitchell, 1973) and the Basin and Range Province of the western United States (Patton and Taylor, 1989).

A nonlinear variation of the Tsai and Aki method (Mitchell, 1975) represents a nuclear explosion with strain release by a superposition of an explosion (with a circular radiation pattern) and a vertical strike-slip fault (represented by a horizontal double couple). Variations of the orientation of the double couple and its strength relative to the explosion produce a wide variety of radiation patterns. The inversion solves for the moment of the explosion, the orientation of the double couple, the strength of the double couple relative to the explosion, and an average attenuation coefficient value for each period of interest. Mitchell applied the method to two nuclear events in Colorado as recorded by stations throughout the United States and found that Q_μ in the upper crust of the eastern United States is about twice as high as it is in the western United States at surface-wave frequencies.

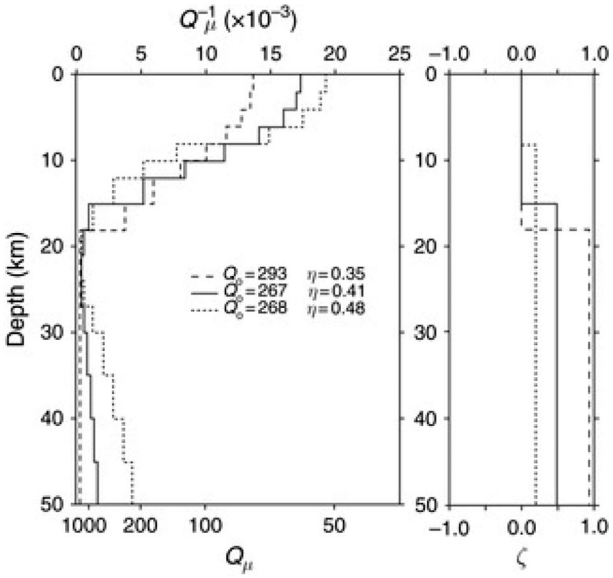

Figure 11 (Left) Three Q_μ models resulting from inversion of Rayleigh-wave attenuation coefficient data from the Basin and Range Province. The numbers refer to the value of Q_0 and η predicted by three models for Q_{Lg}. (Right) Three selected models for the variation of Q_μ frequency dependence with depth in the crust of the Basin and Range Province. Each of these depth distributions was fixed during inversions that produced Q_μ models. Reproduced from Mitchell BJ and Xie J (1994) Attenuation of multiphase surface waves in the Basin and Range province. Part III: Inversion for crustal anelasticity. *Geophysical Journal International* 116: 468–484, with permission from Blackwell Publishing.

The first attempts at mapping regional variations of attenuation or Q utilized crude regionalizations (two or three regions) based upon broad-scale geologic or geophysical information. Studies have produced models for Eurasia (Yacoub and Mitchell, 1977) using the method of Mitchell (1975) and for the Pacific (Canas and Mitchell, 1978) and Atlantic (Canas and Mitchell, 1981) using the two-station method.

1.25.7.2.3 Spectral decay methods in which source effects cancel: Lg coda

Lg coda, like direct Lg, is sensitive to properties through a known depth range (the crust) in which it travels and is a large amplitude phase for which data are plentiful. In addition, since the coda of Lg is comprised of scattered energy, it can continue to oscillate for several hundred seconds following the onset of the direct Lg phase, thus making it possible to stack spectral amplitudes for many pairs of time windows to make a Q estimate. Other positive aspects of using Lg coda for Q studies are that the averaging effect of scattering stabilizes Q_{Lg}^C determinations and, if stacking methods are utilized to determine Q for Lg coda, site effects cancel (Xie and Mitchell, 1990a).

Two methods have been applied to Lg coda to make Q determinations. The first of these was developed by Herrmann (1980) and applied by Singh and Herrmann (1983) to data in the United States. The method extended the coda theory of Aki (1969) utilizing the idea that coda dispersion is due to the combined effects of the instrument response and the Q filter of the Earth. The two studies provided new approximations for the relative variation of Q across the United States. Herrmann later realized, however, that his method did not take into consideration the broadband nature of the recorded signal and overestimates Q by about 30% (R. B. Herrmann, personal communication).

Xie and Nuttli (1988) introduced the stacked spectral ratio (SSR) method, which stacks spectra from several pairs of windows along the coda of Lg. That process leads to

$$R_k = f^{1-\eta}/Q_0 \qquad [16]$$

as the expression for the SSR, or in logarithmic form

$$\log R_k = (1-\eta)\log f_k - \log Q_0 + e \qquad [17]$$

from which Q_0 and η can be obtained by linear regression. f_k, Q_0, η, and e in these equations are, respectively, a discrete frequency, the value of Q at 1 Hz, the frequency dependence of Q at frequencies near 1 Hz, and an estimate for random error. This stacking process provides stable estimates of Q_0 and η with standard errors sufficiently low to allow tomographic mapping of those quantities. A detailed description of the SSR method appears in Xie and Nuttli (1988) and more briefly in Mitchell et al. (1997).

Figure 12 shows an example of Lg coda and its associated SSR for a relatively high-Q path in India, which can be fit over a

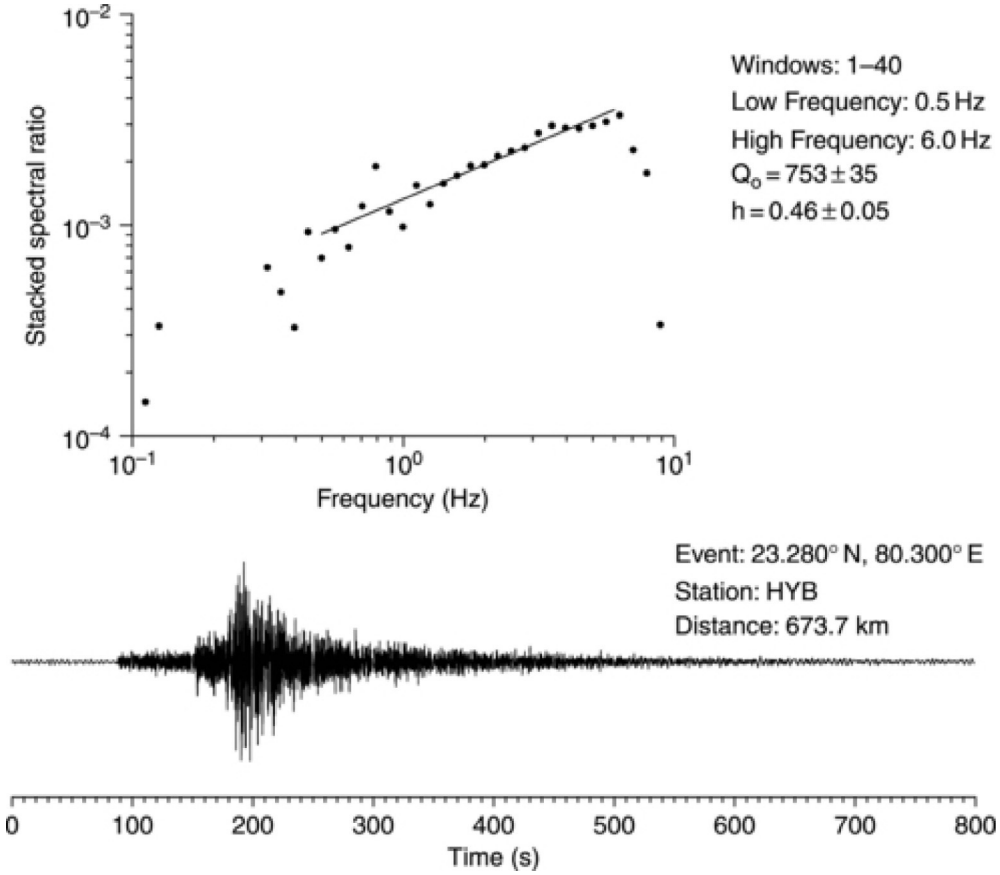

Figure 12 (Bottom) Seismogram. (Top) Stacked spectral ratio as a function of frequency for a relatively high-*Q* path in India.

broad frequency range with a straight line on a log–log plot. The value at 1 Hz provides an estimate of $1/Q$ at that frequency and the slope of the line gives an estimate for η. Inversions of sets of those values over a broad region can yield tomographic maps of those quantities.

Past studies have shown that several factors may contribute to reductions in Q_0; these include thick accumulations of young sediments (Mitchell and Hwang, 1987) and the presence of a velocity gradient rather than a sharp interface at the CMB (Bowman and Kennett, 1991; Mitchell et al., 1998). In addition, decreasing depth of the Moho in the direction of Lg travel or undulations of the Moho surface can be expected to decrease measured Q_{Lg} or Q_{Lg}^C, whereas increasing depth would produce larger values. To our knowledge, this effect has not been quantitatively studied and is expected to be small over large regions. These factors may cause determinations of correlation coefficients between Q_{Lg} or Q_{Lg}^C and various crustal or mantle properties to be relatively low whenever they are determined (e.g., Artemieva et al., 2004; Zhang and Lay, 1994).

1.25.7.2.4 Spectral decay methods for which assumptions are made, or information can be learned, about the source spectrum: regional phases

Hough et al. (1988) studied S waves traveling over relatively short distances near Anza, California, and defined the instrument-corrected acceleration spectrum at a station located a distance r from the source as

$$A(r,f) = A_0 e^{-\pi t^*} \quad [18]$$

where t^* is defined in eqn [12]. For crustal studies, it is common to assume that Q is constant along the path, in which case

$$t^* = \frac{t}{Q} \quad [19]$$

where t is the travel time.

Hough et al. (1988) defined A_0 as

$$A_0 = (2\pi f)^2 S(f) G(r,f) \quad [20]$$

where $S(f)$ is the source displacement spectrum and $G(r, f)$ is the geometric spreading factor, which, if we assume frequency-independent propagation in a homogeneous medium, is $1/r$ for body waves. At higher frequencies, these methods assume a spectral falloff rate (such as ω^{-2} or ω^{-3}) and attribute additional falloff to attenuation. Since a large body of data supports the ω^{-2}, or Brune, model (Brune, 1970), that is the one most commonly used. Taking the natural logarithm of eqn [18] leaves

$$\ln A(f) = \ln A_0 - \pi f t^* \quad [21]$$

For the frequency-independent case, this equation defines a straight line with an intercept of $\ln A_0$ and a slope of $-\pi t/Q_0$.

Anderson and Hough (1984) hypothesized that, to first order, the shape of the acceleration spectrum at high frequencies can be described by

$$\alpha(f) = A_0 e^{-\pi\kappa f} \quad f > f_E \qquad [22]$$

where f_E is the frequency above which the spectral shape is indistinguishable from spectral decay and A_0 depends on source properties and epicentral distance. They found that κ increased slowly with distance, an observation consistent with a Q model of the crust that increases with depth in its shallow layers and that it was systematically smaller on rock sites than at alluvial sites. Hough et al. (1988) studied κ as a function of hypocentral distance, as well as site and source characteristics, and found that $\kappa(0)$ differed for sites at Anza and the Imperial Valley in California but that $d\kappa/dr$ was similar for the two regions. Their interpretation was that $\kappa(0)$ was a component of attenuation that reflects Q_i in the shallow portion of the crust while $d\kappa/dr$ was due to regional structure at great depth. This method was applied to various regions in the world including the Canadian Shield (Hasegawa, 1974), the Pyrenees (Modiano and Hatzfeld, 1982), the New Madrid zone of the central United States (Al-Shukri et al., 1988), and eastern Asia (Phillips et al., 2000).

Shi et al. (1996) studied Q_{Lg} variation for five tectonically different regions of the northeastern United States. They used eight pairs of colocated earthquakes to determine accurate source spectrum corner frequencies by applying an empirical Green's function method to Pg and Lg or Sg phases. Based upon the corner frequencies, Sg or Lg displacement spectra were used to obtain values of Q and η values for 87 event–station paths at frequencies between 1 and 30 Hz. The 1 Hz Q_0 values for the five regions vary between 561 and 905 while η varies between 0.40 and 0.47.

1.25.7.2.5 Spectral decay methods for which assumptions are made about the source spectrum: fundamental-mode surface waves

A multimode spectral method has yielded simple crustal models (two or three layers) of shear-wave Q (Q_μ) in a few regions. The method assumes a flat source spectrum and tries to match theoretical amplitude spectra to two sets of observed spectral amplitude data, one corresponding to the fundamental mode and the other to the superposition of higher modes that forms the longer-period (3–10 s) component of the Lg phase. The higher modes travel faster than all but the longest-period fundamental-mode energy observed on records for relatively small events that are used with this method.

The first study using this method (Cheng and Mitchell, 1981) compared upper crustal Q_μ for three regions of North America and found values of 275 for the eastern United States, 160 for the Colorado Plateau, and 85 for the Basin and Range Province. Kijko and Mitchell (1983) applied the method to the Barents Shelf, a region of relatively high-Q crystalline crust overlain by low-Q sediments. They found the method to be sensitive to Q_μ in the sediments and upper crust but insensitive to Q_μ in the lower crust and to P-wave Q at all depths. Cong and Mitchell (1998) obtained models in which Q_μ is very low at all depths beneath the Iran/Turkish plateaus and somewhat higher but still much lower than expected beneath the Arabian Peninsula. Models they obtained using the multimode method agree well with those they obtained using the two-station method.

Jemberie and Mitchell (2004) applied the method to China and peripheral regions and obtained three-layer crustal models with low Q_μ and wide variation across China. Values decrease with depth beneath regions such as southeastern China and increase with depth beneath other regions such as the eastern Tibetan Plateau.

Seismologists have, in recent years, developed methods to measure the attenuation of regional phases (Pn, Pg, Sn, and Lg) in which the effects of source spectra are considered. One of those (Walter et al., 2007) used source spectra derived from the coda of those phases. It determined apparent Q by subtracting source spectra amplitudes from the observed amplitudes that were corrected for geometric spreading. They tested the method for several paths in Italy and found that they could determine path and recording site attenuation that satisfied the equation $Q(f) = Q_0 f^\eta$ well, for all phases, over the frequency range 0.5–8 Hz. Their measured values were also quite repeatable. Ford et al. (2008) compared several methods, including this one, for determining the attenuation of Lg in northern California. All methods returned similar values for Q_0 and η but with large 95% confidence regions ($Q_0 = 80 \pm 40$; $\eta = 0.65 \pm 0.35$). Another study of broadband Lg attenuation in the Middle East (Pasyanos et al., 2009) used the magnitude and distance amplitude correction developed by Walter and Taylor (2001). The method formulates the source term in terms of a corner frequency ω_c with an ω^{-2} falloff (Aki, 1967 and others) where the corner frequency and source term include constants that depend on medium properties as well as seismic moment. Their studies compared favorably with the results found by other studies in the region and, like those studies, showed a strong correlation with tectonics.

1.25.7.3 Tomographic Mapping of Crustal *Q*

Seismologists are currently attempting to map variations of Q and its frequency variation in the Earth in as much detail as possible. For continents, researchers have obtained tomographic maps for several broad regions using Lg coda, the direct Lg phase, and surface waves. Studies using P and S waves have yielded important results in regions where earthquakes and recording stations are plentiful. Studies of even smaller regions, such as volcanoes and geothermal areas, have utilized P and S waves (e.g., Hough et al., 1999). In this chapter, we restrict our discussion to more broad-scale studies.

An earlier section described three early regionalized studies of surface-wave attenuation in the late 1970s and early 1980s, one for continental paths and two for oceanic paths in which the Eurasian continent, the Pacific Ocean, and Atlantic Ocean were divided into two or three regions. Since then, tomographic mapping using Lg coda has made possible a much finer regionalization of crustal Q in continents. This section will discuss tomography results for continents and for one oceanic region using either direct Lg, fundamental-mode surface waves, or P and S waves.

We emphasize Lg coda since tomographic maps of Q_{Lg}^C, all obtained for the same frequency and using the same methodology, are available for all continents except Antarctica. This

commonality in phase, frequency, and method allows us to compare Q from one continent to that in others and also to various geophysical and geologic properties. These comparisons contribute to our understanding of the mechanisms for seismic-wave attenuation in the crust.

Earlier sections have indicated that Lg coda has several properties that make it useful for tomographic studies. First, it is usually a large amplitude phase making it easily available for study in most regions of the world. Second, it is a scattered wave and the averaging effect of that scattering makes Lg coda relatively insensitive to focusing. Third, the SSR method used to determine Q_0 and η tends to cancel site effects. Fourth, although it is a scattered wave, measurements of Q for seismic coda have been shown theoretically and computationally to yield measures of intrinsic Q (e.g., Frankel and Wennerberg, 1987; Mitchell, 1995; Sarker and Abers, 1999). If that is correct, researchers can interpret Q variation in terms of Earth structure and evolution. Other studies, however (e.g., Aki, 1980; Gusev and Abubakirov, 1996) attribute energy loss to scattering.

Akinci et al. (1995), employing the energy partition method of Frankel and Wennerberg (1987) for a Q study in western Turkey, found that shear-wave scattering predominated at low frequencies (1–4 Hz) and short hypocentral distances (0–80 km). Intrinsic anelasticity, however, became the dominant contributor to attenuation at greater distances. Cicerone et al. (2011) obtained a similar result for northeastern North America, while Sahin et al. (2013) also came to that conclusion when studying Lg attenuation in central Turkey. Those three studies suggest that for typical studies of Lg attenuation at large distances (about 200 km and more), Q values will largely reflect intrinsic properties of the Earth's crust.

Mitchell et al. (2014) proposed that the reason these path length-dependent differences occur can be understood by considering a supposition of rays taken to characterize Lg propagation. At very short lateral distances, most of the rays that comprise shear waves are reflected at angles smaller that the critical angle. For that reason, much of the wave energy at short distances is scattered into the mantle and quickly lost. At large lateral distances, waves that combine to form Lg reflect off the crust–mantle boundary (and other crustal boundaries) at angles that exceed the critical angle. That being the case, Lg and its coda will be largely constrained to travel in the crust, and relatively little energy is lost to the mantle.

As indicated earlier, Lg coda Q (Q_{Lg}^{C}) is typically assumed to follow a power-law frequency dependence, $Q_{Lg}^{C} = Q_0 f^{\eta}$, where Q_0 is the Q value at 1 Hz and η is the frequency dependence of Q near 1 Hz. Tomographic maps of the 1 Hz values of Q_{Lg}^{C} (Q_0 and η) with nearly continent-wide coverage are now available for Eurasia (Mitchell et al., 1997, 2008), Africa (Xie and Mitchell, 1990b), South America (DeSouza and Mitchell, 1998), and Australia (Mitchell et al., 1998). In North America, broad-scale determinations of Q_{Lg}^{C} are currently restricted to the United States (Baqer and Mitchell, 1998). These studies have shown a wide range of average Q_0 values for different continents and a very wide range within each continent. Average Q_0 tend to be highest in continents that contain the most old stable cratonic regions that have not undergone later tectonic or orogenic activity (e.g., Africa and South America).

Tomographic studies have also been completed for more restricted regions using the direct Lg phase in Eurasia, North America, and South America, and high-resolution tomographic maps of Q for P and S waves are available for southern California. For oceanic regions, tomographic mapping of Q variations, to our knowledge, is currently available only for P waves in one broad portion of the East Pacific Rise (Wilcock et al., 1995).

Sarker and Abers (1998) showed that, for comparative studies, it is important that researchers use the same phase and methodology in comparative Q studies. The Lg coda Q maps presented here adhere to that principle; thus, the continental-scale maps of Q_0 and η for Lg coda at 1 Hz that are available can be considered to provide the closest thing to global Q coverage at crustal depth that currently exists. The maps also present the possibility for comparisons of Q_0 variation patterns with variations in seismic velocity, temperature, plate subduction, seismicity, the surface velocity field, and tectonics when that information is available.

A discussion of the inversion method for mapping Q_0 and η appears, in detail, in Xie and Mitchell (1990b) and, more briefly, in Mitchell et al. (1997). The method assumes that the area occupied by the scattered energy of recorded Lg coda can be approximated by an ellipse with the source at one focus and the recording station at the other, as was shown theoretically by Malin (1978) to be the case for single scattering.

Xie and Mitchell (1990b) utilized a back-projection algorithm (Humphreys and Clayton, 1988) to develop a methodology for deriving tomographic images of Q_0 and η over broad regions using a number of Q_0 or η values determined from observed ground motion. **Figures 13–17(a)** show the ellipses that approximate data coverage for the event–station pairs used in Q_{Lg}^{C} studies of Eurasia, Africa, South America, Australia, and the United States. The inversion process assumes that each ellipse approximates the spatial coverage of scattered energy comprising late Lg coda. The areas of the ellipses grow larger with increasing lag time of the Lg coda components. The ellipses in the figure are plotted for maximum lag times used in the determination of Q_0 and η. Ideally, each inversion should utilize many ellipses that are oriented in various directions and exhibit considerable overlap in order to obtain the redundancy needed to obtain the best possible resolution for features of interest. Xie and Mitchell (1990b) discuss the procedure in detail, presenting methods for obtaining standard errors for Q_0 and η and for estimating spatial resolution.

Because Lg coda consists of scattered energy, it must be distributed, for each event–station pair, over an area surrounding the great-circle path between the source and receiver. Because of this areal coverage, our maps may not include effects of Lg blockage in regions where such blockage has been reported. We may have no data from blocked paths but are likely to have other paths, such as those subparallel to the blocking feature or for which the source or recording station, represented by one focus of the scattering ellipse, lies near the blocking feature. In both cases, portions of the scattering ellipses may overlap the blocking feature, but that feature will not substantially contribute to the values we obtain for Q_0 and η. A comparison of mapped Q_0 for all continents (**Figures 13–17(b)**) shows that it is typically highest in the stable portions of the continents and lowest in regions that are, or recently have been, tectonically active. Exceptions occur, however, especially for stable regions. For instance, the Arabian

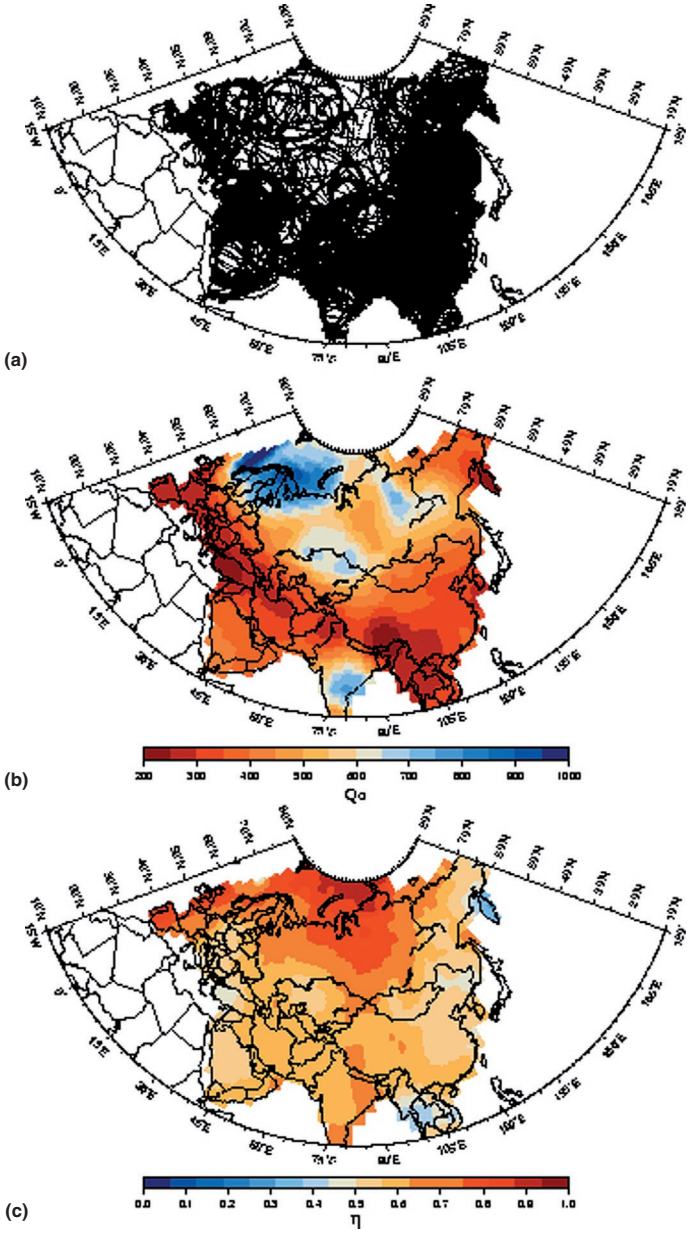

Figure 13 (a) A scattering ellipse map, (b) a Q_0 map, and (c) an η map for Eurasia. Adapted from Mitchell BJ, Cong L, and Ekström G. (2008) A continent-wide 1-Hz map of *Lg* coda *Q* variation across Eurasia and its implications for lithospheric evolution. *Journal of Geophysical Research* 113. http://dx.doi.org/10.1029/2007JB005065.

Peninsula, although being a stable platform, shows Q_0 variations between 300 and 450, values that are one-half or less of maximum values in other Eurasian platforms. Other regions showing lower than expected Q_0 include the Siberian Trap region of northern Siberia and the cratonic regions of Australia.

The frequency dependence values of Q_{Lg}^{C} (η) in Figures 13–17(c) appear to show consistent relationships to Q_0 in some individual continents. For instance, in both Africa and South America, high-*Q* regions are typically regions of low η. That same relationship, however, does not occur consistently in Eurasia, Australia, or the United States. η is high, for instance, throughout much of the northern portions of Eurasia where Q_0 is mostly high but is low in California, Kamchatka, and a portion of southeast Asia where Q_0 is very low.

1.25.7.3.1 Q_{Lg}^{C}, Q_{Lg}, and Q_{μ} tomography in regions of Eurasia

Figure 13 shows maps of data coverage, Q_0, and η across most of Eurasia (Mitchell et al., 2008). These maps represent a major increase in data coverage for northeastern Siberia, southeastern Asia, India, and Spain, compared to those of an earlier study (Mitchell et al., 1997) and provide additional redundancy in regions where there was earlier coverage. As indicated in Figure 13(a), the data coverage is excellent for virtually all of

Eurasia. Low Q_0 values extend through the Tethysides belt that extends across southern Eurasia from western Europe to eastern China, and its southern portions appear to be related to subduction processes occurring at the present time. Q_0 is generally high in the platforms of northern Eurasia and India (600–950). It is, however, low in the Kamchatka Peninsula and regions directly north of there, which, like the Tethysides region, are seismically active. A conspicuous region of relatively low Q_0 lies in central Siberia and corresponds spatially to the Siberian Traps.

The four zones with lowest Q values lie in the Kamchatka Peninsula in northeastern Siberia, the southeastern portions of the Tibetan Plateau and Himalaya, and the Hindu Kush (just north of India) and western Turkey. All of these regions are also highly seismically active, a correspondence that suggests that low-Q regions are associated with regions of high crustal strain.

Other low-Q regions appear to be related to upper mantle processes. A comparison of **Figure 13(b)** with wave velocities at long periods (Ekström et al., 1997), which are not sensitive to crustal properties, shows a correspondence of low-Q regions with regions of low upper mantle velocities. This is most apparent for the broadband of low Q values throughout southern Eurasia but also occurs in the Siberian Trap region of Siberia. Both the low-Q and low-velocity regions largely coincide with high upper mantle temperatures (Artemieva and Mooney, 2001).

Patterns of frequency dependence (η) variation in **Figure 13(c)**, in contrast to those of Q_0 variation, show no clear-cut relationship to tectonics. They similarly show no relation to patterns of Q_0 variation. For instance, Kamchatka has low Q_0 and low η while Spain has low Q_0 and high η.

Seismologists have performed other tomographic studies for portions of Eurasia using Q_{Lg} and shear-wave Q (Q_μ). Xie et al. (2006) used a two-station version of the SSR method to determine more than 5000 spectral ratios over 594 paths in eastern Eurasia. They were able to obtain tomographic models for Q_0 and η with resolution ranging between 4° and 10° in which Q_0 varies between 100 and 900.

Using the single-station multimode method, Cheng and Mitchell (1981) and Jemberie and Mitchell (2004) obtained tomographic maps of shear-wave Q (Q_μ) for depth ranges of 0–10 and 10–30 km. Although large standard errors accompany those determinations, several features of their variation patterns, such as the low-Q regions in southern Tibet, resemble the map of Q_0 variations (**Figure 13(b)**). Q_μ varies between about 30 and 280 in the upper 10 km of the crust and between about 30 and 180 at 10–30 km depth.

1.25.7.3.2 Q^C_{Lg} tomography in Africa

Xie and Mitchell (1990b), in the first tomographic study of Lg coda, determined Q_0 and η for continental Africa. **Figure 14** shows maps of data coverage, Q_0 and η for that entire continent (Xie and Mitchell, 1990b). The feature in the Q_0 map (**Figure 14(b)**) that is most obviously related to tectonics is the low-Q region that broadly coincides with the East African Rift system. The three high-Q regions correspond to Precambrian cratons: the West African Craton in the northwest, the East Sahara Craton in the northeast, and the Kalahari Craton in the south. The Congo Craton, situated just to the north of the Kalahari Craton does not show up as a region of high Q, probably because waves are damped by a broad and deep basin of low-Q sedimentary rock in that region.

Low Q_0 values also occur in the Atlas Mountains (Cenozoic age) of northern Africa, the Cape Fold Belt (Permian–Triassic age) at the southern tip of Africa, and the Cameroon line (Miocene age), which is oriented in an NNE–SSW direction from the point where the western coast changes direction from east–west to north–south.

1.25.7.3.3 Q^C_{Lg} and Q_{Lg} tomography in South America

Figure 15 shows data coverage and values of Q_0 and η obtained for South America (DeSouza and Mitchell, 1998). The data coverage (**Figure 15(a)**) is excellent throughout western South America where seismicity is high but poor in eastern regions, especially the most easterly regions, where there are few earthquakes. **Figure 15(b)** shows that, as expected, the low-Q (250–450) portion of South America is associated with the tectonically active western coastal regions. The lowest Q_0 values occur along the coast between 15° and 25° S latitude where the level of intermediate-depth seismicity is highest in the continent. The slab in this region also dips steeply (>20°) and significant volcanism occurs (Chen et al., 2001). Davies (1999) had studied the role of hydraulic fractures and intermediate-depth earthquakes in generating subduction zone magmatism. He suggested that the level of intermediate-depth earthquakes was high because liberated fluids favored brittle fracture in response to stresses acting on the slab. Q levels may be low there because earthquake activity creates a degree of permeability that allows dehydrated fluids to be transported to the mantle wedge.

Ojeda and Ottemöller (2002) developed maps of Lg attenuation for most of Colombia at various frequencies in the 0.5–5.0 Hz range. They delineated regional variations of Q_{Lg} within that relatively small region.

1.25.7.3.4 Q^C_{Lg} tomography in Australia

Figure 16 shows the data coverage and values of Q_0 and η obtained for Australia (Mitchell et al., 1998). Data coverage (**Figure 16(a)**) there was the poorest of the five continents where Q^C_{Lg} was mapped over continent-scale dimensions. Q_0 variation there is consistent, however, with the other studies, and, for all but peripheral regions where systematic measurement errors can be high, it displays a clear relationship with past tectonic activity. Q_0 in Australia (**Figure 16(b)**) is unusually low for a stable continental region, perhaps because a velocity gradient rather than a sharp interface separates the crust and mantle.

Highest values range between 550 and 600 in the southeastern corner of the continent (the Yilgarn Block) and along the southern coast (the Gawler Block). Values between 400 and 500 characterize much of the remaining cratonic crust. This compares with values of 800 and higher in most of the African and South American cratons. The youngest crust lies in eastern Australia where Q_0 is between 350 and 400. An orogeny occurred there during the Devonian Period, and another occurred in the eastern portion of that region during the Permian Period. Low Q_0 values in the most westerly point of the continent and along the northern coast are probably due to very poor data coverage there (**Figure 16(a)**) and are probably meaningless.

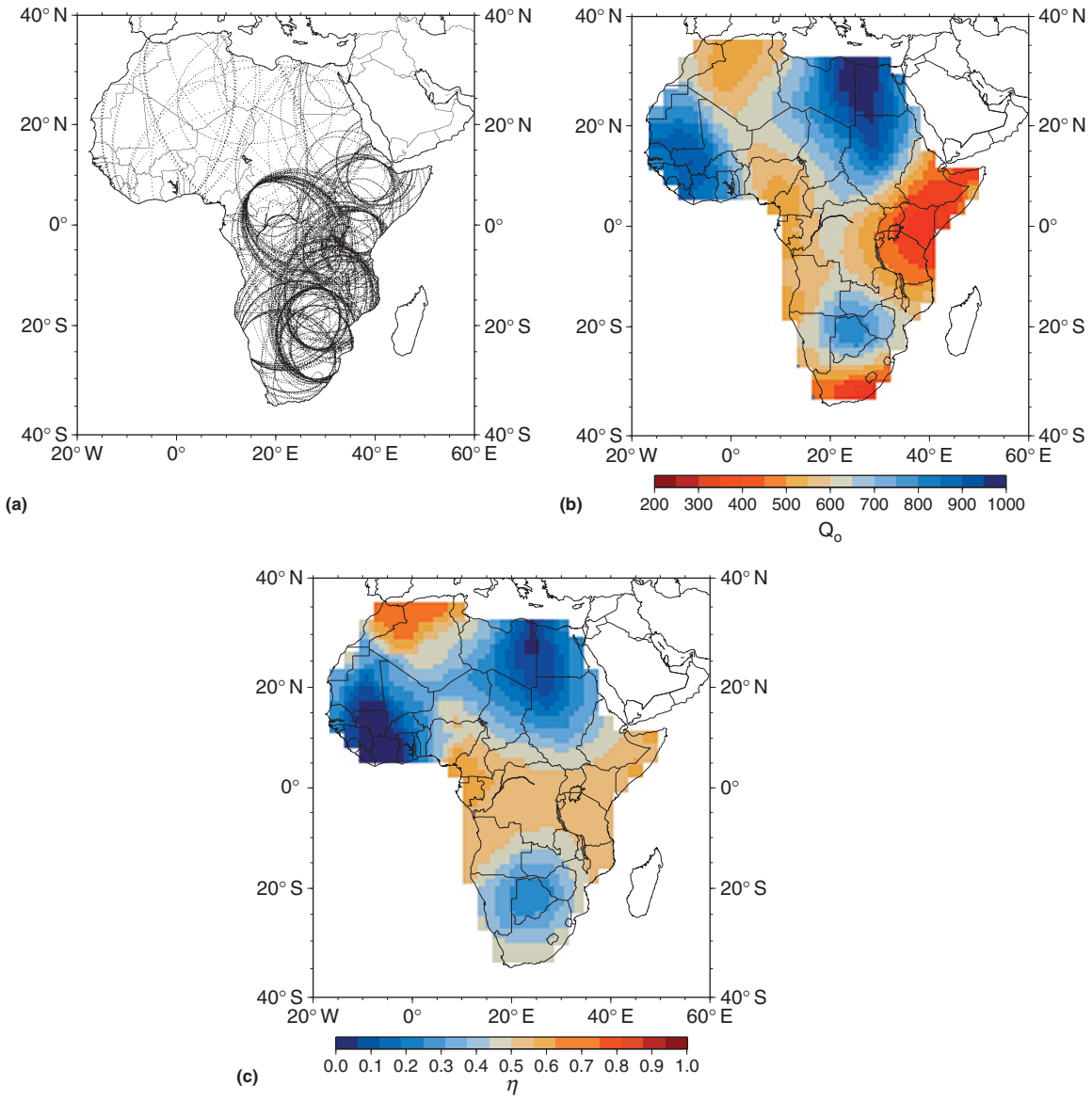

Figure 14 (a) A scattering ellipse map, (b) a Q_0 map, and (c) an η map for Africa. Adapted from Xie J and Mitchell BJ (1990b) A back-projection method for imaging large-scale lateral variations of *Lg* coda *Q* with application to continental Africa. *Geophysical Journal International* 100: 161–181.

1.25.7.3.5 Q^c_{Lg}, Q_{Lg}, and P/S tomography in North America

Figure 17(a) shows approximate data coverage and values of Q_0 and η for the first Lg coda *Q* study of the entire North American continent (Mitchell et al., 2014). This work utilized 1122 event–station pairs distributed across virtually all of North America, a number that represents a more than fivefold increase in data coverage over that of an earlier Lg coda *Q* study of the United States (Baqer and Mitchell, 1998). Data coverage is densest in the westernmost portion of North America where seismicity rates are high but coverage is also more than adequate for most of the rest of the continent. This is especially true for the south-central and northeastern portions of the United States, as well as for southeastern Canada. The ability to use relatively small earthquakes, even in central and north-central Canada where seismicity rates are low, allowed us to achieve quite good data coverage.

The Q_0 map (Figure 17(b)) reveals two major features that cover vast areas of North America. One is a region of high-*Q* values (700–1000) that covers much of the Canadian Shield with a southeastern arm that extends through southern New England and New York to the Atlantic coast. The other is a band of low-*Q* values (about 200–350) that runs continuously, with some variations in width (between about 20 and 500 km), from southern Alaska to southern Central America. The transition from the high-*Q* shield values to low values in western Canada is surprisingly sharp and suggests that the pattern of mapped Q_0 cannot be explained as being produced by temperature variations alone in the crust. One possibility that would nicely explain the sharp transition is a change from high levels of interstitial fluid content in the low-*Q* region compared to lower fluid levels in the high-*Q* region.

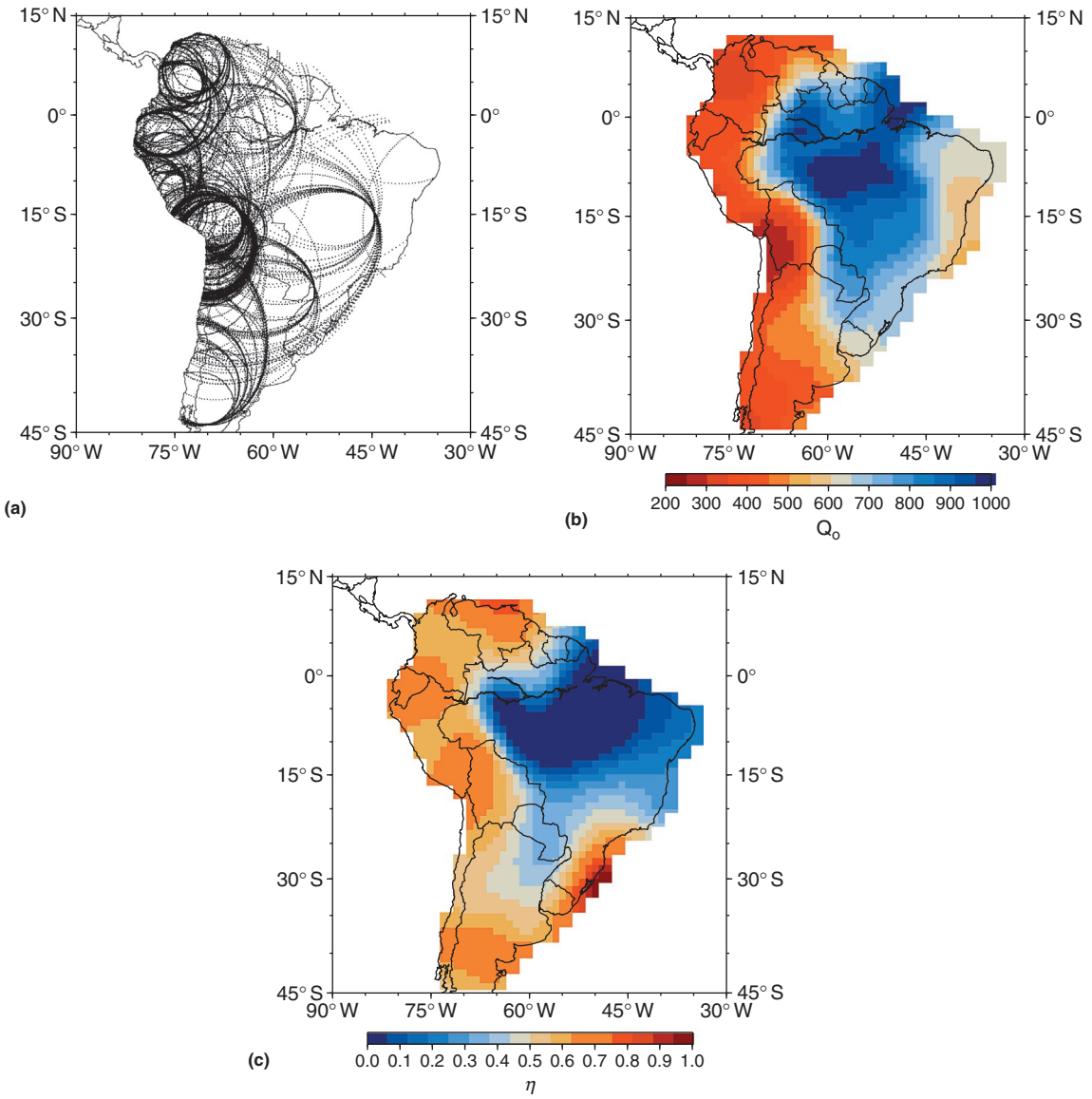

Figure 15 (a) A scattering ellipse map, (b) a Q_0 map, and (c) an η map for South America. Adapted from DeSouza JL and Mitchell BJ (1998) *Lg* coda *Q* variations across South America and their relation to crustal evolution. *Pure and Applied Geophysics* 153: 587–612.

A small but important feature on the map appears as a circular region of high Q_0 values (600–700) with a diameter of about 500–700 km in the central United States. It coincides well with the Ozark uplift of southern Missouri and northern Arkansas. The region of relatively high Q_0 includes the St. Francis Mountains, a region of Precambrian rock, which contains some of the oldest rock in North America.

One region of moderately low Q_0 values includes the east–west band that extends from the eastern edge of very low-Q_0 regions of southern California and northern Mexico through southern portions of the Gulf coast states and northward along the Atlantic coast to an extension of the high-Q_0 Canadian Shield. Another is the relatively low-Q_0 band from northeastern Canada through most of the continental shelf of northern Canada. All of these features are probably due to the accumulations of thick sediments known to occupy those regions.

Figure 17(c) shows the distribution of the frequency dependence parameter (η) for North America. The excellent coverage of this study makes possible a better understanding of the regional variation in η than has been previously possible. The most striking feature of the map is the high-η band stretching from northern Canada to the western coast of the Gulf of Mexico. The highest values stretch northward from Great Slave Lake to the coast and are associated with high errors for both Q_0 and η. This probably indicates that crustal complexity, not intrinsic rock properties, causes anomalous values for η. More moderate η values (0.6–0.8) extend southward from the Great Slave Lake anomaly to the Gulf of Mexico. Lower values (0.3–0.6) characterize four regions of North America: (1) the Canadian Shield, (2) the eastern United States, (3) the western United States, and (4) the region of northwestern Canada and southern Alaska. We have discussed the likelihood that the very

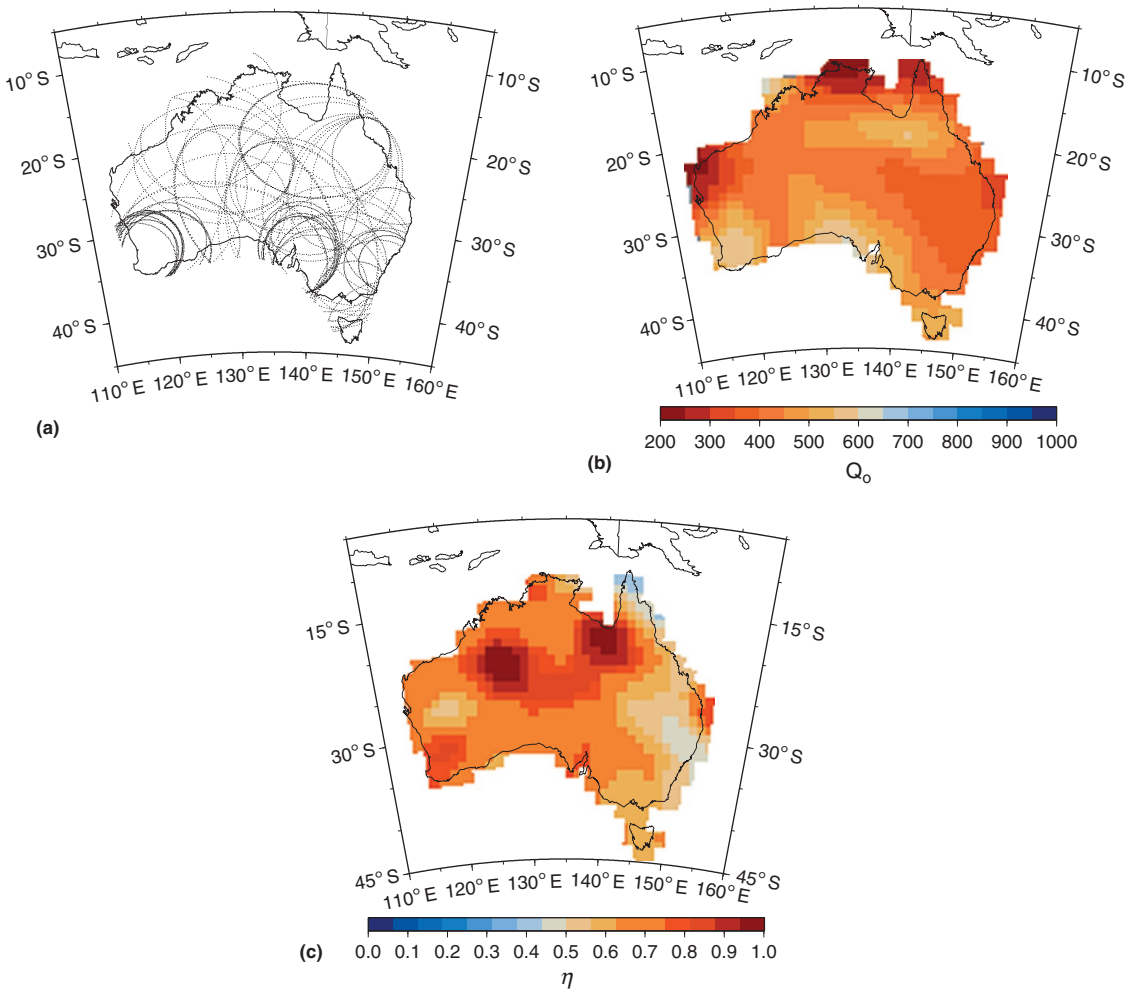

Figure 16 (a) A scattering ellipse map, (b) a Q_0 map, and (c) an η map of Q_{Lg}^{C} for Australia. Adapted from Mitchell BJ, Baqer S, Akinci A, and Cong L (1998) *Lg* coda *Q* in Australia and its relation to crustal structure and evolution. *Pure and Applied Geophysics* 153: 639–653.

high η values (0.8–1.0) in northern Canada are due to scattering causing the crustal complexity known to exist there. A broadband of high η values (0.6–0.8) extends southward from the concentration of highest values forming a long and broad high-η band extending from there to the Gulf of Mexico. That band lies between the Great Plains on its eastern side and the Rocky Mountains on its western side and may be caused by a transition zone with changing east–west crustal thickness.

Two research groups have studied the 3D structure of P-wave and S-wave attenuation in southern California. Schlotterbeck and Abers (2001) fit theoretical spectra to observed spectra using the least-square minimization method of Hough et al. (1988) and determined t^* for P and S waves at frequencies between 0.5 and 25 Hz. Their inversions showed that P and S results were in substantial agreement, and that *Q* varies spatially and correlates with regional tectonics.

The second California study (Hauksson, 2006) also determined t^* from P- and S-wave spectra. They assumed that t^* consists of the sum of the whole-path attenuation and the local site effect at each recording station and utilized an expression of Eberhart-Phillips and Chadwick (2002) for the velocity spectrum. The inversion, in addition to providing t^*, yields parameters defining the velocity amplitude spectra. They determined t^* for about 340 000 seismograms from more than 5000 events of t^* data to obtain 3D, frequency-independent crustal models for Q_P and Q_S in the crust and uppermost mantle in southern California. They found that both Q_P and Q_S generally increase with depth from values of 50 or less in surface sediments to 1000 and greater at midcrustal depths. Their models reflect major tectonic structures to a much greater extent than they reflect the thermal structure of the crust. Al-Eqabi and Wysession (2006) conducted a tomographic study of Q_{Lg} in the Basin and Range Province using a genetic algorithm technique. They found that Q_{Lg} increases (234–312) in a southwest–northeast direction across the Basin and Range Province in good agreement with the variation of Q_{Lg}^{C} reported by Baqer and Mitchell (1998). As part of a broader study of Lg wave propagation in southern Mexico, Ottemöller et al. (2002) used formal inversion methods to separately obtain tomographic maps of Q_{Lg} at three frequencies (0.5, 2.0, and 5.0 Hz) using 1° by 1° cells. Because of uneven path coverage in southern Mexico, they applied regularization conditions to their inversion equations. They found lower than average Q_{Lg} in the Gulf of Mexico coastal plain and the area east of 94° W,

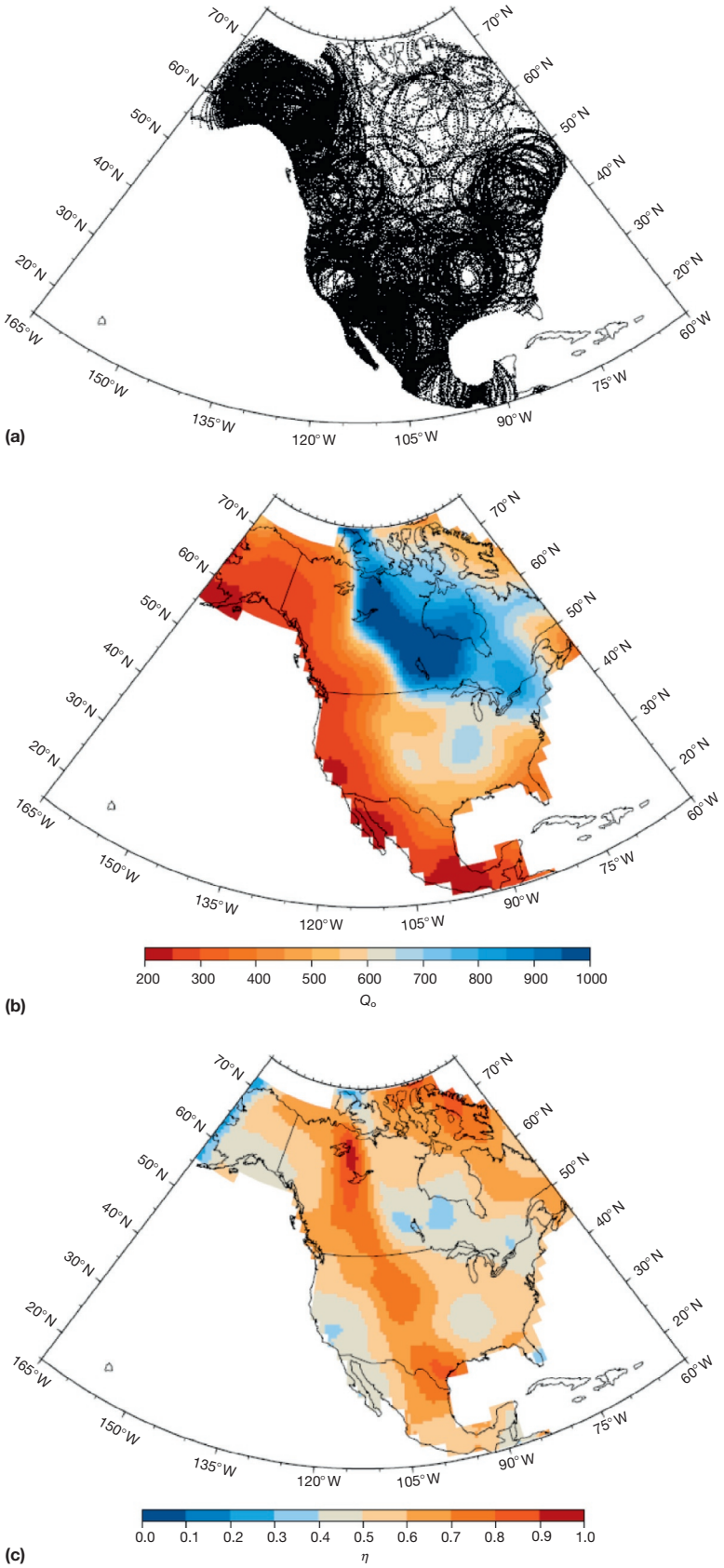

Figure 17 (a) A scattering ellipse map, (b) a Q_0 map, and (c) an η map of Q_{Lg}^{C} for North America. Adapted from Mitchell BJ, Cong L, and Jemberie A (2014) Continent-wide maps of *Lg* coda *Q* for North America and their relationship to crustal structure and evolution. *Bulletin of the Seismological Society of America*.

average values in the northern portion of the Pacific coastal region, and below average values in the southern portion.

1.25.7.3.6 Q_P variation near ocean ridges

Wilcock et al. (1995) developed a spectral technique by which they determined the attenuation of P waves in an active-source experiment centered at the East Pacific Rise at latitude 9°30′N. It is, to date, the only tomographic study of crustal Q variation in an oceanic region. They obtained over 3500 estimates of t^*, the path integral of the product of Q^{-1} and P-wave velocity where both quantities are variable along the path. Wilcock et al. display plots of both cross-axis and along-axis structures for upper crustal and lower crustal Q^{-1} structures. Within the ridge magma chamber, Q reaches minimum values of 20–50, which extend to the base of the crust. Off the ridge axis, they find that Q in the upper crust is 35–50 and at least 500–1000 at depths greater than 2–3 km.

1.25.7.3.7 Variation of crustal Q with time

Several investigators (e.g., Chouet, 1979; Jin and Aki, 1986) have reported temporal variations of Q over timescales of a few years. Although this observation has been reported several times, it continues to be controversial. Spatial patterns of Q variation and their apparent relation to time that has elapsed since the most recent episode of tectonic activity in any region, however, suggest that temporal variations of Q over very long periods of time can easily be detected. Mitchell and Cong (1998) found that variation for Q_{Lg}^{C} at 1 Hz extends between roughly 250, for broad regions that are currently tectonically active, and about 1000 for shields that have been devoid of tectonic activity for a billion years or more (Figure 18). Mitchell et al. (1997) explained those observations as being due to variable volumes of fluids in faulted, fractured, and permeable rock. Fluids may enhance the rate of attenuation of seismic waves either because the waves must expend energy to push those fluids through permeable rock as they propagate or because they may traverse a region of enhanced scattering that causes loss of wave energy into the mantle. Figure 18 points to an evolutionary process in which fluids are relatively abundant in tectonically active regions due to their generation by hydrothermal reactions at high temperatures. With time, fluids are gradually lost, either by migration to the Earth's surface or absorption due to retrograde metamorphism. This process causes low Q values early in the tectonic cycle and gradually increasing values at later times as the fluids dissipate.

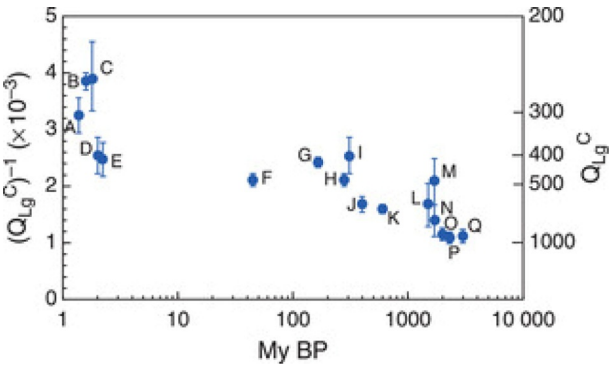

Figure 18 Q_0 for Q_{Lg}^{C} at 1 Hz versus time elapsed in selected regions since the most recent episode of tectonic or orogenic activity. A, the Andes; B, Basin and Range Province in the western United States; C, Tethys region of convergence between the Eurasian and African/Arabian/Indian plates; D, the Arabian Peninsula; E, the East African Rift; F, the Rocky Mountains; G, northeastern China; H, the eastern Altaids in Eurasia; I, the Tasman Province in Australia; J, the Atlantic Shield in South America; K, the African fold belts; L, the portion of the North American Craton in the United States; M, the Australian Craton; N, Eurasian cratons; O, African shields; P, the Brazilian shield; *Q*, the Indian shield. Adapted from Mitchell BJ and Cong L (1998) *Lg* coda *Q* and its relation to the structure and evolution of continents: A global perspective. *Pure and Applied Geophysics* 153: 655–663.

1.25.8 Conclusions

Much progress has been made in the last 15 years in characterizing the lateral variations in attenuation in the crust, especially under continents, and their relation to tectonics. Characterizing the nature and distribution of attenuation deeper in the Earth still remains a challenging subject, because of the persistent difficulties in separating anelastic and scattering effects and the nonuniform sampling achieved with available data.

Still, it is encouraging to see that there is now consistency in the large-scale features of lateral variations in Q in the upper 200 km of the mantle, correlated with tectonics, and that accounting for focusing effects using a single scattering approximation in present-day elastic 3D models is helpful, at least at the longest wavelengths. It is still important to consider that, when the inversion experiment is well designed, the unmodeled scattering effects can be minimized, or even utilized to constrain velocity models (e.g., Dalton and Ekström, 2006b), but the consequence is that significant damping needs to be applied in the inversion for lateral variations in Q. This results in large uncertainties (a factor of 2 or more) in the amplitudes of lateral variations of Q, so that physical interpretations of these models must remain tentative. On the other hand, the spatial distribution of low- and high-Q regions is, in general, more robust. Thus far, only one research group has produced models of lateral variations of Q_μ in the transition zone. While the results are consistent within this group using different methodologies (Gung and Romanowicz, 2004; Romanowicz, 1995) and point to an intriguing correlation with structure at the base of the mantle (Romanowicz and Gung, 2002), these results need to be confirmed by independent studies.

At the regional, uppermost mantle scale, consistent results have been obtained in subduction zones (high Qs) and back-arc regions (very low Qs), less so in oceanic settings. A promising trend, made possible by improved data and techniques, is to combine attenuation, velocity, and other geophysical parameters to better constrain lateral variations of temperature and composition. An ambitious goal would be to do the same at the global, and deeper, scale. Progress in laboratory experiments on Q at seismic frequencies is just starting to provide reliable mineral physics parameters on the behavior of Q at depths down to the upper mantle low-velocity zone, so that joint inversions of seismic waveform data for elastic and anelastic 3D structure can be envisaged (e.g., Cammarano and Romanowicz, 2007, 2008). The challenge

here is in the nonlinearities introduced by the exponential variation of Q with temperature, on the one hand, and the variation in the position of mineral phase changes depending on composition, on the other.

Important uncertainties remain in the characterization of the 1D profile of Q_μ in the mantle – first and foremost, explaining once and for all the discrepancy between free oscillations and surface-wave measurements, which has consequences for the value of Q_μ in the transition zone. Because there are still unexplained discrepancies between elastic models of the upper mantle, and particularly the transition zone, produced from seismic data, on the one hand, and from mineral physics data and computations, on the other (e.g., Cammarano et al., 2003), it is particularly important to apply accurate anelastic corrections when interpreting seismic velocity models in terms of composition. The evidence for a maximum in Q_μ in the lower mantle, and therefore lower Q_μ at the base of the mantle, is now clear; however, the location of this maximum is not well constrained. The confirmation of frequency dependence of Q in the mantle, with $\alpha \sim 0.3$, and a shift of the absorption band to lower frequencies in the lower mantle, seems to emerge from the comparison of 1D Q profiles derived from normal modes/surface-wave data, on the one hand, and body-wave data, on the other. The location in the Earth of the attenuation in bulk required to explain some normal mode data is still the subject of debate.

The presence of hemispheric variations in Q_α at the top of the inner core and the confirmation of increasing Q with depth and of anisotropy in Q_α correlated with anisotropy in velocity are exciting results that need further investigation, in particular in the light of recent studies by Li and Cormier (2002) favoring a scattering interpretation of attenuation in the inner core.

Finally, in the shallow Earth, it has been found over the past four decades that crustal Q, as manifested by regional studies of body waves, Lg and Lg coda, varies tremendously across continents, as well as in average values of different continents. Q_0 for Lg coda varies between about 150 and 1000 for features that can be resolved at 1 Hz frequency and the frequency dependence of Lg coda Q varies between about 0.0 and 1.0. Recent work on energy partitioning to learn the extent to which Lg attenuation is governed by intrinsic rock properties or by scattering shows that while scattering is predominant at short distances, intrinsic rock properties play the larger role at long distances. Most Q determinations at short periods in any region appear to be governed, most prominently, by the time that has elapsed since the most recent episode of tectonic or orogenic activity there.

Further advances in mapping the Q structure in the crust and mantle may come from the implementation of novel methodologies, such as the use of powerful numerical techniques for wavefield computations (e.g., Ruan and Zhou, 2012; Savage et al., 2010) and the use of noise correlation data (e.g., Lawrence and Prieto, 2011; Prieto et al., 2009; **Chapter 1.12**).

Acknowledgment

The research of BJM was partially supported by the Air Force Research Laboratory under Award FA 8718-04-C-0021.

References

Abercrombie RE (1997) Near-surface attenuation and site effects from comparison of surface and deep borehole recordings. *Bulletin of the Seismological Society of America* 87: 731–744.

Abercrombie RE (2000) Crustal attenuation and site effects at Parkfield, California. *Journal of Geophysical Research* 105: 6277–6286.

Aizawa Y, Barnhoorn A, Faul UH, Fitz Gerald JD, Jackson I, and Kovács I (2008) Seismic properties of Anita Bay dunite: An exploratory study of the influence of water. *Journal of Petrology* 49: 841–855. http://dx.doi.org/10.1093/petrology/egn007.

Aki K (1967) Scaling law of seismic spectrum. *Journal of Geophysical Research* 72: 729–740.

Aki K (1969) Analysis of the seismic coda of local earthquakes as scattered waves. *Journal of Geophysical Research* 74: 615–631.

Aki K (1980) Scattering and attenuation of shear waves in the lithosphere. *Journal of Geophysical Research* 85: 6496–6504.

Akinci A, Del Pezzo E, and Ibanez JM (1995) Separation of scattering and intrinsic attenuation in southern Spain and western Anatolia (Turkey). *Geophysical Journal International* 121: 337–353.

Akopyan ST, Zharkov VN, and Lyubimov VM (1976) Corrections to the eigenfrequencies of the Earth due to dynamic shear modulus. *Bulletin of the Seismological Society of America* 12: 625–630.

Alboussière T, Deguen R, and Melzani M (2010) Melting-induced stratification above the Earth's inner core due to convective translation. *Nature* 466: 744–747.

Al-Eqabi GI and Wysession ME (2006) Q_{Lg} distribution in the Basin and Range province of the western United States. *Bulletin of the Seismological Society of America* 96: 348–354.

Al-Khatib HH and Mitchell BJ (1991) Upper mantle anelasticity and tectonic evolution of the western United States from surface wave attenuation. *Journal of Geophysical Research* 96: 18129–18146.

Allen RM, Nolet G, Morgan WJ, et al. (1999) The thin hot plume beneath Iceland. *Geophysical Journal International* 137: 51–63.

Al-Shukri HJ, Mitchell BJ, and Ghalib HAA (1988) Attenuation of seismic waves in the New Madrid seismic zone. *Seismological Research Letters* 59: 133–140.

Anderson DL and Archambeau CB (1966) The anelasticity of the Earth. *Journal of Geophysical Research* 69: 2071–2084.

Anderson DL, Ben-Menahem A, and Archambeau CB (1965) Attenuation of seismic energy in the upper mantle. *Journal of Geophysical Research* 70: 1441–1448.

Anderson DL and Given JW (1982) Absorption band Q model for the Earth. *Journal of Geophysical Research* 87: 3893–3904.

Anderson DL and Hart RS (1976) An Earth model based on free oscillations and body waves. *Journal of Geophysical Research* 81: 1461–1475.

Anderson DL and Hart RS (1978) Q of the Earth. *Journal of Geophysical Research* 83: 5869–5882.

Anderson JG and Hough SE (1984) A model for the shape of Fourier amplitude spectrum of acceleration at high frequencies. In: 1984 *Annual Meeting 30 May–3 June, 1984* Anchorage, Alaska: Seismological Society of America.

Andrews J, Deuss A, and Woodhouse J (2006) Coupled normal mode sensitivity to inner-core shear velocity and attenuation. *Geophysical Journal International* 167: 204–212.

Angenheister GH (1906) Bestimmung der fortpflanzungsgeschwindigkeit und absorption von erdbebenwellen, die durch den gegenpunkt des Herdes gegangen sind. *Nachrichten von der Königlichen Gesellschaft der Wissenschaften zu Göttingen* 110–120.

Angenheister GH (1921) Beobachtungen an pazifischen beben. *Nachrichten von der Königlichen Gesellschaft der Wissenschaften zu Göttingen* 113–146.

Artemieva IM, Billien M, Lévêque JJ, and Mooney WD (2004) Shear-wave velocity, seismic attenuation, and thermal structure of the continental upper mantle. *Geophysical Journal International* 157: 607–628.

Artemieva IM and Mooney WD (2001) Thermal evolution of precambrian lithosphere: A global study. *Journal of Geophysical Research* 106: 16387–16414.

Asada T and Takano K (1963) Attenuation of short-period *P* waves in the mantle. *Journal of Physics of the Earth* 11: 25–34.

Baqer S and Mitchell BJ (1998) Regional variation of *Lg* coda *Q* in the continental United States and its relation to crustal structure and evolution. *Pure and Applied Geophysics* 153: 613–638.

Barazangi M and Isaaks B (1971) Lateral variations of seismic-wave attenuation in the upper mantle above the inclined earthquake zone of the Tonga Island Arc: Deep anomaly in the upper mantle. *Journal of Geophysical Research* 76: 8493–8516.

Barazangi M, Pennington W, and Isaaks B (1975) Global study of seismic wave attenuation in the upper mantle behind Island Arcs using P waves. *Journal of Geophysical Research* 80: 1079–1092.

Ben-Menahem A (1965) Observed attenuation and Q values of seismic surface waves in the upper mantle. *Journal of Geophysical Research* 70: 4641–4651.

Benz HM, Frankel A, and Boore DM (1997) Regional *Lg* attenuation for the continental United States. *Bulletin of the Seismological Society of America* 87: 606–619.

Bhattacharyya J, Masters G, and Shearer P (1996) Global lateral variations of shear wave attenuation in the upper mantle. *Journal of Geophysical Research* 101: 22273–22289.

Bhattacharyya J, Shearer P, and Masters G (1993) Inner core attenuation from short period *PKP*(*BC*) versus *PKP*(*DF*) waveforms. *Geophysical Journal International* 114: 1–11.

Billien M and Lévêque J (2000) Global maps of Rayleigh wave attenuation for periods between 40 and 150 seconds. *Geophysical Research Letters* 27: 3619–3622.

Bollinger GA (1979) Attenuation of the *Lg* phase and determination of m_b in the Southeastern United States. *Bulletin of the Seismological Society of America* 69: 45–63.

Bolt BA (1977) The detection of PKIIKP and damping in the inner core. *Annali di Geofisica* 30: 507–520.

Bowers RJ (2000) Observations of PKP(DF) and PKP(BC) across the United Kingdom: Implications for studies of attenuation in the Earth's core. *Geophysical Journal International* 140: 374–384.

Bowman JR (1988) Body wave attenuation structure in the Tonga subduction zone. *Journal of Geophysical Research* 93: 2125–2139.

Bowman JR and Kennett BLN (1991) Propagation of *Lg* waves in the North Australian craton: Influence of crustal velocity gradients. *Bulletin of the Seismological Society of America* 81: 592–610.

Boyd OS and Sheehan AF (2005) Attenuation tomography beneath the rocky mountain front: Implications for the physical state of the upper mantle. In: Karlstrom KE and Keler GR (eds.) *The Rocky Mountain Region: An evolving lithosphere*. *Geophysical Monograph Series*, vol. 154, pp. 361–377. Washington, DC: American Geophysical Union.

Brune JN (1970) Tectonic stress and the spectra of seismic shear waves from earthquakes. *Journal of Geophysical Research* 75: 4997–5009.

Buland R and Gilbert F (1978) Improved resolution of complex eigenfrequencies in analytically continued seismic spectra. *Geophysical Journal of the Royal Astronomical Society* 52: 457–470.

Cammarano F, Goes S, Vacher P, and Giardini D (2003) Inferring upper-mantle temperatures from seismic velocities. *Physics of the Earth and Planetary Interiors* 138: 197–222.

Cammarano F and Romanowicz B (2007) Insights into the nature of the transition zone from physically constrained inversion of long period seismic data. *Proceedings of the National Academy of Sciences of the United States of America* 104: 9139–9144. http://dx.doi.org/10.1073/pnas.0608075104.

Cammarano F and Romanowicz B (2008) Radial profiles of seismic attenuation in the upper mantle based on physical models. *Geophysical Journal International* 175: 116–134.

Campillo M, Plantet JL, and Bouchon M (1985) Frequency-dependent attenuation in the crust beneath central France from *Lg* waves: Data analysis and numerical modeling. *Bulletin of the Seismological Society of America* 75: 1395–1411.

Canas JA and Mitchell BJ (1978) Lateral variation of surface-wave anelastic attenuation across the Pacific. *Bulletin of the Seismological Society of America* 68: 1637–1650.

Canas JA and Mitchell BJ (1981) Rayleigh-wave attenuation and its variation across the Atlantic Ocean. *Geophysical Journal of the Royal Astronomical Society* 67: 159–176.

Cao A and Romanowicz B (2004) Hemispherical transition of seismic attenuation at the top of the Earth's inner core. *Earth and Planetary Science Letters* 228: 243–253.

Cao A and Romanowicz B (2009) Constraints on shear wave attenuation in the Earth's inner core from an observation of PKJKP. *Geophysical Research Letters* 36: L09301. http://dx.doi.org/10.1029/2009GL038342.

Cao A, Romanowicz B, and Takeuchi N (2005) An observation of *PKJKP*: Inferences on inner core shear properties. *Science* 308: 1453–1455.

Carcione JM and Cavallini F (1995) A rheological model for anelastic anisotropic media with applications to seismic wave propagation. *Geophysical Journal International* 119: 338–348.

Carpenter PJ and Sanford AR (1985) Apparent *Q* for upper crustal rocks of the central Rio Grande Rift. *Journal of Geophysical Research* 90: 8661–8674.

Chan WW and Der ZA (1988) Attenuation of multiple *ScS* in various parts of the world. *Geophysical Journal International* 92: 303–314.

Chavez D and Priestley KF (1986) Measurement of frequency dependent *Lg* attenuation in the Great Basin. *Geophysical Research Letters* 60: 551–554.

Chen PF, Bina CR, and Okal EA (2001) Variations in slab dip along the subducting Nazca plate, as related to stress patterns and moment release of intermediate-depth seismicity and to surface volcanism. *Geochemistry, Geophysics, Geosystems* 2. http://dx.doi.org/10.1029/2001GC000153.

Cheng HX and Kennett BLN (2002) Frequency dependence of seismic wave attenuation in the upper mantle in the Australian region. *Geophysical Journal International* 150: 45–47.

Cheng CC and Mitchell BJ (1981) Crustal *Q* structure in the United States from multi-mode surface waves. *Bulletin of the Seismological Society of America* 71: 161–181.

Chouet B (1979) Temporal variation in the attenuation of earthquake coda near Stone Canyon, California. *Geophysical Research Letters* 6: 143–146.

Choy G and Cormier VF (1983) The structure of the inner core inferred from short-period and broadband GDSN data. *Geophysical Journal International* 63: 457–470.

Chun KY, West GF, Kikoski RJ, and Samson C (1987) A novel technique for measuring *Lg* attenuation – Results from eastern Canada between 1-Hz and 10-Hz. *Bulletin of the Seismological Society of America* 77: 398–419.

Cicerone RD, Doll CG, and Toksöz MN (2011) Scattering and attenuation of seismic waves in northeastern North America. *Bulletin of the Seismological Society of America* 101: 2897–2903.

Cong L and Mitchell BJ (1998) Seismic velocity and *Q* structure of the Middle Eastern crust and upper mantle from surface-wave dispersion and attenuation. *Pure and Applied Geophysics* 153: 503–538.

Cormier VF (1981) Short period *PKP* phases and the anelastic mechanism of the inner core. *Physics of the Earth and Planetary Interiors* 24: 291–301.

Cormier VF (2007) Texture of the uppermost inner core from forward- and back-scattered seismic waves. *Earth and Planetary Science Letters* 258: 442–453.

Cormier VF and Li X (2002) Frequency-dependent seismic attenuation in the inner core. Part 2: A scattering and fabric interpretation. *Journal of Geophysical Research* 107. http://dx.doi.org/10.1029/2002JB001796.

Cormier VF and Richards P (1976) Comments on the damping of core waves by Anthony Qamar and Alfredo Eisenberg. *Journal of Geophysical Research* 81: 3066–3068.

Cormier VF and Richards P (1988) Spectral synthesis of body waves in Earth models specified by vertically varying layers. In: Doornbos D (ed.) *Seismological Algorithms*, pp. 3–45. San Diego, CA: Academic Press.

Cormier VF and Stroujkova A (2005) Waveform search for the innermost inner core. *Earth and Planetary Science Letters* 236: 96–105.

Cormier VF, Xu L, and Choy GL (1998) Seismic attenuation of the inner core: Viscoelastic or stratigraphic? *Geophysical Research Letters* 25: 4019–4022.

Creager KC (1992) Anisotropy of the inner core from differential travel times of the phases *PKP* and *PKIKP*. *Nature* 356: 309–314.

Creager KC (1999) Large-scale variations in inner core anisotropy. *Journal of Geophysical Research* 104: 23127–23139.

Dainty AM (1981) A scattering model to explain *Q* observations in the lithosphere between 1 and 30 Hz. *Geophysical Research Letters* 8: 1126–1128.

Dalton C and Ekström G (2006a) Constraints on global maps of phase velocity from surface-wave amplitudes. *Geophysical Journal International* 167: 820–826.

Dalton C and Ekström G (2006b) Global models of surface wave attenuation. *Journal of Geophysical Research* 111. http://dx.doi.org/10.1029/2005JB003997.

Dalton CA, Ekström G, and Dziewonski AM (2008) The global attenuation structure of the upper mantle. *Journal of Geophysical Research* 113. http://dx.doi.org/10.1029/2007JB005429.

Dalton CA, Ekström G, and Dziewonski AM (2009) Global seismological shear velocity and attenuation: A comparison with experimental observations. *Earth and Planetary Science Letters* 284: 65–75.

Dalton CA and Faul U (2010) The oceanic and cratonic upper mantle: Clues from joint interpretation of global velocity and attenuation models. *Lithos* 120: 160–172.

Davies JH (1990) Mantle plumes, mantle stirring and hotspot geometry. *Earth and Planetary Science Letters* 99: 94–109.

Davies JH (1999) The role of hydraulic fractures and intermediate-depth earthquakes in generating subduction-zone magmatism. *Nature* 398: 142–145.

Der ZA, McElfresh TW, and O'Donnell A (1982) An investigation of the regional variations and frequency dependence of anelastic attenuation in the mantle under the United States in the 0.5–4 Hz band. *Geophysical Journal of the Royal Astronomical Society* 69: 67–99.

Deschamps A (1977) Inversion of the attenuation data of free oscillations of the Earth (fundamental and first higher modes). *Geophysical Journal of the Royal Astronomical Society* 50: 699–722.

DeSouza JL and Mitchell BJ (1998) *Lg* coda *Q* variations across South America and their relation to crustal evolution. *Pure and Applied Geophysics* 153: 587–612.

Ding CY and Grand SP (1993) Upper mantle Q structure under the East Pacific Rise. *Journal of Geophysical Research* 98: 1973–1975.

Doornbos DJ (1974) The anelasticity of the inner core. *Geophysical Journal of the Royal Astronomical Society* 38: 397–415.

Doornbos DJ (1983) Observable effects of the seismic absorption band in the Earth. *Geophysical Journal of the Royal Astronomical Society* 57: 381–395.

Durand S, Chambat F, Matas J, and Ricard Y (2012) Constraining the kinetics of mantle phase changes with seismic data. *Geophysical Journal International* 189: 1557–1564.

Durand S, Matas J, Ford S, Ricard Y, Romanowicz B, and Montagner JP (2013) Insights from ScS–S measurements on deep mantle attenuation. *Geophysical Journal International* 374: 101–110.

Durek JJ and Ekström G (1995) Evidence for bulk attenuation in the asthenosphere from recordings of the Bolia earthquake. *Geophysical Research Letters* 22: 2309–2312.

Durek JJ and Ekström G (1996) A radial model of anelasticity consistent with long-period surface wave attenuation. *Bulletin of the Seismological Society of America* 86: 144–158.

Durek JJ and Ekström G (1997) Investigating discrepancies among measurements of traveling and standing wave attenuation. *Journal of Geophysical Research* 102: 24529–24544.

Durek JJ, Ritzwoller MH, and Woodhouse JH (1993) Constraining upper mantle anelasticity using surface wave amplitude anomalies. *Geophysical Journal International* 114: 249–272.

Dziewonski AM and Anderson DL (1981) Preliminary reference Earth model. *Physics of the Earth and Planetary Interiors* 25: 297–356.

Dziewonski AM and Steim JM (1982) Dispersion and attenuation of mantle waves through waveform inversion. *Geophysical Journal of the Royal Astronomical Society* 70: 503–527.

Eberhart-Phillips D and Chadwick M (2002) Three-dimensional attenuation model of the shallow Hikurangi subduction zone in the Raukumara Peninsula, New Zealand. *Journal of Geophysical Research* 107. http://dx.doi.org/10.1029/2000JB000; 046.

Ekström G and Dziewonski AM (1997) The unique anisotropy of the Pacific upper mantle. *Nature* 394: 168–172.

Ekström G, Tromp J, and Larson EWF (1997) Measurements and global models of surface wave propagation. *Journal of Geophysical Research* 102: 8137–8157.

Evernden JF (1955) Tripartite results for the Kamchatka earthquake of November 4, 1952. *Bulletin of the Seismological Society of America* 45: 167–178.

Farla RM, Jackson I, FitzGerald JD, Faul UH, and Zimmerman ME (2012) Dislocation damping and anisotropic seismic wave attenuation in earth's upper mantle. *Science* 336: 332–335.

Faul U, FitzGerald J, and Jackson I (2004) Shear wave attenuation and dispersion in melt-bearing olivine polycrystals. Part 2: Microstructural interpretation and seismological implications. *Journal of Geophysical Research* 109. http://dx.doi.org/10.1029/2003JB002407.

Faul U and Jackson I (2005) The seismological signature of temperature and grain size variations in the upper mantle. *Earth and Planetary Science Letters* 234: 119–134.

Fearn DR, Loper DE, and Roberts PH (1981) Structure of the Earth's inner core. *Nature* 292: 232–233.

Fisher JL and Wysession ME (2003) Small-scale lateral variations in D″ attenuation and velocity structure. *Geophysical Research Letters* 30. http://dx.doi.org/10.1029/2002GL016179.

Flanagan MP and Wiens DA (1990) Attenuation structure beneath the Lau back arc spreading center from teleseismic S phases. *Geophysical Research Letters* 17: 2117–2120.

Flanagan MP and Wiens DA (1994) Radial upper mantle structure of inactive back-arc basins from differential shear wave measurements. *Journal of Geophysical Research* 99: 15469–15485.

Flanagan MP and Wiens DA (1998) Attenuation of broadband P and S waves in Tonga: Observations of frequency dependent Q. *Pure and Applied Geophysics* 153: 345–375.

Ford SR, Dreger DS, Mayeda K, Walter WR, Malagnini L, and Phillips WS (2008) Regional attenuation in northern California: A comparison of five 1D Q methods. *Bulletin of the Seismological Society of America* 98: 2033–2046.

Ford SR, Garnero EJ, and Thorne MS (2012) Differential t* measurements via instantaneous frequency matching: Observations of lower mantle shear attenuation heterogeneity beneath western Central America. *Geophysical Journal International* 189: 513–523.

Frankel A and Wennerberg L (1987) Energy-flux model for seismic coda: Separation of scattering and intrinsic attenuation. *Bulletin of the Seismological Society of America* 77: 1223–1251.

Futterman A (1962) Dispersive body waves. *Journal of Geophysical Research* 67: 5279–5291.

Gao J, Yang S, Wang D, and Wu R (2011) Estimation of quality factor Q from the instantaneous frequency at the envelope peak of a seismic signal. *Journal of Computational Acoustics* 19: 155–179. http://dx.doi.org/10.1142/S0218396x11004390.

Garcia R (2002) Constraints on upper inner-core structure from waveform inversion of core phases. *Geophysical Journal International* 150: 651–664.

Geller RJ and Stein S (1978) Time domain measurements of attenuation of fundamental modes ($_0S_6$–$_0S_{28}$). *Bulletin of the Seismological Society of America* 69: 1671–1691.

Getting IC, Dutton SJ, Burnley PC, Karato SI, and Spetzler HA (1997) Shear attenuation and dispersion in MgO. *Physics of the Earth and Planetary Interiors* 99: 249–257.

Giardini DXDL and Woodhouse JH (1988) Splitting functions of long period normal modes of the Earth. *Journal of Geophysical Research* 93: 13716–13742.

Gilbert F and Dziewonski AM (1975) An application of normal mode theory to the retrieval of structural parameters and source mechanisms from seismic spectra. *Philosophical Transactions of the Royal Society of London, Series A* 278: 187–269.

Gomer BM and Okal EA (2003) Multiple-ScS probing of the Ontong-Java Plateau. *Physics of the Earth and Planetary Interiors* 138: 317–331.

Gueguen Y, Darot M, Mazot P, and Woirgard J (1989) Q^{-1} of forsterite single crystals. *Physics of the Earth and Planetary Interiors* 55: 254–258.

Gung Y, Panning M, and Romanowicz BA (2003) Anisotropy and thickness of the lithosphere. *Nature* 422: 707–711.

Gung Y and Romanowicz BA (2004) Q tomography of the upper mantle using three component long period waveforms. *Geophysical Journal International* 157: 813–830.

Gusev AA and Abubakirov IR (1996) Simulated envelopes of non-isotropically scattered body waves as compared to observed ones: Another manifestation of fractal inhomogeneity. *Geophysical Journal International* 127: 49–60.

Gutenberg B (1924) Dispersion und extinktion von seismischen oberflächenwellen und der aufbau der obersten erdschichten. *Physikalische Zeitschrift* 25: 377–381.

Gutenberg B (1945a) Amplitudes of *P*, *PP*, and *SS* and magnitude of shallow earthquakes. *Bulletin of the Seismological Society of America* 35: 57–69.

Gutenberg B (1945b) Amplitudes of surface waves and magnitudes of shallow earthquakes. *Bulletin of the Seismological Society of America* 35: 3–12.

Gutenberg B (1958) Attenuation of seismic waves in the Earth's mantle. *Bulletin of the Seismological Society of America* 48: 269–282.

Haberland C and Rietbrock A (2001) Attenuation tomography in the western central Andes: A detailed insight into the structure of a magmatic arc. *Journal of Geophysical Research* 106: 11151–11167.

Hasegawa HS (1974) Theoretical synthesis and analysis of strong motion spectra of earthquakes. *Canadian Geotechnical Journal* 11: 278–297.

Hasegawa HS (1985) Attenuation of *Lg* waves in the Canadian shield. *Bulletin of the Seismological Society of America* 75: 1569–1582.

Hauksson E (2006) Attenuation models (Q_P and Q_S) in three dimensions of the Southern California crust: Inferred fluid saturation at seismogenic depths. *Journal of Geophysical Research* 111(B05): 302. http://dx.doi.org/10.1029/2005JB003947.

He X and Tromp J (1996) Normal-mode constraints on the structure of the Earth. *Journal of Geophysical Research* 101: 20053–20082.

Helffrich G, Kaneshima S, and Kendall JM (2002) A local, crossing-path study of attenuation and anisotropy of the inner core. *Geophysical Research Letters* 29. http://dx.doi.org/10.1029/2001GL014059.

Herrmann RB (1980) *Q* estimates using the coda of local earthquakes. *Bulletin of the Seismological Society of America* 70: 447–468.

Herrmann RB and Mitchell BJ (1975) Statistical analysis and interpretation of surface-wave anelastic attenuation data for the stable interior of North America. *Bulletin of the Seismological Society of America* 65: 1115–1128.

Hough SE, Anderson JG, Brune J, et al. (1988) Attenuation near Anza, California. *Bulletin of the Seismological Society of America* 78: 672–691.

Hough SE, Lees JM, and Monastero F (1999) Attenuation and source properties at the Coso geothermal area, California. *Bulletin of the Seismological Society of America* 89: 1606–1619.

Humphreys E and Clayton RW (1988) Adaptation of back projection tomography to seismic travel time problems. *Journal of Geophysical Research* 93: 1073–1086.

Hwang HJ and Mitchell BJ (1987) Shear velocities, Q_β, and the frequency dependence of Q_β in stable and tectonically active regions from surface wave observations. *Geophysical Journal of the Royal Astronomical Society* 90: 575–613.

Hwang YK and Ritsema J (2011) Radial Q_β structure of the lower mantle from teleseismic body-wave spectra. *Earth and Planetary Science Letters* 303: 369–375.

Hwang YK, Ritsema J, and Goes S (2009) Spatial variations of P wave attenuation in the mantle beneath North America. *Journal of Geophysical Research* 114: B06312.

Hwang YK, Ritsema J, and Goes S (2011) Global variations of body-wave attenuation in the upper mantle from teleseismic P wave and S wave spectra. *Geophysical Research Letters* 38: L06308.

Ichikawa M and Basham PW (1965) Variations in short-period records from Canadian seismograph stations. *Canadian Journal of Earth Sciences* 2: 510–542.

Iritani R, Takeuchi N, and Kawakatsu H (2010) Seismic attenuation structure of the top half of the inner core beneath the northeastern Pacific. *Geophysical Research Letters* 37: L19303.

Ishii M and Dziewonski AM (2002) The innermost inner core of the earth: Evidence for a change in anisotropic behavior at the radius of about 300 km. *Proceedings of the National Academy of Sciences of the United States of America* 22: 14026–14030.

Isse T and Nakanishi I (1997) The effect of the crust on the estimation of mantle Q from spectral ratios of multiple ScS phases. *Bulletin of the Seismological Society of America* 87: 778–781.

Ivan M, Marza V, de Farias Caixeta D, and de Melo Arraes T (2005) Uppermost inner core attenuation from PKP data at South American seismological stations. *Geophysical Journal International* 164: 441–448.

Jackson I (1993) Progress in the experimental study of seismic wave attenuation. *Annual Review of Earth and Planetary Sciences* 21: 375–406.

Jackson I (2000) Laboratory measurement of seismic wave dispersion and attenuation: Recent progress. *Journal of Geophysical Research* 109. http://dx.doi.org/10.1029/2003JB002406.

Jackson I (2007) Properties of rocks and minerals – Physical origins of anelasticity and attenuation in rock. In: Romanowicz B and Dziewonski AM (eds.) *Treatise on Geophysics*, vol. 1, pp. 493–525. USA: Elsevier.

Jackson I and Faul UH (2010) Grainsize-sensitive viscoelastic relaxation in olivine: Towards a robust laboratory-based model for seismological application. *Physics of the Earth and Planetary Interiors* 183: 151–163. http://dx.doi.org/10.1016/j.pepi.2010.09.005.

Jackson I, Faul UH, Fitzgerald JD, and Tan BH (2004) Shear wave attenuation and dispersion in melt-bearing olivine polycrystals. Part 1: Specimen fabrication and mechanical testing. In: Karato S-I, Forte AM, Liebermann RC, Masters G, and Stixrude L (eds.) *Earth's Deep Interior: Mineral Physics and Tomography from the Atomic to the Global Scale*. *Geophysical Monograph Series*, vol. 117, pp. 265–289. Washington, DC: American Geophysical Union.

Jeffreys H (1939) The times of the core waves. *Monthly Notices of the Royal Astronomical Society of Geophysics* (supplement 4): 498.

Jeffreys H (1967) Radius of the Earth's core. *Nature* 215: 1365–1366.

Jemberie AL and Mitchell BJ (2004) Shear-wave *Q* structure and its lateral variation in the crust of China and surrounding regions. *Geophysical Journal International* 157: 363–380.

Jin A and Aki K (1986) Temporal change in coda *Q* before the Tangshan earthquake of 1976 and the Haicheng earthquake of 1975. *Journal of Geophysical Research* 91: 665–673.

Jobert N and Roult G (1976) Periods and damping of free oscillations observed in France after 16 earthquakes. *Geophysical Journal of the Royal Astronomical Society* 45: 155–176.

Jordan TH and Sipkin SS (1977) Estimation of the attenuation operator for multiple ScS waves. *Geophysical Research Letters* 4: 167–170.

Kanamori H (1970) Velocity and Q of mantle waves. *Physics of the Earth and Planetary Interiors* 2: 259–275.

Kanamori H and Anderson DL (1977) Importance of physical dispersion in surface-wave and free oscillation problems. *Reviews of Geophysics* 15: 105–112.

Karato SI (1993) Importance of anelasticity in the interpretation of seismic tomography. *Geophysical Research Letters* 20: 1623–1626.

Karato SI (1998) A dislocation model of seismic wave attenuation and micro-creep in the Earth: Harold Jeffreys and the rheology of the solid Earth. *Pure and Applied Geophysics* 153: 239–256.

Karato SI and Karki BB (2001) Origin of lateral variation of seismic wave velocities and density in the deep mantle. *Journal of Geophysical Research* 106: 21771–21783.

Karato SI and Spetzler H (1990) Defect microdynamics in minerals and solid state mechanisms of seismic wave attenuation and velocity dispersion in the mantle. *Reviews of Geophysics* 28: 399–421.

Kazama T, Kawakatsu H, and Takeuchi N (2008) Depth-dependent attenuation structure of the inner core inferred from short-period Hi-net data. *Physics of the Earth and Planetary Interiors* 167: 155–160.

Kijko A and Mitchell BJ (1983) Multimode Rayleigh wave attenuation and Q_β in the crust of the Barents shelf. *Journal of Geophysical Research* 88: 3315–3328.

Knopoff L (1964) Q. *Reviews of Geophysics* 2: 625–660.

Komatitsch D, Ritsema J, and Tromp J (2002) The spectral-element method, Beowulf computing, and global seismology. *Science* 298: 1737–1742.

Kovach RL and Anderson DL (1964) Attenuation of shear waves in the upper and lower mantle. *Bulletin of the Seismological Society of America* 54: 1855–1864.

Krasnoshchekov DN, Kaazik PB, and Ovtchinnikov VM (2005) Seismological evidence for mosaic structure of the surface of the Earth's inner core. *Nature* 435: 483–487.

Kumazawa M, Imanashi Y, Fukao Y, Furumoto M, and Yananoto A (1990) A theory of spectral analysis based on the characteristic property of a linear dynamical system. *Geophysical Journal International* 101: 613–630.

Kuster GT (1972) *Seismic Wave Propagation in Two-Phase Media and Its Application to the Earth's Interior*. PhD Dissertation, Cambridge, MA: MIT.

Lawrence JF and Prieto G (2011) Attenuation tomography of the western United States from ambient seismic noise. *Journal of Geophysical Research* 116: B06302. http://dx.doi.org/10.1029/2010JB007836.

Lawrence JF, Shearer P, and Masters G (2006) Mapping attenuation beneath North America using waveform cross-correlation and cluster analysis. *Geophysical Research Letters* 33. http://dx.doi.org/10.1029/2006GL025813.

Lawrence JF and Wysession ME (2006a) QLM9: A new radial quality factor (Q_{mu}) model for the lower mantle. *Earth and Planetary Science Letters* 241: 962–971.

Lawrence JF and Wysession ME (2006b) Seismic evidence for subduction-transported water in the lower mantle. In: *Earth's Deep Water Cycle*. *Geophysics Monograph Series*, vol. 168, p. 251. Washington, DC: American Geophysical Union.

Lay T and Kanamori H (1985) Geometric effects of global lateral heterogeneity on long-period surface wave propagation. *Journal of Geophysical Research* 90: 605–621.

Lay T and Wallace T (1983) Multiple ScS travel times and attenuation beneath Mexico and Central America. *Geophysical Research Letters* 10: 301–304.

Lay T and Wallace T (1988) Multiple ScS attenuation and travel times beneath Western North America. *Bulletin of the Seismological Society of America* 78: 2041–2061.

Lee WB and Solomon SC (1979) Simultaneous inversion of surface-wave phase velocity and attenuation: Rayleigh and Love waves over continental and oceanic paths. *Bulletin of the Seismological Society of America* 69: 65–95.

Lekic V, Matas J, Panning M, and Romanowicz B (2009) Measurement and implications of frequency dependence of attenuation. *Earth and Planetary Science Letters* 282: 285–293.

Leyton P and Koper KD (2007) Using PKiKP coda to determine inner core structure: 2. Determination of Q_C. *Journal of Geophysical Research* 112: B05317.

Li XD (1990) *Asphericity of the Earth from Free Oscillations*. PhD Dissertation, Cambridge, MA: Harvard University.

Li L (2010) Bulk attenuation in the earth's mantle due to phase transitions. *Physics of the Earth and Planetary Interiors* 183: 473–477.

Li X and Cormier VF (2002) Frequency-dependent seismic attenuation in the inner core. Part 1: A viscoelastic interpretation. *Journal of Geophysical Research* 107. http://dx.doi.org/10.1029/2002JB001795.

Li XD and Romanowicz B (1995) Comparison of global waveform inversions with and without considering cross branch coupling. *Geophysical Journal International* 121: 695–709.

Liu HP, Anderson DL, and Kanamori H (1976) Velocity dispersion due to anelasticity: Implication for seismology and mantle composition. *Geophysical Journal of the Royal Astronomical Society* 47: 41–58.

Lomnitz C (1957) Linear dissipation in solids. *Journal of Applied Physics* 28: 201–205.

Loper DE and Fearn DR (1983) A seismic model of a partially molten inner core. *Journal of Geophysical Research* 88: 1235–1242.

Loper DE and Roberts PH (1981) A study of conditions at the inner core boundary of the Earth. *Physics of the Earth and Planetary Interiors* 24: 302–307.

Luh P (1974) Normal modes of a rotating, self gravitating inhomogeneous Earth. *Geophysical Journal of the Royal Astronomical Society* 38: 187–224.

Lundquist GM and Cormier VC (1980) Constraints on the absorption band model of Q. *Journal of Geophysical Research* 85: 5244–5256.

Malin PE (1978) *A First Order Scattering Solution for Modeling Lunar and Terrestrial Seismic Coda*. PhD Dissertation, Princeton, NJ: Princeton University.

Masters G and Gilbert F (1981) Structure of the inner core inferred from observations of its spheroidal shear modes. *Geophysical Research Letters* 8: 569–571.

Masters G and Gilbert F (1983) Attenuation in the Earth at low frequencies. *Philosophical Transactions of the Royal Society of London, Series XI* 308: 479–522.

Masters G and Laske G (1997) On bias in surface wave and free oscillation attenuation measurements. *Eos Transactions of the American Geophysical Union* 78: F485.

McCarthy C and Takei Y (2011) Anelasticity and viscosity of partially molten rock analogue: Toward seismic detection of small quantities of melt. *Geophysical Research Letters* 38: L18306. http://dx.doi.org/10.1029/2011GL048776.

McCarthy C, Takei Y, and Hiraga T (2011) Experimental study of attenuation and dispersion over a broad frequency range: 2. The universal scaling of polycrystalline materials. *Journal of Geophysical Research* 116: B09207. http://dx.doi.org/10.1029/2011JB008384.

Mills J and Hales A (1978) Great circle Rayleigh wave attenuation and group velocity. Part III: Inversion of global average group velocity and attenuation coefficients. *Physics of the Earth and Planetary Interiors* 17: 307–322.

Minster B and Anderson DL (1981) A model of dislocation controlled rheology for the mantle. *Philosophical Transactions of the Royal Society of London, Series A* 299: 319–356.

Mitchell BJ (1973) Radiation and attenuation of Rayleigh waves from the Southeastern Missouri earthquake of October 21, 1965. *Journal of Geophysical Research* 78: 886–899.

Mitchell BJ (1975) Regional Rayleigh wave attenuation on North America. *Journal of Geophysical Research* 35: 4904–4916.

Mitchell BJ (1995) Anelastic structure and evolution of the continental crust and upper mantle from seismic surface wave attenuation. *Reviews of Geophysics* 33: 441–462.

Mitchell BJ, Baqer S, Akinci A, and Cong L (1998) *Lg* coda *Q* in Australia and its relation to crustal structure and evolution. *Pure and Applied Geophysics* 153: 639–653.

Mitchell BJ and Cong L (1998) *Lg* coda *Q* and its relation to the structure and evolution of continents: A global perspective. *Pure and Applied Geophysics* 153: 655–663.

Mitchell BJ, Cong L, and Ekström G (2008) A continent-wide 1-Hz map of Lg coda Q variation across Eurasia and its implications for lithospheric evolution. *Journal of Geophysical Research* 113. http://dx.doi.org/10.1029/2007JB005065.

Mitchell BJ and Helmberger DV (1973) Shear velocities at the base of the mantle from observations of *S* and *ScS*. *Journal of Geophysical Research* 78: 6009–6020.

Mitchell BJ and Hwang HJ (1987) The effect of low-*Q* sediments and crustal *Q* on *Lg* attenuation in the United States. *Bulletin of the Seismological Society of America* 77: 1197–1210.

Mitchell BJ, Pan Y, Xie J, and Cong L (1997) *Lg* coda *Q* across Eurasia and its relation to crustal evolution. *Journal of Geophysical Research* 102: 22767–22779.

Mitchell BJ and Xie J (1994) Attenuation of multiphase surface waves in the Basin and Range province. Part III: Inversion for crustal anelasticity. *Geophysical Journal International* 116: 468–484.

Mitchell BJ, Cong L, and Jemberie A (2014) Continent-wide maps of Lg coda Q for North America and their relationship to crustal structure and evolution. *Bulletin of the Seismological Society of America*. http://dx.doi.org/10.1785/0120130235.

Modiano T and Hatzfeld D (1982) Experimental study of the spectral content for shallow earthquakes. *Bulletin of the Seismological Society of America* 72: 1739–1758.

Molnar P and Oliver J (1969) Lateral variations in attenuation in the upper mantle and discontinuities in the lithosphere. *Journal of Geophysical Research* 74: 2648–2682.

Monnereau M, Calvet M, Margerin L, and Souriau A (2010) Lopsided growth of Earth's inner core. *Science* 328: 1014–1017.

Montagner JP and Kennett BLN (1996) How to reconcile body-wave and normal-mode reference Earth models. *Geophysical Journal International* 125: 229–248.

Montagner JP and Tanimoto T (1991) Global upper mantle tomography of seismic velocities and anisotropy. *Journal of Geophysical Research* 96: 20337–20351.

Morelli A, Dziewonski AM, and Woodhouse JH (1986) Anisotropy of the core inferred from PKIKP travel times. *Geophysical Research Letters* 13: 1545–1548.

Morris SJS and Jackson I (2009) Diffusionally-assisted grain-boundary sliding and viscoelasticity of polycrystals. *Journal of the Mechanics and Physics of Solids* 57: 744–761.

Mueller G (1986) Rheological properties and velocity dispersion of a medium with power law dependence of Q in frequency. *Journal of Geophysics* 54: 20–29.

Myers SC, Beck S, Zandt G, and Wallace T (1998) Lithospheric-scale structure across the Bolivian Andes from tomographic images of velocity and attenuation for P and S waves. *Journal of Geophysical Research* 103: 21233–21252.

Nakajima J and Hasegawa A (2003) Estimation of thermal structure in the mantle wedge of northeastern Japan from seismic attenuation data. *Geophysical Research Letters* 30(14): 1760. http://dx.doi.org/10.1029/2003GL017185.

Nakanishi I (1978) Regional differences in the phase velocity and the quality factor Q of mantle Rayleigh waves. *Science* 200: 1379–1381.

Nakanishi I (1979a) Attenuation of multiple ScS waves beneath the Japanese Arc. *Physics of the Earth and Planetary Interiors* 19: 337–347.

Nakanishi I (1979b) Phase velocity and Q of mantle Rayleigh waves. *Geophysical Journal of the Royal Astronomical Society* 58: 35–59.

Nakanishi I (1981) Shear velocity and shear attenuation models inverted from the worldwide and pure-path average data of mantle Rayleigh waves ($_0S_{25}$ to $_0S_{80}$) and fundamental spheroidal modes ($_0S_2$ to $_0S_{24}$). *Geophysical Journal of the Royal Astronomical Society* 66: 83–130.

Niazi M and Johnson LR (1992) Q in the inner core. *Physics of the Earth and Planetary Interiors* 74: 55–62.

Niu F and Wen L (2001) Hemispherical variations in seismic velocity at the top of the Earth's inner core. *Nature* 410: 1081–1084.

Nuttli OW (1973) Seismic wave attenuation and magnitude relations for Eastern North America. *Journal of Geophysical Research* 78: 876–885.

Nuttli OW (1978) A time-domain study of the attenuation of 10-Hz waves in the New Madrid seismic zone. *Bulletin of the Seismological Society of America* 68: 343–355.

Nuttli OW (1980) The excitation and attenuation of seismic crustal phases in Iran. *Bulletin of the Seismological Society of America* 70: 469–484.

O'Connell RJ and Budiansky B (1978) Measures of dissipation in viscoelastic media. *Geophysical Research Letters* 5: 5–8.

Ojeda A and Ottemöller L (2002) Q_{Lg} tomography in Colombia. *Physics of the Earth and Planetary Interiors* 130: 253–270.

Okal EA and Jo BG (2002) *Q* measurements for phase X overtones. *Pure and Applied Geophysics* 132: 331–362.

Oki S, Fukao Y, and Obayashi M (2000) Reference frequency of teleseismic body waves. *Journal of Geophysical Research* 109. http://dx.doi.org/10.1029/2003JB002821.

Oki S and Shearer PM (2008) Mantle Q structure from S–P differential attenuation measurements. *Journal of Geophysical Research* 113. http://dx.doi.org/10.1029/2007JB005567.

Oreshin SI and Vinnik LP (2004) Heterogeneity and anisotropy of seismic attenuation in the inner core. *Geophysical Research Letters* 31. http://dx.doi.org/10.1029/2003GL018591.

Ottemöller L, Shapiro NM, Singh SK, and Pacheco JF (2002) Lateral variation of *Lg* wave propagation in southern Mexico. *Journal of Geophysical Research* 107(B1): Art No. 2008. http://dx.doi.org/10.1029/2001JB000, 206.

Park J (1987) Asymptotic coupled-mode expressions for multiplet amplitude anomalies and frequency shift on a laterally heterogeneous Earth. *Geophysical Journal of the Royal Astronomical Society* 90: 129–170.

Pasyanos ME, Matzel EM, Walter WR, and Rodgers AJ (2009) Broad-band Lg attenuation modelling in the Middle East. *Geophysical Journal International* 177: 1166–1176.

Patton HJ and Taylor SR (1989) *Q* structure of the Basin and Range from surface waves. *Journal of Geophysical Research* 89: 6929–6940.

Peacock S and Hudson JA (1990) Seismic properties of rocks with distributions of small cracks. *Geophysical Journal International* 102: 471–484.

Phillips S, Hartse HE, Taylor SR, and Randall GE (2000) 1 Hz *Lg* Q tomography in central Asia. *Geophysical Research Letters* 27: 3425.

Pozgay SH, Wiens DA, Conder JA, Shiobara H, and Sugioka S (2009) Seismic attenuation tomography of the Mariana subduction system: Implications for thermal structure, volatile distribution, and slow spreading dynamics. *Geochemistry, Geophysics, Geosystems* 19: Q04X05.

Press F (1956) Rigidity of the Earth's core. *Science* 124: 1204.

Prieto GA, Lawrence JF, and Beroza GC (2009) Anelastic Earth structure from the coherency of the ambient seismic field. *Journal of Geophysical Research* 114: B07303. http://dx.doi.org/10.1029/2008JB006067.

Randall MJ (1976) Attenuative dispersion and frequency shifts of the Earth's free oscillations. *Physics of the Earth and Planetary Interiors* 12: P1–P4.

Reid FJL, Woodhouse JH, and van Heist H (2001) Upper mantle attenuation and velocity structure from measurements of differential S phases. *Geophysical Journal International* 145: 615–630.

Resovsky JS and Ritzwoller MH (1998) New and refined constraints on three-dimensional Earth structure from normal modes below 3 MHz. *Journal of Geophysical Research* 103: 783–810.

Resovsky JS, Trampert J, and van der Hilst RD (2005) Error bars for the global seismic Q profile. *Earth and Planetary Science Letters* 230: 413–423.

Revenaugh J and Jordan TH (1989) A study of mantle layering beneath the western Pacific. *Journal of Geophysical Research* 94: 5787–5813.

Revenaugh J and Jordan TH (1991) Mantle layering from ScS reverberations. Part 2: The transition zone. *Journal of Geophysical Research* 96: 19763–19780.

Ricard Y, Matas J, and Chambat F (2009) Seismic attenuation in a phase change coexistence loop. *Physics of the Earth and Planetary Interiors* 176(1–2): 124–131. http://dx.doi.org/10.1016/j.pepi.2009.04.007.

Richards PG and Menke W (1983) The apparent attenuation of a scattering medium. *Bulletin of the Seismological Society of America* 73: 1005–1021.

Romanowicz B (1987) Multiplet–multiplet coupling due to lateral heterogeneity: Asymptotic effects on the amplitude and frequency of the Earth's normal modes. *Geophysical Journal of the Royal Astronomical Society* 90: 75–100.

Romanowicz B (1990) The upper mantle degree. Part 2: Constraints and inferences on attenuation tomography from global mantle wave measurements. *Journal of Geophysical Research* 95: 11051–11071.

Romanowicz B (1994a) On the measurement of anelastic attenuation using amplitudes of low-frequency surface waves. *Physics of the Earth and Planetary Interiors* 84: 179–191.

Romanowicz B (1994b) Anelastic tomography: A new perspective on upper-mantle thermal structure. *Earth and Planetary Science Letters* 128: 113–121.

Romanowicz B (1995) A global tomographic model of shear attenuation in the upper mantle. *Journal of Geophysical Research* 100: 12375–12394.

Romanowicz B (1998) Attenuation tomography of the Earth's mantle: A review of current status. *Pure and Applied Geophysics* 153: 257–272.

Romanowicz B (2002) Inversion of surface waves: A review. In: Lee WHK (ed.) *Handbook of Earthquake and Engineering Seismology, IASPEI, Part A*, pp. 149–174. Amsterdam: Academic Press.

Romanowicz B and Durek J (2000) Seismological constraints on attenuation in the Earth: A review. In: Karato S-I, Forte AM, Liebermann RC, Masters G, and Stixrude L (eds.) *Earth's Deep Interior: Mineral Physics and Tomography from the Atomic to the Global Scale. Geophysical Monograph Series*, vol. 117, pp. 161–180. Washington, DC: American Geophysical Union.

Romanowicz B and Gung Y (2002) Superplumes from the core–mantle boundary to the lithosphere: Implications for heat-flux. *Science* 296: 513–516.

Romanowicz B and Mitchell BJ (2007) Deep earth structure: Q of the Earth from crust to core. In: Romanowicz B and Dziewonski AM (eds.) *Treatise on Geophysics*, vol. 1. chapter 1.21. USA: Elsevier.

Romanowicz B, Roult G, and Kohl T (1987) The upper mantle degree two pattern: Constraints from geoscope fundamental spheroidal model eigenfrequency and attenuation measurements. *Geophysical Research Letters* 14: 1219–1222.

Rosat S, Sato T, Imanishi Y, et al. (2005) High resolution analysis of the gravest seismic normal modes after the 2005 Mw = 9 Sumatra earthquake using superconducting gravimeter data. *Geophysical Research Letters* 32. http://dx.doi.org/10.1029/2005GL023128.

Roth E, Wiens DA, Dorman LM, Hildebrand J, and Webb SC (1999) Seismic attenuation tomography of the Tonga–Fiji region using phase pair methods. *Journal of Geophysical Research* 104: 4795–4809.

Roth E, Wiens DA, and Zhao D (2000) An empirical relationship between seismic attenuation and velocity anomalies in the upper mantle. *Geophysical Research Letters* 27: 601–604.

Roult G (1975) Attenuation of seismic waves of very low frequency. *Physics of the Earth and Planetary Interiors* 10: 159–166.

Roult G (1982) The effect of young oceanic regions on the periods and damping of free oscillation of the Earth. *Journal of Geophysical Research* 51: 38–43.

Roult G and Clévédé E (2000) New refinements in attenuation measurements from free oscillations and surface wave observations. *Physics of the Earth and Planetary Interiors* 121: 1–37.

Roult G, Romanowicz B, and Montagner JP (1984) 3D upper mantle shear velocity and attenuation from fundamental mode free oscillation data. *Geophysical Journal International* 101: 61–80.

Roult G, Rosat S, Clévédé E, Millot-Langet R, and Hinderer J (2006) New determination of Q quality factors eigenfrequencies for the whole set of singlets of Earth's normal modes ${}_0S_0$, ${}_0S_2$, ${}_0S_3$, and ${}_2S_1$, using superconducting Gravimeter data from the GGP network. *Journal of Geodynamics* 41: 345–357.

Ruan Y and Zhou Y (2010) The effects of 3-D anelasticity (Q) structure on surface wave phase delays. *Geophysical Journal International* 181: 479–492.

Ruan Y and Zhou Y (2012) The effects of 3-D anelasticity (Q) structure on surface wave amplitudes. *Geophysical Journal International* 189: 967–983.

Rychert CA, Fischer KM, Abers GA, and Plank T (2008) Strong along-arc variations in attenuation in the mantle wedge between Costa Rica and Nicaragua. *Geochemistry, Geophysics, Geosystems* 9: Q10S10.

Sacks IS (1969) Anelasticity of the inner core. *Annual Report of the Director of Department of Terrestrial Magnetism* 69: 416–419.

Sacks IS (1980) Q_s of the lower mantle – A body wave determination. *Annual Report of the Director of Department of Terrestrial Magnetism* 79: 508–512.

Sahin S, Xueyang B, Turkelli N, Sandvol E, Teoman U, and Kahraman M (2013) Lg wave attenuation in the Isparta Angle and Anatolian Plateau. *Pure and Applied Geophysics* 170: 337–351.

Sailor RV and Dziewonski AM (1978) Measurements and interpretation of normal mode attenuation. *Geophysical Journal of the Royal Astronomical Society* 53: 559–581.

Sarker G and Abers GA (1998) Comparison of seismic body wave and coda wave measures of Q. *Pure and Applied Geophysics* 153: 665–683.

Sarker G and Abers GA (1999) Lithospheric temperature estimates from seismic attenuation across range fronts in southern and central Eurasia. *Geology* 27: 427–430.

Sato R and Espinosa AF (1967) Dissipation in the Earth's mantle and rigidity and viscosity in the Earth's core determined from waves multiply-reflected from the mantle–core boundary. *Bulletin of the Seismological Society of America* 57: 829–856.

Sato H, Sacks IS, Murase T, Muncill G, and Fukuyama F (1989) Q_P-melting temperature relation in peridotite at high pressure and temperature: Attenuation mechanism and implications for the mechanical properties of the upper mantle. *Journal of Geophysical Research* 94: 10647–10661.

Savage B, Komatitsch D, and Tromp J (2010) Effects of 3D attenuation on seismic wave amplitude and phase measurements. *Bulletin of the Seismological Society of America* 100: 1241–1251.

Schlotterbeck BA and Abers GA (2001) Three-dimensional attenuation variations in Southern California. *Journal of Geophysical Research* 106: 30719–30735.

Schurr B, Asch G, Rietbrock A, Trumbull R, and Haberland C (2003) Complex patterns of fluid and melt transport in the central Andean subduction zone revealed by attenuation tomography. *Earth and Planetary Science Letters* 215(1–2): 105–119. http://dx.doi.org/10.1016/S0012-821X(03)00441-2.

Selby ND and Woodhouse JH (2000) Controls on Rayleigh wave amplitudes: Attenuation and focusing. *Geophysical Journal International* 142: 933–940.

Selby ND and Woodhouse JH (2002) The Q structure of the upper mantle: Constraints from Rayleigh wave amplitudes. *Journal of Geophysical Research* 107. http://dx.doi.org/10.1029/2001JB000,257.

Shearer P (1994) Constraints on inner core anisotropy from PKP(DF) travel times. *Journal of Geophysical Research* 99: 19647–19659.

Sheehan A and Solomon SC (1992) Differential shear wave attenuation and its lateral variation in the north Atlantic region. *Journal of Geophysical Research* 97: 15339–15350.

Shi J, Kim WY, and Richards PG (1996) Variability of crustal attenuation in the northeastern United States from *Lg* waves. *Journal of Geophysical Research* 101: 25231–25242.

Shito A, Karato S-I, Matsukage KN, and Nishibara Y (2006) Towards mapping the three-dimensional distribution of water in the upper mantle from velocity and attenuation tomography. In: Jacobsen SD and vanderLee S (eds.) *Earth's Deep Water Cycle. Geophysical Monograph Series*, vol. 168, pp. 225–236. Washington, DC: AGU.

Shito A, Karato S, and Park J (2004) Frequency dependence of Q in Earth's upper mantle inferred from continuous spectra of body waves. *Geophysical Research Letters* 31. http://dx.doi.org/10.1029/2004GL019582.

Shito A and Shibutan T (2003a) Anelastic structure of the upper mantle beneath the northern Philippine Sea. *Physics of the Earth and Planetary Interiors* 140: 319–329.

Shito A and Shibutan T (2003b) Nature of heterogeneity of the upper mantle beneath the northern Philippine Sea as inferred from attenuation and velocity tomography. *Physics of the Earth and Planetary Interiors* 140: 331–341. http://dx.doi.org/10.1016/j.pepi.2003.09.010.

Singh S and Herrmann RB (1983) Regionalization of crustal Q in the continental United States. *Journal of Geophysical Research* 88: 527–538.

Singh SC, Taylor MJ, and Montagner JP (2000) On the presence of liquid in the Earth's inner core. *Science* 287: 2471–2474.

Sipkin SA and Jordan TH (1979) Frequency dependence of Q_{ScS}. *Bulletin of the Seismological Society of America* 69: 1055–1079.

Sipkin SA and Jordan TH (1980) Regional variation of Q_{ScS} phases. *Bulletin of the Seismological Society of America* 70: 1071–1102.

Sipkin SA and Revenaugh J (1994) Regional variation of attenuation and travel times in China from analysis of multiple ScS phases. *Journal of Geophysical Research* 99: 2687–2699.

Smith S (1972) The anelasticity of the mantle. *Tectonophysics* 13: 601–622.

Smith ML and Dahlen FA (1981) The period and Q of the Chandler wobble. *Geophysical Journal of the Royal Astronomical Society* 64: 223–282.

Smith MF and Masters G (1989) Aspherical structure constraints from free oscillation frequency and attenuation measurements. *Journal of Geophysical Research* 94: 1953–1976.

Sobolev SV, Zeyen H, Soll G, Werling F, Altherr R, and Fuchs K (1996) Upper mantle temperatures from teleseismic tomography of French Massif Central including the effects of composition, mineral reactions, anharmonicity, anelasticity and partial melt. *Earth and Planetary Science Letters* 139: 147–163.

Solomon SC (1973) Seismic wave attenuation and melting beneath the mid-Atlantic Ridge. *Journal of Geophysical Research* 78: 6044–6059.

Solomon SC and Toksöz MN (1970) Lateral variation of attenuation of P and S waves beneath the United States. *Bulletin of the Seismological Society of America* 60: 819–838.

Song XD and Helmberger D (1993) Anisotropy of the Earth's inner core. *Geophysical Research Letters* 20: 285–288.

Souriau A and Calvet M (2015) The Earth's cores. *Treatise on Geophysics*, vol. 1. USA: Elsevier.

Souriau A and Romanowicz B (1996) Anisotropy in inner core attenuation: A new type of data to constrain the nature of the solid core. *Geophysical Research Letters* 23: 1–4.

Souriau A and Romanowicz B (1997) Anisotropy in the inner core: Relation between P-velocity and attenuation. *Physics of the Earth and Planetary Interiors* 101: 33–47.

Souriau A and Roudil P (1995) Attenuation in the uppermost inner core from broadband GEOSCOPE PKP data. *Geophysical Journal International* 123: 572–587.

Stachnik JC, Abers GA, and Christensen DH (2004) Seismic attenuation and mantle wedge temperatures in the Alaska subduction zone. *Journal of Geophysical Research* 109: B10304. http://dx.doi.org/10.1029/2004JB003018.

Street RL (1976) Scaling northeastern United States/southeastern Canadian earthquakes by the *Lg* waves. *Bulletin of the Seismological Society of America* 66: 1525–1537.

Strick E (1967) The determination of *Q*, dynamic viscosity and creep curves from wave propagation measurements. *Geophysical Journal of the Royal Astronomical Society* 13: 197–218.

Su WJ and Dziewonski AM (1990) Inner core anisotropy in three dimensions. *Journal of Geophysical Research* 100: 9831–9852.

Suda N and Fukao Y (1990) Structure of the inner core inferred from observations of seismic core modes. *Geophysical Journal International* 103: 403–413.

Suda N, Nawa K, and Fukao Y (1998) Earth's background free oscillations. *Science* 279: 2089–2091.

Suda N, Shibata N, and Fukao Y (1991) Degree 2 pattern of attenuation structure in the upper mantle from apparent complex frequency measurements of fundamental spheroidal modes. *Geophysical Research Letters* 18: 1119–1122.

Suetsugu D (2001) A low Q_{ScS} anomaly near the South Pacific Superswell. *Geophysical Research Letters* 28: 391–394.

Sumita I and Olson P (1999) A laboratory model for convection in Earth's core driven by a thermally heterogeneous mantle. *Geophysical Research Letters* 286: 1547–1549.

Sundberg M and Cooper RF (2010) A composite viscoelastic model for incorporating grain boundary sliding and transient diffusion creep; correlating creep and attenuation responses for materials with a fine grain size. *Philosophical Magazine* 90(20): 2817–2840. http://dx.doi.org/10.1080/14786431003746656.

Sutton GH, Mitronovas W, and Pomeroy PW (1967) Short-period seismic energy radiation patterns from underground explosions and small-magnitude earthquakes. *Bulletin of the Seismological Society of America* 57: 249–267.

Takanami T, Sacks S, and Hasegawa A (2000) Attenuation structure beneath the volcanic front in northeastern Japan from broad-band seismograms. *Physics of the Earth and Planetary Interiors* 121: 339–357.

Tanaka S and Hamaguchi H (1997) Degree one heterogeneity and hemispherical variation of anisotropy in the inner core from PKP(BC)-PKP(DF) times. *Journal of Geophysical Research* 102: 2925–2938.

Teng TL (1968) Attenuation of body waves and the Q structure of the mantle. *Journal of Geophysical Research* 73: 2195–2208.

Thouvenot F (1983) Frequency dependence of the quality factor in the upper crust: A deep seismic sounding approach. *Geophysical Journal of the Royal Astronomical Society* 73: 427–447.

Trampert J and Woodhouse JH (1995) Global phase velocity maps of Love and Rayleigh waves between 40 and 150 seconds. *Geophysical Journal International* 122: 675–690.

Tryggvason E (1965) Dissipation of Rayleigh-wave energy. *Journal of Geophysical Research* 70: 1449–1455.

Tsai YB and Aki K (1969) Simultaneous determination of the seismic moment and attenuation of seismic surface waves. *Bulletin of the Seismological Society of America* 59: 275–287.

Tseng TL, Huang BS, and Chin BH (2001) Depth-dependent attenuation in the uppermost inner core from the Taiwan short period PKP data. *Geophysical Research Letters* 28: 459–462.

Tsumura N, Matsumoto S, Horiuchi S, and Hasegawa A (2000) Three-dimensional attenuation structure beneath the northeastern Japan arc estimated from spectra of small earthquakes. *Tectonophysics* 319(4): 241–260. http://dx.doi.org/10.1016/S0040-1951(99)00297-8.

Ulug A and Berckhemer G (1984) Frequency dependence of Q for seismic body waves in the Earth's mantle. *Journal of Geophysics* 56: 9–19.

Utsu T (1967) Anomalies in seismic wave velocity and attenuation associated with a deep earthquake zone. *Journal of the Faculty of Science, Hokkaido University* 7: 1–25.

Vidale JE and Earle PS (2000) Fine-scale heterogeneity in the Earth's inner core. *Nature* 404: 273–275.

Vinnik LP, Romanowicz B, and Bréger L (1994) Anisotropy in the center of the inner core. *Geophysical Research Letters* 21: 1671–1674.

Walter WR, Mayeda K, Malagnini L, and Scognamiglio L (2007) Regional body-wave attenuation using a coda source normalization method: Application to MEDNET records of earthquakes in Italy. *Geophysical Research Letters* 34.

Walter WR and Taylor SR (2001) A revised magnitude and distance amplitude correction (MDAC2) procedure for regional seismic discriminants. *Theory and Testing at NTS Lawrence Livermore National Laboratory Technical Report*, UCRL-ID-146882.

Warren LM and Shearer PM (2000) Investigating the frequency dependence of mantle Q by stacking P and PP spectra. *Journal of Geophysical Research* 105: 25391–25402.

Warren LM and Shearer PM (2002) Mapping lateral variation in upper mantle attenuation by stacking *P* and *PP* spectra. *Journal of Geophysical Research* 107. http://dx.doi.org/10.1029/2001JB001195.

Waszek L and Deuss A (2013) A low attenuation layer in Earth's uppermost inner core. *Geophysical Journal International* 195: 2005–2015. http://dx.doi.org/10.1093/gji/ggt368.

Wen L and Niu F (2002) Seismic velocity and attenuation structures in the top of the Earth's inner core. *Journal of Geophysical Research* 107. http://dx.doi.org/10.1029/2001JB000170.

Widmer R, Masters G, and Gilbert F (1991) Spherically symmetric attenuation within the Earth from normal mode data. *Geophysical Journal International* 104: 541–553.

Wiens DA, Conder JA, and Faul UH (2008) The seismic structure and dynamics of the mantle wedge. *Annual Review of Earth and Planetary Sciences* 36: 421–455. http://dx.doi.org/10.1146/annurev.earth.33.092203.122633.

Wilcock WSD, Solomon SC, Purdy GM, and Toomey D-R (1995) Seismic attenuation structure of the East Pacific Rise near 9°30′N. *Journal of Geophysical Research* 100: 24147–24165.

Wong YK (1989) *Upper Mantle Heterogeneity from Phase and Amplitude Data of Mantle Waves*. PhD Dissertation, Cambridge, MA: Harvard University.

Woodhouse JH and Wong YK (1986) Amplitude, phase and path anomalies of mantle waves. *Geophysical Journal of the Royal Astronomical Society* 87: 753–773.

Xie J (2007) Pn attenuation beneath the Tibetan Plateau. *Bulletin of the Seismological Society of America* 97: 2040–2052.

Xie J, Gok R, Ni J, and Aoki Y (2004) Lateral variations of crustal seismic attenuation along the INDEPTH profiles in Tibet from *Lg Q* inversion. *Journal of Geophysical Research* 109(B10): 988. http://dx.doi.org/10.1029/2004JB002.

Xie J and Mitchell BJ (1990a) Attenuation of multiphase surface waves in the Basin and Range province. Part I: *Lg* and *Lg* coda. *Geophysical Journal International* 102: 121–127.

Xie J and Mitchell BJ (1990b) A back-projection method for imaging large-scale lateral variations of *Lg* coda *Q* with application to continental Africa. *Geophysical Journal International* 100: 161–181.

Xie J and Nuttli OW (1988) Interpretation of high-frequency coda at large distances: Stochastic modeling and method of inversion. *Geophysical Journal* 95: 579–595.

Xie J, Wu X, Liu R, Schaff D, Liu Y, and Liang J (2006) Tomographic regionalization of crustal *Lg Q* in eastern Eurasia. *Geophysical Research Letters* 33(L03). http://dx.doi.org/10.1029/2005GL024; 410.

Yacoub NK and Mitchell BJ (1977) Attenuation of Rayleigh wave amplitudes across Eurasia. *Bulletin of the Seismological Society of America* 67: 751–769.

Yang Y, Forsyth DW, and Weeraratne DS (2007) Seismic attenuation near the East Pacific Rise and the origin of the low-velocity zone, Earth planet. *Science Letters* 258: 260–268. http://dx.doi.org/10.1016/j.epsl.2007.03.040.

Yoshida M and Tsujiura M (1975) Spectrum and attenuation of multiply-reflected core phases. *Journal of Physics of the Earth* 23: 31–42.

Yu W and Wen L (2006a) Seismic velocity and attenuation structures in the top 400 km of the Earth's inner core along equatorial paths. *Journal of Geophysical Research* 111. http://dx.doi.org/10.1029/2005JB003995.

Yu W and Wen L (2006b) Inner core attenuation anisotropy. *Earth and Planetary Science Letters* 245: 581–594.

Zhang T and Lay T (1994) Analysis of short-period regional phase path effects associated with topography in Eurasia. *Bulletin of the Seismological Society of America* 84: 119–132.

Zhou Y (2009) Surface wave sensitivity to 3-D anelasticity. *Geophysical Journal International* 178: 1403–1410.

Zou Z, Koper KD, and Cormier VF (2008) The structure of the base of the outer core inferred from seismic waves diffracted around the inner core. *Journal of Geophysical Research* 113. http://dx.doi.org/10.1029/2007JB005316.

Relevant Websites

http://mahi.ucsd.edu/galai/rem.dir/rem.home.html – The Reference Earth Model.